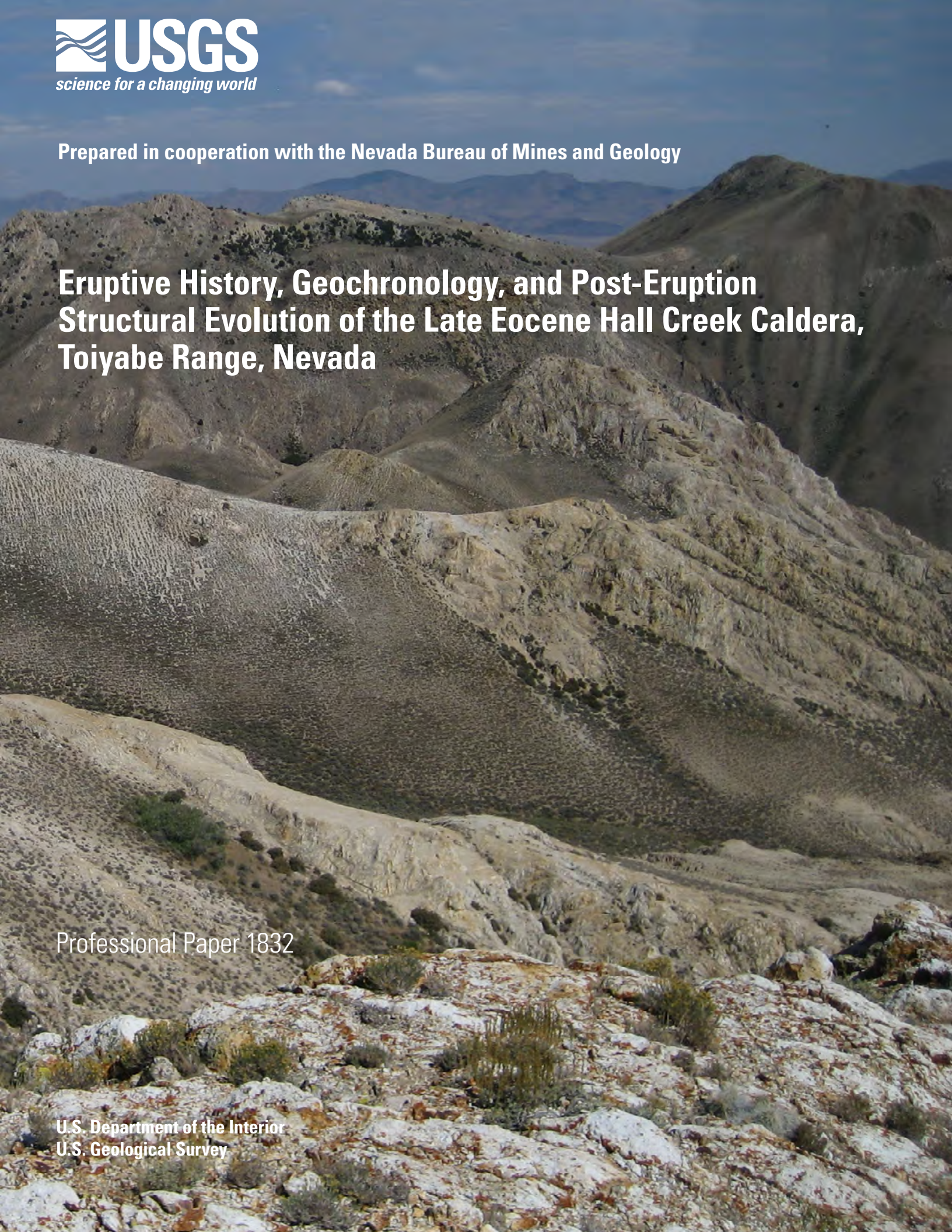

USGS
science for a changing world

Prepared in cooperation with the Nevada Bureau of Mines and Geology

Eruptive History, Geochronology, and Post-Eruption Structural Evolution of the Late Eocene Hall Creek Caldera, Toiyabe Range, Nevada

Professional Paper 1832

U.S. Department of the Interior
U.S. Geological Survey

Cover. View east of thick intracaldera tuff of Hall Creek filling the southern part of the Hall Creek caldera in the central Toiyabe Range. White color and orange staining of tuff in foreground are from post-eruption hydrothermal alteration (Photograph by Joseph P. Colgan, September 2011).

Eruptive History, Geochronology, and Post-Eruption Structural Evolution of the Late Eocene Hall Creek Caldera, Toiyabe Range, Nevada

By Joseph P. Colgan and Christopher D. Henry

Prepared in cooperation with the Nevada Bureau of Mines and Geology

Professional Paper 1832

U.S. Department of the Interior
U.S. Geological Survey

U.S. Department of the Interior
SALLY JEWELL, Secretary

U.S. Geological Survey
Suzette M. Kimball, Director

U.S. Geological Survey, Reston, Virginia: 2017

Suggested citation:
Colgan, J.P., and Henry, C.D., 2017, Eruptive history, geochronology, and post-eruption structural evolution of the late Eocene Hall Creek Caldera, Toiyabe Range, Nevada: U.S. Geological Survey Professional Paper 1832, 44 p., https://doi.org/10.3133/pp1832.

ISSN 2330-7102 (online)

Acknowledgments

Joseph Colgan was supported by the U.S. Geological Survey's National Cooperative Geologic Mapping Program, and Christopher Henry was supported by the Nevada Bureau of Mines and Geology. David John and Kathryn Watts of the U.S. Geological Survey assisted with field work and sample collection. We thank Bill McIntosh, Matt Heizler, and Lisa Peters for assistance with $^{40}Ar/^{39}Ar$ dating at the New Mexico Geochronology Research Laboratory (New Mexico Institute of Mining and Technology). David John reviewed an early draft of the manuscript, and we thank Charles Bacon and Eric Christiansen for insightful comments during the review process.

Contents

Figures

Appendix Figures

Tables

Conversion Factors

U.S. customary units to International System of Units

Multiply	By	To obtain
	Length	
inch (in.)	2.54	centimeter (cm)
inch (in.)	25.4	millimeter (mm)
foot (ft)	0.3048	meter (m)
mile (mi)	1.609	kilometer (km)
mile, nautical (nmi)	1.852	kilometer (km)
yard (yd)	0.9144	meter (m)
	Area	
square mile (mi^2)	2.590	square kilometer (km^2)
	Volume	
cubic mile (mi^3)	4.168	cubic kilometer (km^3)

Datum

Vertical coordinate information is referenced to the North American Vertical Datum of 1988 (NAVD 88)].

Horizontal coordinate information is referenced to North American Datum of 1927 (NAD 27)].

Elevation, as used in this report, refers to distance above the vertical datum.

Eruptive History, Geochronology, and Post-Eruption Structural Evolution of the Late Eocene Hall Creek Caldera, Toiyabe Range, Nevada

By Joseph P. Colgan[1] and Christopher D. Henry[2]

Abstract

The magmatic, tectonic, and topographic evolution of what is now the northern Great Basin remains controversial, notably the temporal and spatial relation between magmatism and extensional faulting. This controversy is exemplified in the northern Toiyabe Range of central Nevada, where previous geologic mapping suggested the presence of a caldera that sourced the late Eocene (34.0 mega-annum [Ma]) tuff of Hall Creek. This region was also inferred to be the locus of large-magnitude middle Tertiary extension (more than 100 percent strain) localized along the Bernd Canyon detachment fault, and to be the approximate location of a middle Tertiary paleodivide that separated east and west-draining paleovalleys. Geologic mapping, $^{40}Ar/^{39}Ar$ dating, and geochemical analyses document the geologic history and extent of the Hall Creek caldera, define the regional paleotopography at the time it formed, and clarify the timing and kinematics of post-caldera extensional faulting. During and after late Eocene volcanism, the northern Toiyabe Range was characterized by an east-west trending ridge in the area of present-day Mount Callaghan, probably localized along a Mesozoic anticline. Andesite lava flows erupted around 35–34 Ma ponded hundreds of meters thick in the erosional low areas surrounding this structural high, particularly in the Simpson Park Mountains. The Hall Creek caldera formed ca. 34.0 Ma during eruption of the approximately 400 cubic kilometers (km^3) tuff of Hall Creek, a moderately crystal-rich rhyolite (71–77 percent SiO_2) ash-flow tuff. Caldera collapse was piston-like with an intact floor block, and the caldera filled with thick (approximately 2,600 meters) intracaldera tuff and interbedded breccia lenses shed from the caldera walls. The most extensive exposed megabreccia deposits are concentrated on or close to the caldera floor in the southwestern part of the caldera. Both silicic and intermediate post-caldera lavas were locally erupted within 400 thousand years of the main eruption, and for the next approximately 10 million years sedimentary rocks and distal tuffs sourced from calderas farther west ponded in the caldera basin surrounding low areas nearby. Patterns of tuff deposition indicate that the area was characterized by east-west trending paleovalleys and ridges in the late Eocene and Oligocene, which permitted tuffs to disperse east-west but limited their north-south extent. Although a low-angle fault contact of limited extent separates Cambrian and Ordovician strata in the southwestern part of the study area, there is no evidence that this fault cuts overlying Tertiary rocks. Total extensional strain across the caldera is on the order of 15 percent, and there is no evidence for progressive tilting of 34–25 Ma rocks that would indicate protracted Eocene–Oligocene extension. The caldera appears to have been tilted as an intact block after 25 Ma, probably during the middle Miocene extensional faulting well documented to the north and south of the study area.

Introduction

From the Eocene to the Miocene, the northern Great Basin in the western United States was the locus of intense silicic caldera-forming volcanic eruptions often referred to as the "ignimbrite flareup" (for example, Coney, 1978; Best and others, 2013). Over the same time period, the region underwent widespread extensional faulting that eventually formed the modern Basin and Range Province (for example, Dickinson, 2006). Silicic magmatism was broadly time transgressive (fig. 1), sweeping southwest across the Basin and Range from northern Nevada in the Eocene to south central Nevada in the early Miocene (for example, Armstrong and others, 1969; Henry and John, 2013). Extensional faulting locally began during this time and has continued episodically up to the present, but the relation between extension and magmatism—both locally and at the province scale—has been debated for several decades as new studies gradually unraveled the relative timing of volcanism and extensional faulting. Many studies have inferred major (high strain) extension to be synchronous with Eocene to early Miocene silicic volcanism as it migrated south across the Great Basin, perhaps because of thermal weakening and thinning of the brittle crust (for example, Miller and others, 1983; Gans and others, 1989; Hudson and others, 2000). Other studies have concluded

[1]U.S. Geological Survey, Denver, Colo.

[2]Nevada Bureau of Mines and Geology, Reno, Nev.

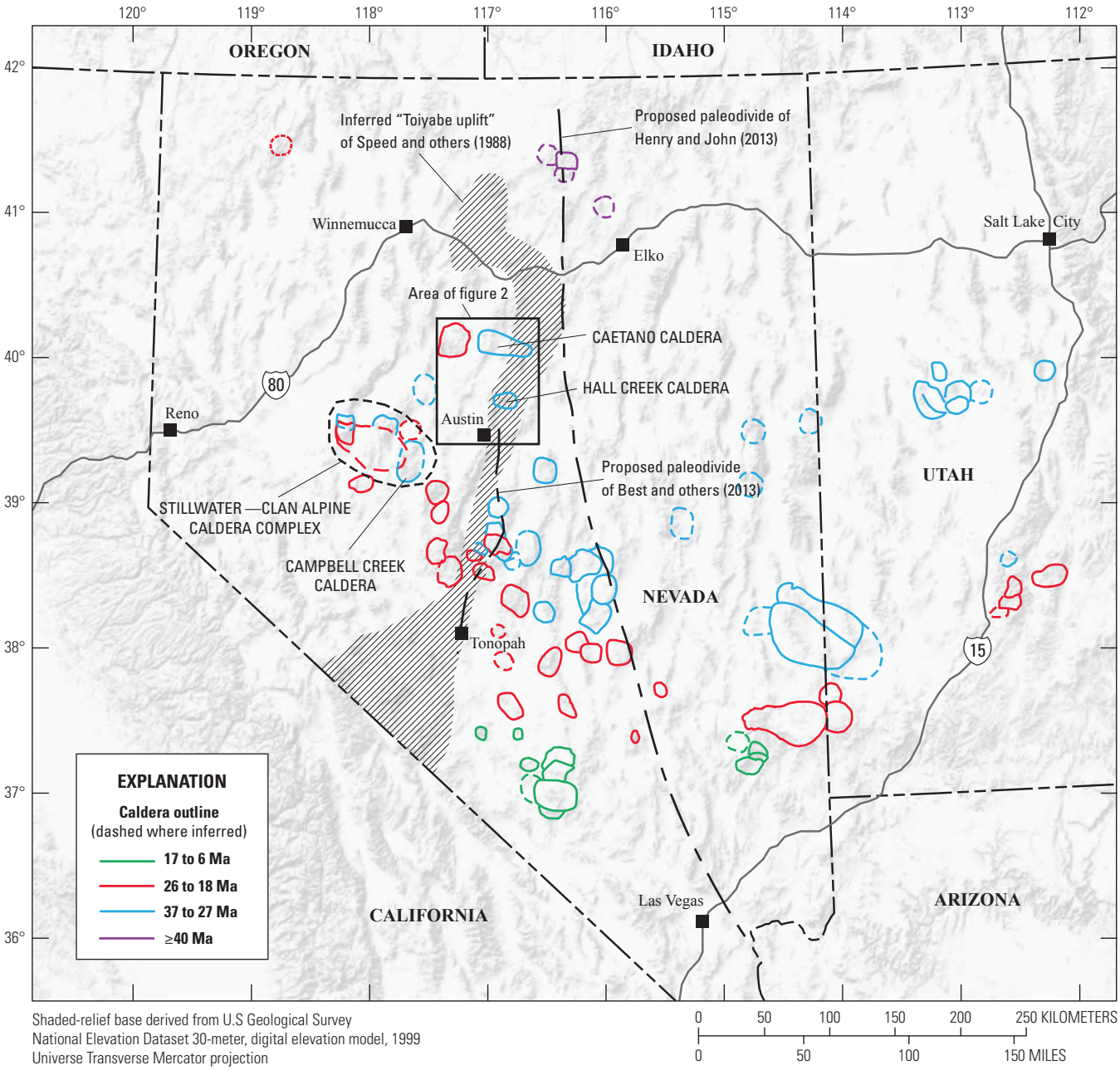

Figure 1. Northern Great Basin, showing distribution of middle Tertiary ignimbrite calderas from Henry and John (2013) and proposed middle Tertiary drainage divides from Best and others (2009) and Henry and John (2013) (Ma, mega-annum).

instead that the most widespread and high-strain extension did not begin until the middle Miocene, after the most voluminous phase of Eocene to early Miocene ignimbrite magmatism had ended (for example, Best and Christiansen, 1991; Colgan and Henry, 2009; Cassel and others, 2014).

Stewart and McKee (1968) first mapped a sequence of ash-flow tuffs in the northern Toiyabe Range of central Nevada that they suspected might be within or near a caldera related to the Eocene tuff of Hall Creek. Smith (1989, 1992) subsequently remapped and interpreted part of the same area, also inferring the presence of a caldera but concluding that it had been deformed by large magnitude extension (up to 200 percent strain) accommodated primarily by a gently-dipping detachment fault. Smith (1989, 1992) concluded that this deformation took place synchronously with volcanism from the Eocene to the Miocene, making the northern Toiyabe Range an example of large-magnitude, syn-volcanic middle Tertiary extension in the Basin and Range Province (Gans and others, 1989). In contrast, recent work in the Eocene Caetano caldera at the north end of the Toiyabe Range (fig. 2) also documented large-magnitude (approximately 100 percent strain) extension, but concluded that it took place in the middle Miocene (around 17–16 to 12–10 Ma), long after formation of the 34 Ma Caetano caldera (Colgan and others; 2011, Colgan and others; 2008, John and others; 2008).

Although inferred to exist on the basis of sound field observations by both Stewart and McKee (1968) and Smith (1992), most of the Hall Creek caldera has not been mapped; previous studies covered only the southwest corner in any detail. Understanding how one of the northernmost and oldest calderas of the ignimbrite flareup (fig. 1) formed is important for understanding how middle Tertiary magmatism evolved in time and space as it migrated southwest across the northern Basin and Range. The large magnitude of inferred extensional strain and tilting would make it an ideal place to study the evolution of large silicic magma systems in general, as such deformation may expose deeper parts of the magma system that are not directly observable in modern calderas or in less-extended middle Tertiary ones (for example, du Bray and Pallister, 1991; John, 1995; John and others, 2008). The inferred timing of extension at Hall Creek (mostly Oligocene to early Miocene) contrasts strongly with the middle Miocene faulting in both the Caetano caldera approximately 30 kilometers (km) to the north (Colgan and others, 2008) and in the Toiyabe Range at the latitude of Austin approximately 20 km to the south (fig. 2) (Stockli, 1999); if correct, this suggests a much different tectonic setting for deformation as well as requiring the existence of east-west striking faults or accommodation zones between the different areas.

Many of the ash-flow tuffs erupted from the calderas shown in figure 1 dispersed widely across the landscape by flowing along paleovalleys carved into the pre-Tertiary bedrock in the late Mesozoic or earlier in the Cenozoic (for example, Henry, 2008). Their distribution thus informs knowledge of regional topography prior to formation of the modern Basin and Range Province, when the region was thought to be a broad, high orogenic plateau, much of which drained to the Pacific Ocean (for example, DeCelles, 2004; Cassel and others, 2009; Henry and John, 2013). Best and others (2009, 2013) interpreted a major north-south topographic high between Austin and Tonopah, Nevada (fig. 1) that formed the middle Tertiary drainage divide and served as a barrier to the east-west dispersal of ash-flow tuffs. Best and others (2009; 2013) interpreted this barrier as the western edge of a high continental plateau coincident with a crustal-scale, east-vergent thrust fault; the edge of the plateau was enhanced by precipitation and consequent erosion and isostatic uplift on the westward (Pacific Ocean) side compared to the dry eastern side (for example, Masek and others, 1994). Henry and John (2013) interpreted several tuffs sourced from calderas in western Nevada to have flowed east through the area of this proposed topographic barrier and suggested a drainage divide further east (fig. 1). The Hall Creek caldera lies on or near these proposed Eocene topographic features, and the distribution of its outflow tuff and other tuffs in the study area can provide direct evidence for the nature of late Eocene–early Oligocene topography in the area.

The goals of this study are: (1) to map the full extent of the Hall Creek caldera to understand the geometry and size of the caldera and the physical process of caldera collapse, (2) to collect new argon-argon ($^{40}Ar/^{39}Ar$) dates and geochemical data from caldera-related rocks to understand the composition and evolution of the intracaldera tuff and related lavas and intrusive rocks (if any), (3) to document the distribution of outflow tuff, which bears on the topography of the region at the time of the eruption, and (4) to better document the timing and amount of offset on the system of normal faults that apparently accommodated large-magnitude extension in the area.

Geologic Overview and Previous Work

The northern Toiyabe Range was mapped in reconnaissance by Stewart and McKee (1977) as part of the 1:250,000-scale geologic map of Lander County, Nevada. In the course of that study, a 1:62,500-scale geologic map of the Mount Callaghan quadrangle was published (Stewart and McKee, 1968), which includes the southern edge of the study area for this report, as well as a 1:62,500-scale Open-File Report of the Hall Creek quadrangle (Stewart and McKee, 1969), which covers much of the northern part of the study area for this report. Smith (1989, 1992) mapped an area at 1:24,000 scale that included roughly the southwestern quarter of the Hall Creek caldera (fig. 3).

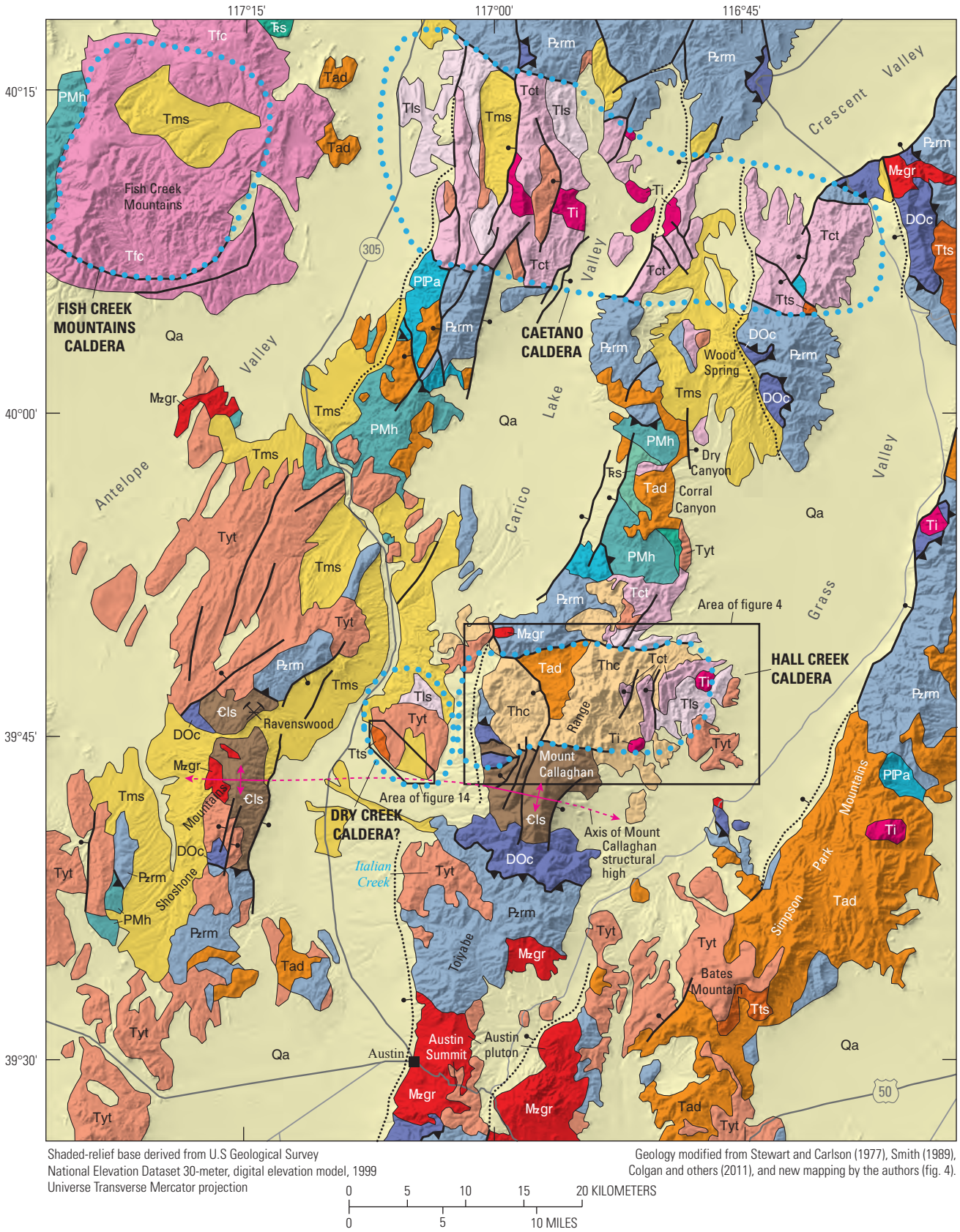

Figure 2. Northern Toiyabe Range and nearby areas, modified from Stewart and Carlson (1977), Smith (1989), Colgan and others (2011) and new mapping for this study.

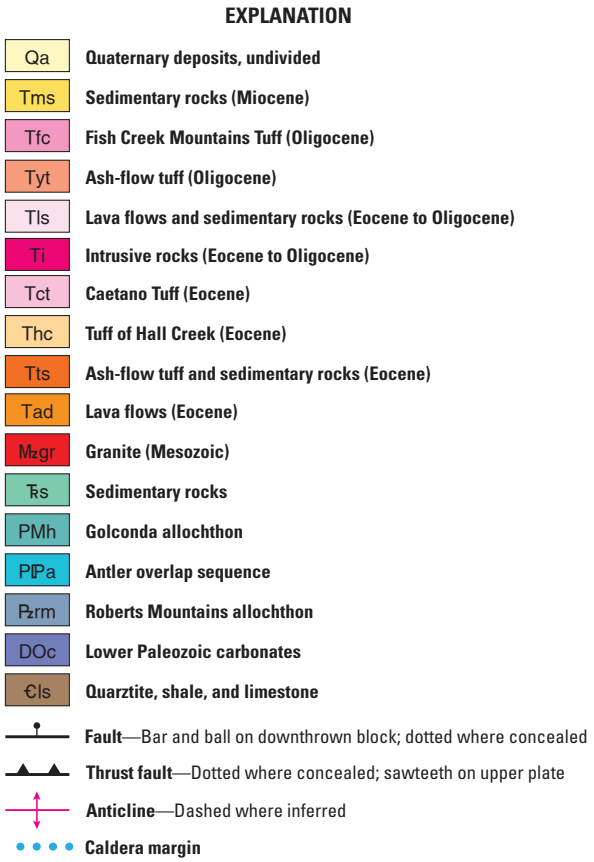

Figure 2. Northern Toiyabe Range and nearby areas, modified from Stewart and Carlson (1977), Smith (1989), Colgan and others (2011) and new mapping for this study.—Continued

Pre-Tertiary Rocks and Structure

The oldest exposed rocks in the northern Toiyabe Range are Early Cambrian to Silurian siliciclastic and carbonate rocks deposited on the western margin of the North American craton during the early Paleozoic (Stewart and McKee, 1977). Lower Paleozoic slope-shelf strata are structurally overlain by the Roberts Mountains allochthon, a highly deformed package of Upper Cambrian to Devonian chert, argillite, quartzite, and greenstone (Stewart and McKee, 1977). These deep-water rocks were deformed and thrust over the coeval slope-shelf sequence along the Roberts Mountains thrust during the Late Devonian-Mississippian Antler orogeny (for example, Roberts and others, 1958; Miller and others, 1992). The deformed Roberts Mountains allochthon is overlain on an erosional unconformity by Pennsylvanian and Permian clastic rocks and limestone (Stewart and McKee, 1977) referred to as the "Antler overlap sequence" (for example, Roberts and others, 1958). The overlap sequence is itself overlain along the Early Triassic Golconda thrust (Stewart and McKee, 1977) by a package of Mississippian to Permian deep-water rocks collectively referred to as the Havallah sequence (for example Silberling and Roberts, 1962; Brueckner and Snyder, 1985; Murchey, 1990). Paleozoic strata are locally intruded by Mesozoic granitic rocks; the most extensive of these is the Jurassic (168 Ma; Silberman and McKee, 1971) Austin pluton underlying the town of Austin, Nevada (fig. 2).

The entire Paleozoic to Triassic stratigraphic and structural package dips broadly north across the study area (fig. 2), exposing progressively younger rocks from Lower Cambrian quartzites on Mount Callaghan to the Havallah sequence just north of the study area. South of the study area, the Paleozoic section dips south, forming a structural dome centered on Mount Callaghan (fig. 2). Speed and others (1988) interpreted this structure as part of a chain of diapiric domes related to Jurassic plutonism, which they suggested gave rise to the "Toiyabe uplift," a north-south trending topographic high that stretched for hundreds of kilometers along strike (fig. 1). Geologic relations shown in figure 2 seem at odds with this, however, as Mesozoic intrusive rocks do not crop out in the vicinity of Mount Callaghan (although they could still be present at depth) and Paleozoic rocks do not appear to be domed around the large Jurassic pluton (unit Mzgr) east of Austin (fig. 2). Instead, the Mount Callaghan structural high appears to continue westward into the Ravenswood district in the Shoshone Mountains (fig. 2), in the form of an east-west trending anticline. Best and others (2009, 2013) interpreted part of the Speed and others (1988) "Toiyabe uplift" as a north-south trending middle Tertiary drainage divide (fig. 1) that served as a barrier to the east-west dispersal of Eocene to early Miocene ash-flow tuffs, which they attributed to a major west-dipping Mesozoic reverse fault at the latitude of the Toiyabe Range.

Tertiary Rocks and Structure

Paleozoic sedimentary rocks and Jurassic plutonic rocks in the northern Toiyabe Range are overlain unconformably by a sequence of Eocene to late Oligocene volcanic rocks, mainly exposed in an east-west belt across the study area inferred to include the caldera source for the tuff of Hall Creek. The oldest Tertiary rocks are Eocene andesitic lava flows that underlie the tuff of Hall Creek; similar rocks crop out extensively in the Simpson Park Mountains to the east (fig. 2), where they have been potassium argon K-Ar dated to around 35 Ma (McKee and Silberman, 1970). The single thickest and most widespread Tertiary unit in the area is the tuff of Hall Creek (Thc, fig. 2), named by Stewart and McKee (1968) for exposures along Hall Creek (fig. 3). Based on its thickness, extent, and inclusion of extensive meso- and megabreccia deposits, both Stewart and McKee (1968, 1977) and Smith (1992) interpreted it to be within or close to its source caldera. The tuff of Hall Creek is 34.0 Ma (Henry and John, 2013) and underlies the 34.0 Ma (John and others, 2008) Caetano Tuff, mapped in the northern Toiyabe Range as the "tuff of Cowboy Rest" by Stewart and McKee (1968) and the "tuff of China Spring" by Smith (1992).

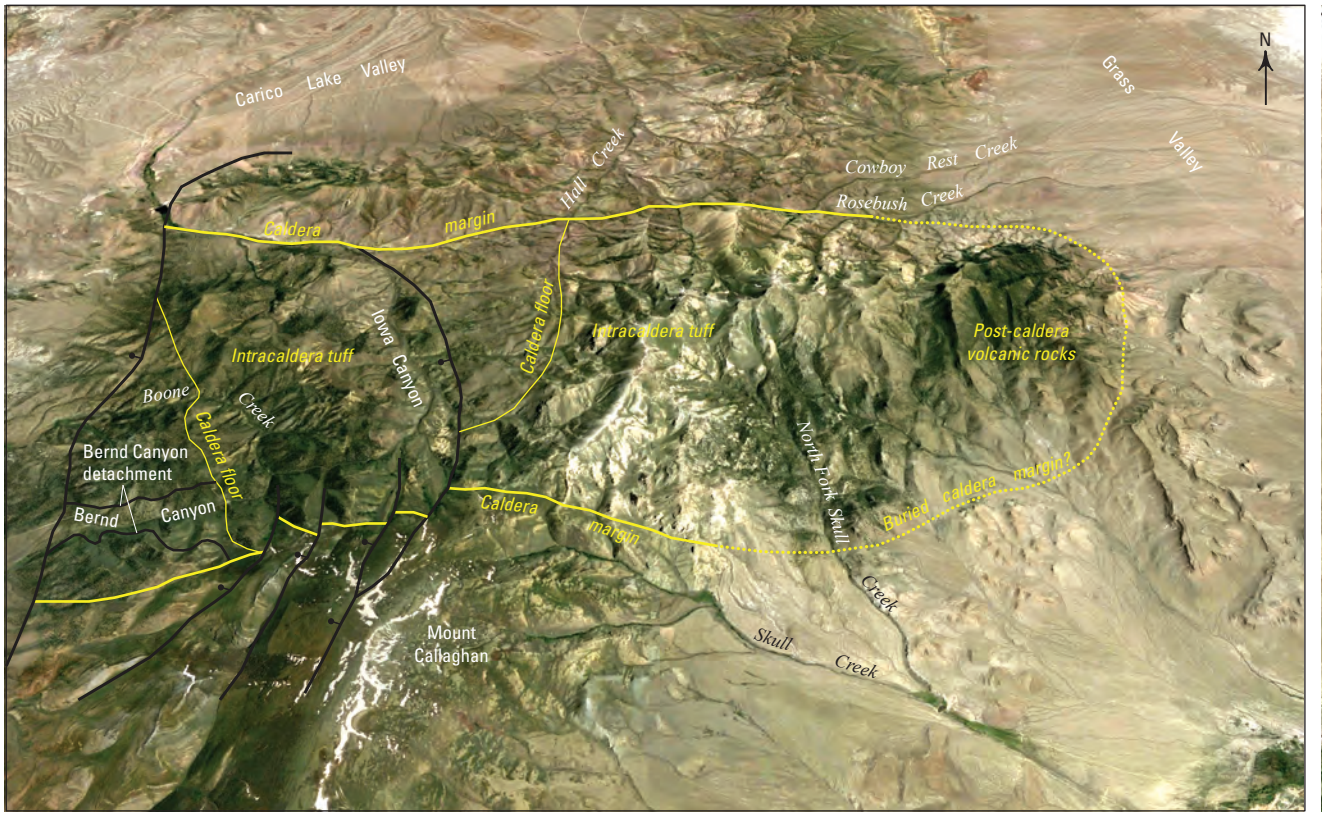

Base map data from Google, Landsat, 2014

Figure 3. Hall Creek caldera, viewed from the south. East-west distance across center of caldera is approximately 25 kilometers. Black lines—normal faults, ball and bar on downthrown side; Solid yellow lines—margin of Hall Creek caldera; Dashed yellow lines—inferred buried caldera margin. "Caldera margin" refers to the caldera structural margin; location of the unexposed caldera topographic rim is discussed in the text.

Caetano Tuff, older Tertiary rocks, and pre-Tertiary bedrock are locally overlain by a sequence of Oligocene ash-flow tuffs interbedded with tuffaceous sedimentary rocks and lava flows (units Tls and Tyt, fig. 2). These rocks are thickest in the central part of the study area where they overlie the tuff of Hall Creek and Caetano Tuff, while thinner sections are exposed in Italian Creek to the south (fig. 2) and Corral and Dry Canyons to the north (fig. 2). Most of these rocks are undated, but Stewart and McKee (1968, 1977) recognized two units of the Bates Mountain tuff in this sequence—unit C, now known to correlate with the 28.9 Ma tuff of Campbell Creek (Henry and others, 2012), and unit D, now known to correlate with the 25.4 Ma Nine Hill Tuff (Henry and John, 2013).

Smith (1989, 1992) conducted a detailed (1:24,000 scale) geologic map-based study of Cenozoic normal faulting in the northern Toiyabe Range, over an area that included roughly the southwestern quarter of the Hall Creek caldera. He interpreted the area as a locus of high extensional strain (50–200 percent) accommodated by closely-spaced, initially steeply west-dipping normal faults. The main extensional structure is the Bernd Canyon detachment fault, which crops out in Bernd Canyon on the west side of the range (fig. 3). This fault is presently subhorizontal, but Smith (1992) inferred that it initiated at an angle closer to 60 degrees (°) and rotated to 25–30° during slip, prior to being passively rotated to its present orientation during slip on younger faults. Smith (1992) interpreted Eocene and Oligocene volcanic rocks in the northern Toiyabe Range to be progressively less tilted upsection, recording protracted slip on the Bernd Canyon detachment and related faults beginning prior to eruption of the 34 Ma tuff of Hall Creek and continuing until eruption of the Bates Mountain tuffs around 25 Ma, with additional post-25 Ma extension recorded by tilting of the Bates Mountain Tuff. Extension was of large magnitude, began synchronously with—and was related to—Eocene magmatism, and took place continuously over a protracted time span, with slip on the Bernd Canyon detachment lasting at least 10 million years and subsequent faulting continuing into the Pliocene.

New Geologic Mapping and $^{40}Ar/^{39}Ar$ Geochronology

New geologic mapping and $^{40}Ar/^{39}Ar$ ages from key volcanic units document formation of the Hall Creek caldera and clarify the timing and kinematics of extensional faulting in the northern Toiyabe Range. Sample localities and ages are summarized in table 1, data from individual samples are presented

Table 1. Geochronology and geochemistry sample locations and descriptions.

Sample number	Latitude[1]	Longitude[1]	Map unit	Lithologic unit	$^{40}Ar/^{39}Ar$ age[2]	Min[3]	Geochemistry
				Hall Creek caldera (fig. 4)			
H11-156	39.77246	–116.85967	Tyr	younger rhyolite dome	25.20 ± 0.04	san	whole rock, devitrified
H11-158	39.73989	–116.86465	Tyr	younger rhyolite dome	25.22 ± 0.04	san	whole rock, vitrophyre
H11-40	39.78592	–116.78084	Tts	post-caldera lava flow			whole rock, crystalline
H14-111	39.82405	–116.87604	Ta	post-caldera lava flow	33.62 ± 0.03	bio	whole rock, crystalline
06-DJ75	39.80814	–116.79772	Tct	Caetano tuff			whole rock, vitrophyre
06-DJ76	39.80622	–116.79814	Tct	Caetano tuff			whole rock, devitrified
H11-154	39.76043	–116.85406	Tct	Caetano tuff			pumice clast, vitrophyre
H11-42	39.78952	–116.79417	Tr	ring-fracture rhyolite			whole rock, devitrified
H11-43	39.79062	–116.79182	Tr	ring-fracture rhyolite	36.61 ± 0.08	san	whole rock, vitrophyre
H11-44	39.78750	–116.78566	Tr	ring-fracture rhyolite	33.51 ± 0.06	san	whole rock, devitrified
H08-30B	39.77943	–116.95010	Thc	tuff of Hall Creek	33.92 ± 0.07	san	–
H11-155	39.76000	–116.85888	Thc	tuff of Hall Creek			whole rock, vitrophyre
H11-159	39.74702	–116.93628	Thc	tuff of Hall Creek			pumice clast, vitrophyre
H11-160	39.74844	–116.92722	Thc	tuff of Hall Creek			pumice clast, vitrophyre
H11-167	39.76799	–116.99119	Thc	tuff of Hall Creek	33.95 ± 0.07	san	pumice clast, vitrophyre
H11-20	39.77231	–116.95010	Thc	tuff of Hall Creek			pumice clast, vitrophyre
H11-21	39.76894	–116.92299	Thc	tuff of Hall Creek			pumice clast, devitrified
H11-22	39.76894	–116.92299	Thc	tuff of Hall Creek	33.90 ± 0.07	san	–
JC12-HC42	39.79794	–116.90934	Thc	tuff of Hall Creek			whole rock, devitrified
JC12-HC43	39.80079	–116.90576	Thc	tuff of Hall Creek			pumice clast, devitrified
JC12-HC44	39.80011	–116.90266	Thc	tuff of Hall Creek			pumice clast, vitrophyre
JC12-HC45	39.79735	–116.89986	Thc	tuff of Hall Creek			pumice clast, vitrophyre
JC12-HC46	39.78827	–116.89469	Thc	tuff of Hall Creek			pumice clast, vitrophyre
H13-52	39.74483	–117.01105	Thci	tuff of Hall Creek dike	33.95 ± 0.02	san	–
JC12-HC40	39.78015	–116.94494	Tad	pre-caldera andesite			whole rock, vitrophyre
JC12-HC41	39.79734	–116.94322	Tad	pre-caldera andesite			whole rock, vitrophyre
H12-166	39.78010	–116.94565	Tad	pre-caldera andesite	34.83 ± 0.04	hbl	–
JC12-HC48	39.80016	–116.92244	Tad	pre-caldera andesite			whole rock, vitrophyre
JC13-16	39.77522	–117.00526	Tad	pre-caldera andesite	34.47 ± 0.16	plag	–
				Bernd Creek area (fig. 14)			
H15-19	39.76062	–117.11272	Tr	ring-fracture rhyolite	33.80 ± 0.03	san	whole rock, devitrified
H15-16	39.75145	–117.11785	Tdc	tuff of Dry Creek	34.79 ± 0.03	san	whole rock, devitrified
15-JC-2	39.73470	–117.10472	Ta	post-caldera lava flow			whole rock, crystalline
				Italian Creek paleovalley (fig. 17)			
H12-177	39.65130	–117.05667		tuff of Cove Spring	30.37 ± 0.01	san	whole rock, devitrified
H12-187	39.63918	–117.04290		tuff of Sutcliffe			whole rock, devitrified
H12-174	39.65391	–117.04966		tuff of Sutcliffe	30.57 ± 0.01	san	whole rock, devitrified
H12-175A	39.65365	–117.05059		unknown tuff			pumice clast, devitrified
H12-175B	39.65365	–117.05059		unknown tuff			pumice clast, devitrified
H12-170	39.64857	–117.05945		tuff of Rattlesnake Canyon	31.25 ± 0.01	san	pumice clast, devitrified
H12-171	39.64951	–117.05847		tuff of Rattlesnake Canyon			whole rock, devitrified
H12-169	39.64811	–117.06184		tuff of Hardscrabble Canyon	31.46 ± 0.01	san	whole rock, devitrified
H12-188	39.63098	–117.04084		Caetano Tuff			whole rock, devitrified
H12-185	39.63754	–117.04500		Caetano Tuff	33.93 ± 0.02	san	whole rock, devitrified
H12-182	39.63014	–117.04584		tuff of Hall Creek	33.92 ± 0.02	san	pumice clast, vitrophyre
H12-183	39.63267	–117.04613		tuff of Hall Creek			whole rock, vitrophyre

Table 1. Geochronology and geochemistry sample locations and descriptions—Continued.

Sample number	Latitude[1]	Longitude[1]	Map unit	Lithologic unit	$^{40}Ar/^{39}Ar$ age[2]	Min[3]	Geochemistry
				Dry Canyon and Caetano caldera			
H11-32	39.95897	–116.83357		Caetano Tuff			whole rock, devitrified
H11-26	39.98363	–116.79420		Caetano Tuff	33.90 ± 0.07	san	whole rock, vitrophyre
H11-27	39.98336	–116.79505		tuff of Hall Creek			whole rock, vitrophyre
06-DJ11	40.05343	–116.81087		tuff of Hall Creek			whole rock, devitrified
				Bates Mountain (fig. 19)			
H11-36	39.53561	–116.78124		tuff of Axehandle Canyon	31.44 ± 0.04		whole rock, devitrified
H11-33	39.53394	–116.78287		tuff of Dry Creek	34.66 ± 0.07		whole rock, devitrified
H11-35	39.53538	–116.78169		tuff of Dry Creek	34.73 ± 0.04		whole rock, devitrified

[1]NAD27 datum.

[2]All ages ±2σ.

[3]Mineral phase dated; san = sanidine; bio = biotite, hbl = hornblende, plag = plagioclase.

in tables 2 and 3, and a description of $^{40}Ar/^{39}Ar$ dating methods and raw data for each sample are presented in Appendix 1. Reported uncertainties for all ages cited in the text are ±2 sigma. New mapping was focused on caldera-related rocks and structures—caldera margins, caldera floor, intracaldera tuff, post-caldera volcanic units—and on the Bernd Canyon detachment and related faults in the southwestern part of the caldera. The new geologic map of the Hall Creek caldera (fig. 4) was compiled from new mapping by the authors and previous mapping by Stewart and McKee (1968, 1969, and 1977) and Smith (1989) (map data sources in figure 5). This section describes the major rock units and structures together with supporting age data. We (this study), Stewart and McKee (1969, 1977), and Smith (1992) each arrived at different interpretations from mapping the geology of the southwestern quarter of figure 4 in this report, with respect to both the Hall Creek caldera and extensional faults. All three interpretations of this area are shown in figure 6.

Pre-Tertiary Bedrock

Pre-Tertiary bedrock in the Hall Creek caldera study area (fig. 4) includes Cambrian to Silurian siliciclastic and carbonate rocks of the lower Paleozoic continental shelf, structurally overlain along the Roberts Mountains thrust by coeval deep-water rocks of the Roberts Mountains allochthon. Stewart and McKee (1968, 1977) mapped the Paleozoic stratigraphy in the study area and assigned ages to the units based on paleontologic data. Although Smith (1992) mapped the distribution of units and fault contacts differently in the southwestern part of the study area, Smith largely adhered to the Stewart and McKee (1968) stratigraphic assignments for the lower Paleozoic rocks, which this study also follows.

Mount Callaghan (fig. 4) is underlain by a sequence of Lower Cambrian quartzite, siltstone, and limestone up to 450 meters (m) thick (the base is not exposed). Stewart and McKee (1968) subdivided this sequence into three units; figures 4 and 6*A* subdivide it into just the distinct basal quartzite (Ꞓ Zq) and an overlying siltstone and limestone unit (Ꞓ s). Early Cambrian rocks are overlain by a thick package of limestone, shale, and siltstone (unit Ꞓ ls, fig. 4). Stewart and McKee (1968) estimated this unit to be 1,800 m thick and assigned it a Middle Cambrian age (as shown in figure 4), while Smith (1992) estimated it to be about 2,400 m thick and correlated it with the Cambrian to Ordovician Broad Canyon Formation (fig. 6*B*). We did not measure a section through these rocks, but estimated the east-dipping section in Bernd Canyon to be 1,600–1,800 m thick based on our mapping, similar to the Stewart and McKee (1968) estimate.

Cambrian rocks in the vicinity of Bernd Canyon (unit Ꞓ ls, fig. 4) northwest of Mount Callaghan are overlain by a sequence of mostly carbonate rocks up to 700 m thick. Stewart and McKee (1968) assigned the bulk of this sequence to the Lower and Middle Ordovician Pogonip Group, with a thin layer of Silurian Roberts Mountains Formation near the top of the section. Smith (1992) largely followed this interpretation (fig. 6*B*). Figure 4 shows these units as a single package of undivided Silurian to Ordovician carbonates (unit SOc). On the south side of Boone Creek in the southwestern part of figure 4, lower Paleozoic carbonates are overlain along a north-dipping contact by highly-deformed chert, quartzite, and argillite of the Roberts Mountains allochthon, shown as a single unit (Pzrm) in figure 4. The nature of this contact is unclear, but as it is subparallel to bedding in the underlying limestone, we interpret it as the Roberts Mountains thrust itself. The high ridge in the northwestern part of the study area is underlain entirely by the Roberts Mountains allochthon, where it is intruded by an undated but probably Mesozoic granitic pluton (unit KJgr, fig. 4).

Pre-Caldera Andesite Lava Flows

The oldest Tertiary rocks in the study area are andesitic lava flows and breccias locally resting on Paleozoic basement beneath the tuff of Hall Creek (unit Tad, fig. 4). These rocks crop out most extensively in the central part of the study area (fig. 4), forming the floor of the Hall Creek caldera. They are also

Table 2. Single crystal laser-fusion sanidine $^{40}Ar/^{39}Ar$ ages.

Sample description	Sample	Age (Ma)[1]	±2σ	K/Ca	±2	n[2]	Instrument
Late rhyolite domes							
Tyr, rhyolite dome, Hall Creek caldera	H11-156	**25.20**	**0.04**	116.9	40.6	14/14	MAP215-50
Tyr, rhyolite dome, Hall Creek caldera	H11-158	**25.22**	**0.04**	117.9	89.3	12/14	MAP215-50
Hall Creek Caldera							
Caldera-related rhyolite domes							
6917T dome	H11-44	**33.51**	**0.06**	80.4	107.6	11/14	MAP215-50
Western rhyolite dome	H15-19	**33.806**	**0.027**	68.50	25.1	22/27	ARGUS VI
Intracaldera Tuff							
tuff of Hall Creek	H11-22	**33.90**	**0.07**	71.7	24.0	12/14	MAP215-50
tuff of Hall Creek	H08-30B	**33.92**	**0.07**	82.9	32.6	10	MAP215-50
tuff of Hall Creek	H11-167	**33.95**	**0.07**	69.5	28.6	14/14	MAP215-50
Ring-fracture rhyolite, pyroclastic feeder	H13-52	**33.95**	**0.02**	64.7	39.6	15/18	ARGUS VI
Pre-caldera rhyolite dome, 7369T	H11-43	**36.61**	**0.08**	144.7	70.9	13/14	MAP215-50
Dry Creek caldera							
Intracaldera-megabreccia tuff	H15-16	**34.79**	**0.03**	38.9	4.0	16/30	ARGUS VI
Italian Creek paleovalley							
tuff of Cove Spring	H12-177	**30.37**	**0.01**	29.0	6.5	12/13	ARGUS VI
tuff of Sutcliffe	H12-174	**30.57**	**0.01**	31.7	5.3	14/14	ARGUS VI
tuff of Rattlesnake Canyon	H12-170	**31.25**	**0.01**	39.7	4.6	13/14	ARGUS VI
tuff of Hardscrabble Canyon	H12-169	**31.46**	**0.01**	67.4	28.1	14/14	ARGUS VI
Caetano Tuff	H12-185	**33.93**	**0.01**	80.3	41.0	12/14	ARGUS VI
tuff of Hall Creek, outflow	H12-182	**33.92**	**0.02**	65.1	31.3	11/14	ARGUS VI
Corral Canyon							
Caetano Tuff	H11-26	**33.90**	**0.07**	101.3	21.2	13/14	MAP215-50
Bates Mountain							
tuff of Bottle Summit	H11-36	**31.44**	**0.04**	46.2	14.3	14/17	MAP215-50
tuff of Dry Creek	H11-35	**34.73**	**0.04**	39.3	4.5	17/24	MAP215-50
tuff of Dry Creek	H11-33	**34.66**	**0.07**	41.2	3.6	14/14	MAP215-50

[1]Mega-annum; weighted mean.

[2]Number of single grains used in age calculation/total number of grains analyzed.

Table 3. $^{40}Ar/^{39}Ar$ step-heating ages.

Sample description	Sample	Material	Plateau age				Isochron age					Total gas age	
			Age (Ma)[1]	±2σ	%^{39}Ar[2]	Steps	Age (Ma)[1]	±2σ	$^{40}Ar/^{36}Ar$	±2σ	MSWD	Age (Ma)[1]	±2σ
Post-caldera lava, north caldera margin (Ta)	H14-111	biotite	**33.62**	**0.06**	84.1	4/16	33.83	0.05	276.9	3.9	23.4	33.61	0.03
Pre-caldera lava, west caldera floor (Tad)	JC13-16	plagioclase	**34.47**	**0.16**	42.9	5/10	34.47	0.20	295.5	0.8	0.5	32.68	0.09
Pre-caldera lava, east caldera floor (Tad)	H12-166	hornblende	**34.83**	**0.04**	97.0	9/10	34.83	0.03	295.8	1.7	2.93	34.87	0.05

[1] Mega-annum.

[2] %^{39}Ar = percentage of ^{39}Ar used to define plateau age.

All samples analyzed on the ARGUS VI instrument.

Ages cited in text are plateau ages.

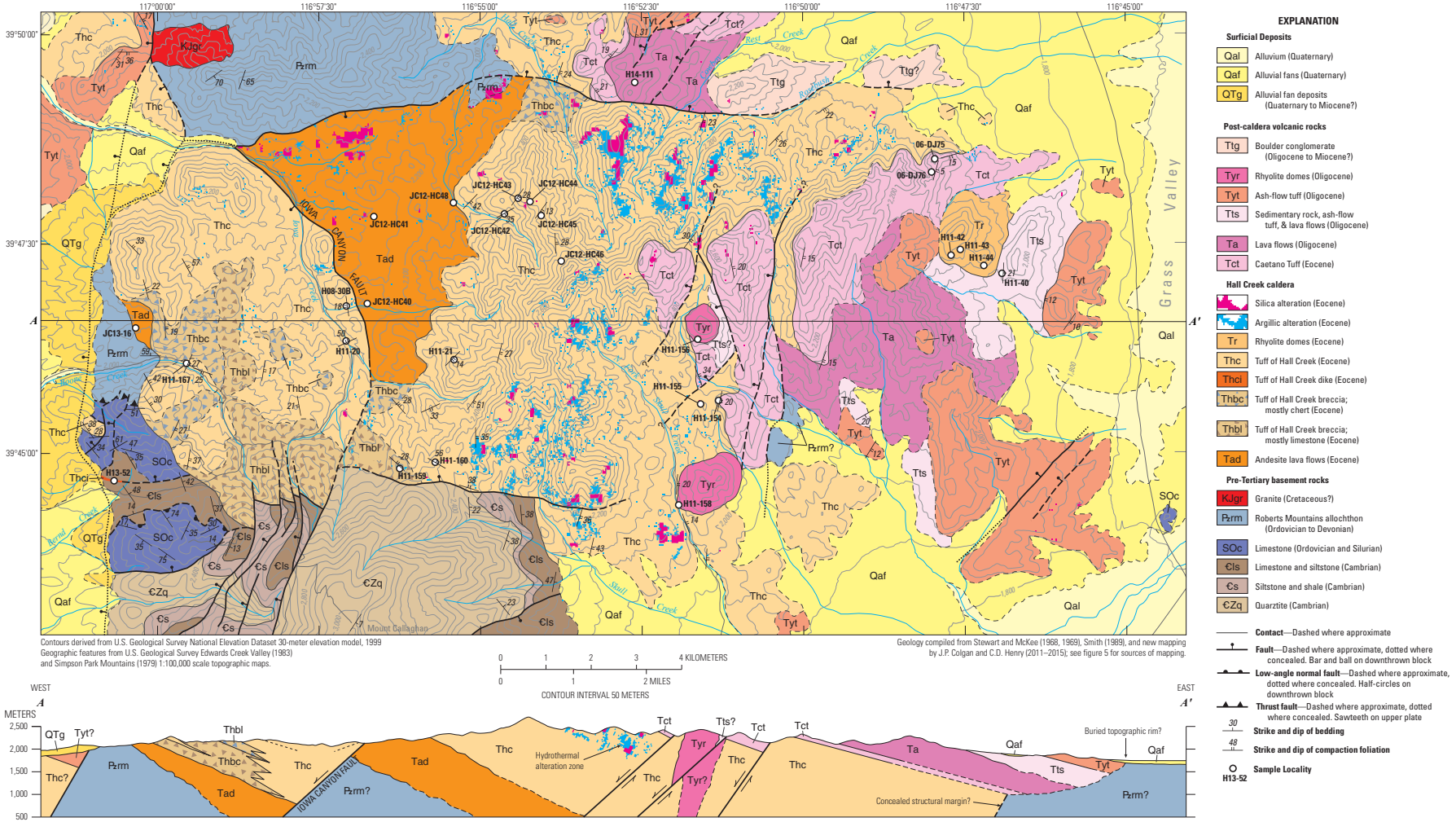

Figure 4. Hall Creek caldera, compiled from Stewart and McKee (1968, 1969), Smith (1989), and new mapping by the authors (see fig. 5 for index to sources of mapping). Click to view figure in full size.

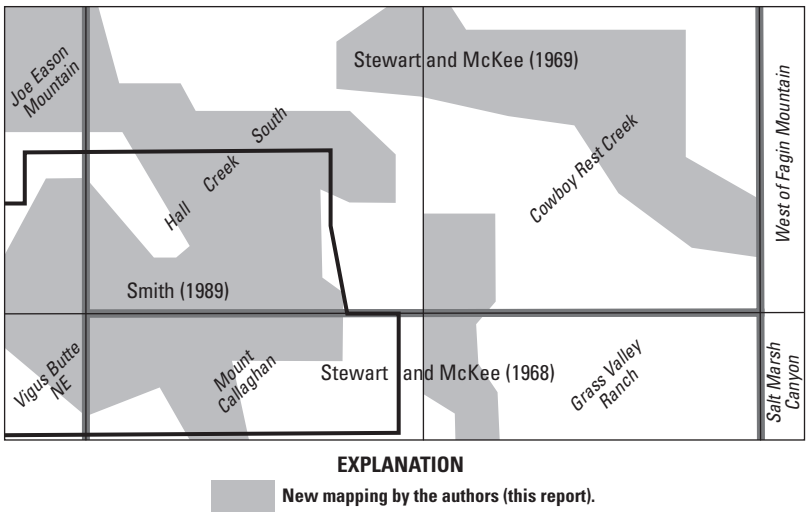

Figure 5. Sources of mapping in fig. 3, showing 1:24,000-scale quadrangle locations, boundaries of source maps, and area of new mapping for this study (gray shading).

exposed in a small area on the north side of Boone Creek, where they rest on siliceous rocks of Roberts Mountains allochthon. They crop out as massive to vesicular lava flows several meters thick, and as angular, matrix-supported breccias interpreted as dry block-and-ash-flow deposits (fig. 7). Flows are moderately porphyritic with phenocrysts of plagioclase and prominent hornblende (locally up to 1 centimeter[cm] long). Andesite flows are locally fresh with devitrified groundmass preserved, but more typically they are weakly propylitically altered and cut by small cm-scale veins filled with calcite and quartz.

The total thickness of the andesite flows is unknown but highly variable. They are absent south of Boone Creek, where the tuff of Hall Creek is deposited directly on Cambrian and Ordovician basement rocks. About 200–300 m are exposed on the north side of Boone Creek canyon. The thickness of the most extensive section east of the Iowa Canyon fault is problematic as there are no reliable bedding indicators in the unit. Simply assuming the andesite dips 25 to –30° east like the overlying tuff, up to 2,000 m may be exposed along the north margin of the caldera. This seems unreasonably large given that similar flows are 600 m thick in the nearby Simpson Park Mountains (Stewart and McKee, 1968; 1977), a large part of which is composed entirely of andesite flows (fig. 2). If the section beneath the tuff of Hall Creek dips less or is repeated by unmapped splays of the Iowa Canyon fault, the total thickness could be significantly less. Andesite flows are absent immediately north of the northern caldera margin, where tuff of Hall Creek rests directly on Paleozoic basement. The age of unit Tad is constrained by $^{40}Ar/^{39}Ar$ ages from two samples: sample JC13-16 from the Boone Creek area yielded a plagioclase step-heating age of 34.47 ± 0.16 Ma, and sample H12-166 from the main outcrop area in the central part of the study area yielded a hornblende step-heating age of 34.83 ± 0.40 Ma (table 3).

The andesite flows mostly filled topographic lows eroded into pre-Cenozoic rocks, similar to the way these lows were later filled by regional ash-flow tuffs (Henry and others, 2012; Henry and John, 2013), rather than building major stratovolcanoes above a flat pre-volcanic landscape of eroded bedrock. Topographic control on flow deposition is well shown south of Mount Callaghan and in the Simpson Park Range to the east (fig. 2), where andesite was deposited in large erosional lows in pre-Cenozoic rocks (McKee, 1968; Stewart and McKee, 1968, 1977). In these areas, and at Hall Creek, andesite flows are overlain by only slightly younger ash-flow tuffs along a mostly planar and (before later extensional tilting) subhorizontal contact. The greatest relief on this contact is about 150 m over a 1 km distance at Bates Mountain in the southern Simpson Park Range (Stewart and McKee, 1968). These characteristics require either that primary topography on top of the andesite flows was never significant or that any topography was subdued soon after deposition.

Figure 6 (following page). Three different interpretations of the southwest corner in figure 4 in the vicinity of Bernd and Boone Creeks. *A*, This study; note abundance of megabreccia in tuff of Hall Creek deposited on Paleozoic basement, tuff of Hall Creek dike (unit Thci), and lack of detachment faults cutting Tertiary rocks. *B*, Smith (1989, 1992); note numerous low-angle detachment faults cutting the tuff of Hall Creek, and lava flows (units Tad, Tr) intruding Paleozoic basement. *C*, Stewart and McKee (1977); note younger-on-older thrust faults in Paleozoic rocks, in-place Paleozoic bedrock where subsequent workers mapped breccia in the tuff of Hall Creek, and Quaternary alluvium where subsequent workers mapped in-place Paleozoic bedrock.

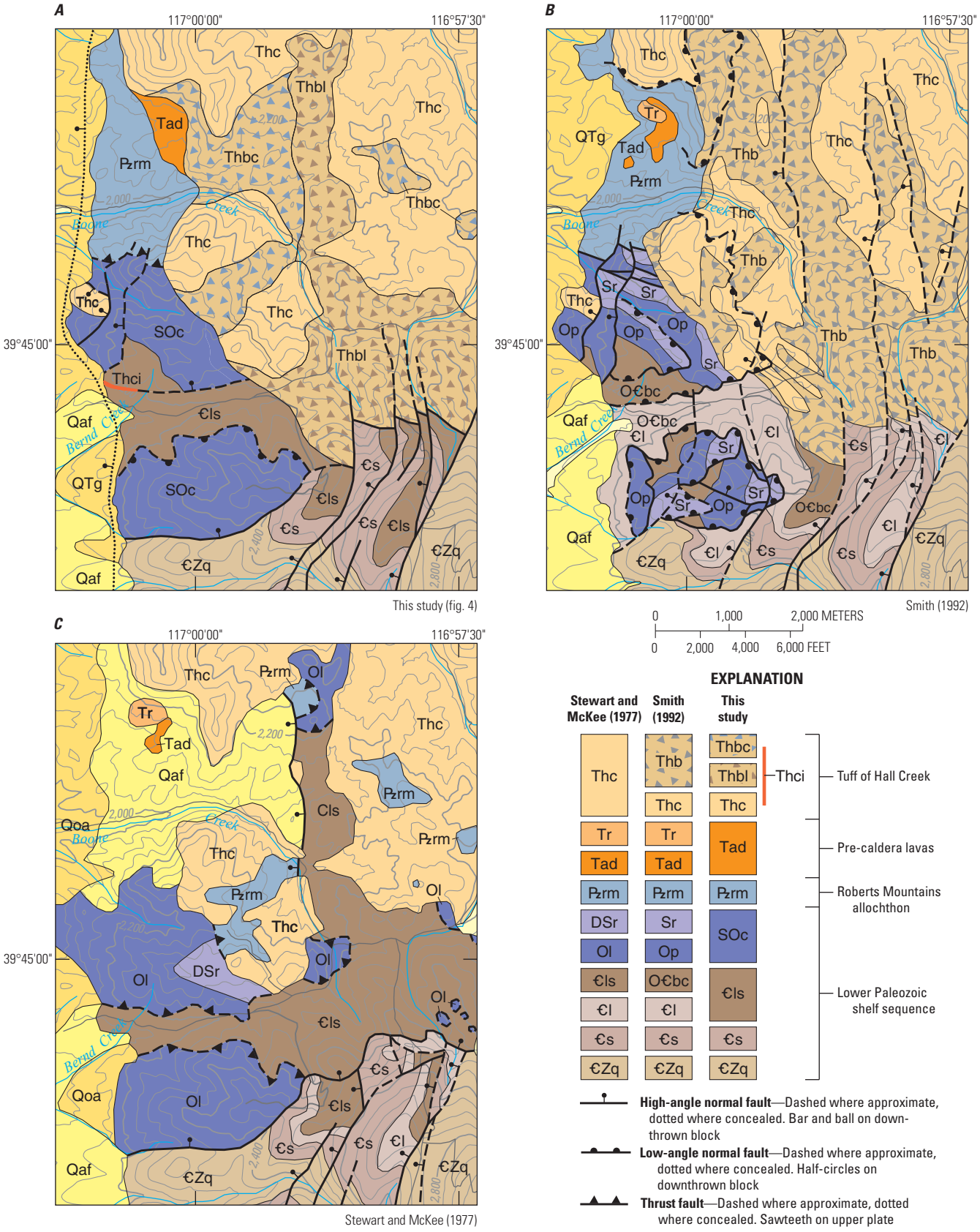
A
117°00'00"
116°57'30"
39°45'00"
Thc
Thbl
Tad
Pzrm
Thbc
Boone Creek
2,200
2,000
Thci
SOc
Qaf
Bernd Creek
€ls
QTg
€s
€Zq
2,400
2,800
This study (fig. 4)
B
Tr
Sr
Op
O€bc
€l
Thb
Smith (1992)
0 1,000 2,000 METERS
0 2,000 4,000 6,000 FEET
C
Ol
DSr
Qoa
Stewart and McKee (1977)
EXPLANATION
Stewart and McKee (1977)
Smith (1992)
This study
Tuff of Hall Creek
Pre-caldera lavas
Roberts Mountains allochthon
Lower Paleozoic shelf sequence
High-angle normal fault—Dashed where approximate, dotted where concealed. Bar and ball on downthrown block
Low-angle normal fault—Dashed where approximate, dotted where concealed. Half-circles on downthrown block
Thrust fault—Dashed where approximate, dotted where concealed. Sawteeth on upper plate

Figure 7. Porphyritic andesite breccia making up floor of Hall Creek caldera (unit Tad, fig. 4). Note radial jointing in block, which indicates it cooled after deposition. Hammer is 40 centimeters.

Hall Creek Caldera

Tuff of Hall Creek and Caldera Geometry

The tuff of Hall Creek (unit Thc) is a tan-weathering, pale gray, moderately crystal-rich (10–15 volume percent), high-silica rhyolite ash-flow tuff with phenocrysts of sanidine, plagioclase, minor quartz, and trace biotite and hornblende (fig. 8). In the area of figure 4, the tuff is densely welded, contains abundant collapsed pumice (fiamme), and is very lithic rich; most lithics consist of small Paleozoic bedrock chips, with sparser lava clasts (probably from the pre-caldera andesite sequence) and rare granitic rock fragments. In the study area, the tuff of Hall Creek ranges from fresh and glassy (vitrophyre is abundant) to devitrified and hydrothermally altered. Where hydrothermally altered, plagioclase and more rarely sanidine are replaced by a fine white clay mineral (probably kaolinite), and the groundmass is silicified in more intensely altered areas (fig. 9). We did not map the full distribution of hydrothermal alteration in the field, but hydrothermal minerals interpreted from Advanced Spaceborne Thermal Emission and Reflection Radiometer (ASTER) data (Mars, 2013) overlaid on the geologic map (fig. 4) clearly show that zones of argillic alteration (blue) and silicification (pink) are concentrated in the upper part of the intracaldera tuff and are perhaps more intense closer to the caldera margins. Three $^{40}Ar/^{39}Ar$ ages constrain the age of the intracaldera tuff of Hall Creek. Sample H11-22, from near the base of the intracaldera tuff in the central part of the caldera, yielded a sanidine laser fusion age of 33.90 ± 0.07 Ma. Sample H08-30B, from intracaldera tuff in the upper hanging wall of the Iowa Canyon fault in Iowa Canyon, yielded a sanidine laser fusion age of 33.92 ± 0.07 Ma. Sample H11-167, from near the base of the intracaldera tuff in Boone Creek, yielded a sanidine laser fusion age of 33.95 ± 0.07 Ma (table 2).

Overall, new geologic mapping confirms that the tuff of Hall Creek in the study area is filling its source caldera, herein named the Hall Creek caldera. Key evidence for a caldera includes the great thickness (about 2,600 m) of intracaldera tuff, well-exposed caldera floor and walls, extensive deposits of meso- and megabreccia composed of Paleozoic caldera wallrock, and the overall lithic-rich character of the tuff. In map view, collapse calderas typically have an inner "structural" margin—the fault that accommodated caldera collapse—and an outer "topographic" margin or rim, formed by catastrophic erosion of the caldera during collapse (for example, Lipman, 1984, 1997). In the following sections, the caldera wall or margin refers to the structural margin of the

Figure 8. Lithic and pumice rich intracaldera tuff of Hall Creek (unit Thc, fig. 4). Note large black glassy collapsed pumice (fiamme). Hammer is 40 centimeters.

Figure 9. View east of hydrothermally altered intracaldera tuff of Hall Creek along southern caldera margin. Alteration is weakly to moderately argillic, with plagioclase and locally sanidine replaced by clay minerals (probably kaolinite) and tuff matrix silicified and bleached white. Corresponds to areas of argillic and silicic alteration shown by ASTER imagery in the headwaters of Skull Creek (fig. 4).

Hall Creek caldera, which is easy to locate in the field. The topographic rim is concealed by younger rocks or modified by faults, and evidence for its presence is less clear. Its possible location and relation to pre-caldera topography is considered further in the "Discussion" section of this report.

The south wall of the caldera is well exposed along the north flank of Mount Callaghan on the east (footwall) side of the Iowa Canyon fault. Here, intracaldera tuff dips ~35° east and is more than 3 km thick (the base is not exposed). Much of the margin is developed against Cambrian quartzite (unit €Zq), the oldest exposed bedrock in the Toiyabe Range. Immediately to the south of the caldera margin fault in the Skull Creek drainage, the tuff of Hall Creek is deposited on Cambrian siltstone and limestone (unit €ls, fig. 4) and is about 1,000 m thick, indicating that a large volume of tuff ponded outside the caldera structural margin during the eruption. West of the Iowa Canyon fault, the southern caldera margin is stepped downward by a series of down-to-the-west faults (fig. 4). Intracaldera "tuff" along the margin here consists of extensive meso- and megabreccia deposits, primarily limestone chips and blocks (fig. 10), with rare chert blocks and sparse float and outcrops of lithic-rich tuff. Stewart and McKee (1968, 1977) mapped most of this megabreccia as in-place Cambrian and Ordovician bedrock in the hanging wall of a down-to-the-north normal fault (fig. 6*C*), whereas Smith (1992) subsequently recognized it as fundamentally part of the intracaldera tuff (fig. 6*B*). Smith (1992) mapped the Ordovician and Silurian section south of Bernd Canyon as entirely in low-angle fault contact with underlying Cambrian rocks (fig. 6*B*), which it is along the northern margin of this exposure on the south side of Bernd Canyon. However, we examined this area in detail as part of this study and concur with Stewart and McKee (1968) that the southern margin is a high-angle, down to the north normal fault (fig. 6*C*) that strikes west down the drainage south of Bernd Canyon. We interpret this fault as the down-plunge continuation of the caldera margin fault, structurally beneath the caldera floor (fig. 6*A*).

The caldera floor is well exposed in both the hanging wall and footwall of the Iowa Canyon fault. The base of the tuff of Hall Creek on the caldera floor is exposed for roughly 7 km along strike on the west side of the caldera. Here, the tuff rests on progressively younger rocks to the north, from Cambrian shale, to Ordovician limestone, to the Roberts Mountains allochthon, to Eocene andesite lava flows. Extensive deposits of meso- and megabreccia are interbedded with the tuff in this area, ranging from very lithic-rich tuff, to meter-scale chert and limestone boulders, to individual chert blocks over 100 m across (fig. 11). One chert block is so large it was the site of a small barite mine. As is the case near the caldera margin, Stewart and McKee (1977) mapped much of the megabreccia as in-place bedrock (fig. 6*C*), while Smith (1992) recognized most of it as belonging to the caldera. Our mapping of the caldera floor and megabreccia in this area (fig. 6*A*) is similar to Smith (fig. 6*B*), although we also were able to roughly classify the breccia based on source lithology—mostly carbonate (unit Thbl) and chert and quartzite (unit Thbc)—using rock types shown on the Stewart and McKee (1977) map together with our field observations. Unit Thbl is composed mostly of limestone from the lower Paleozoic rocks that make up the southern caldera wall and also includes quartzite, phyllite, dolomite, and rare granitic clasts. Unit Thbc predominantly contains chert blocks from rocks of the Roberts Mountains allochthon. Blocks of porphyritic andesite are present in unit Thbc along the northern caldera margin in Hall Creek. With respect to the caldera floor, the main difference between the mapping for this study and that of Smith (1992) is that we interpret tuff of Hall Creek megabreccia to be deposited directly on older andesite flows west of the Iowa Canyon fault (fig. 6*A*), rather than those flows intruding the bedrock (fig. 6*B*). The caldera floor is also exposed for about 8 km along strike in the footwall of the Iowa Canyon fault, where the tuff of Hall Creek is deposited on andesite flows (fig. 4). The contact between tuff and andesite is fairly planar and dips ~25° east, subparallel to the average compaction foliation in the overlying tuff. This contact turns sharply west and is truncated by the Iowa Canyon fault ~2 km north of the southern caldera margin.

Figure 10. Texture in limestone megabreccia block along southern caldera margin. Hammer is 40 centimeters.

Figure 11. Pale gray lithic-rich tuff of Hall Creek injected into dark chert breccia block, close to caldera floor in Boone Creek drainage, near sample locality H11-167. Hammer is 40 centimeters.

Intracaldera tuff in the central and northern part of the caldera is about 2,600 m thick and is repeated by several small-offset normal faults that can be mapped where they offset the overlying Caetano Tuff (fig. 4), but not where they juxtapose hydrothermally altered tuff of Hall Creek with itself. The north wall of the caldera is exposed for an east-west distance of approximately 15 km, from the mouth of Iowa Canyon in the west to the lower reaches of Rosebush Creek in the northeastern corner of the study area (fig. 4). The western part of the caldera margin here places pre-caldera andesite (unit Tad) down to the south against a high ridge of Paleozoic Roberts Mountains allochthon bedrock (fig. 4). Along Rosebush Creek to the east, the caldera margin places post-caldera rocks down to the north against intracaldera tuff of Hall Creek to the south—the opposite sense of slip. Immediately north of the caldera margin here, along Hall Creek, the east-dipping tuff of Hall Creek is about 400 m thick. It is deposited directly on the Roberts Mountains allochthon, and is overlain by Caetano Tuff that crops out east of Hall Creek at 2,200 m elevation (fig. 4). South of the caldera margin, the Thc-Tcc contact crops out at elevations of 2,600–2,800 m (fig. 4), indicating at least 400 m down-to-the-north vertical displacement following deposition of the Caetano Tuff. Although the most recent motion on the eastern part of this fault is down to the north, the tuff of Hall Creek thickens from about 400 to 2,500 m south across the fault, requiring that the fault originally moved as a down-to-the south caldera margin fault active during deposition of the tuff of Hall Creek. The fault was later reactivated with the opposite sense of slip sometime after deposition of the post-caldera lava and tuff sequence.

The eastern caldera margin is not exposed and is no farther east than the lone outcrop of unit SOc in the southeast corner of figure 4, which is roughly 700 m long and has coherent bedding with no signs of the intense fracturing typical of megabreccia. The eastern structural margin is probably no further west than the rhyolite dome (Tr) interpreted as a post-caldera ring-fracture intrusion (described in the "Rhyolite Dome" section). Post-caldera units in this area—Tct, Ta, Tts, and Tyt (fig. 4; described in the "Post-caldera sedimentary rocks, tuffs, and lava flows" section)—are interpreted to be within the caldera. Whether they are within the structurally defined caldera or between the structural and topographic margins of the caldera (Lipman, 1997) is unclear, although the latter interpretation seems more likely (shown in the cross section in figure 4). Based on the thickness and dimensions of the caldera described here (fig. 4), corrected for post-caldera extension (see Discussion section of this report), erupted volume of the tuff of Hall Creek was about 400 km^3, not including an unknown amount of outflow dispersed beyond the study area.

Tuff Dike

A tan, friable rhyolite dike cuts Paleozoic bedrock beneath the caldera floor in the southwest part of the map area (unit Thci, figs. 4, 6*A*). The dike is traceable as float and rare outcrop for about 0.5 km along a slightly north of west trend. Strong flow bands and faint, wispy collapsed pumice in outcrop strike 120° and are near vertical. The dike may have intruded along a high-angle, down to the north normal fault. Sparse phenocrysts of sanidine, slightly smoky quartz, plagioclase, and minor biotite are similar to those of the tuff of Hall Creek. A sanidine $^{40}Ar/^{39}Ar$ date of 33.95 ± 0.02 Ma (sample H13-52) is within uncertainty of that of the tuff of Hall Creek, and the presence of pumice suggests a pyroclastic feeder dike.

Rhyolite Dome

A roughly 1.5 x 2 km rhyolite dome intrudes Caetano Tuff close to the northern margin of the caldera, and is partly overlain by post-caldera sedimentary rocks and ash-flow tuff (unit Tr, fig. 4). Lava on the flanks of this dome is strongly flow-banded and distinctly biotite-rich with phenocrysts of sanidine and plagioclase. A sample of this rhyolite dome (H11-44) yielded a sanidine laser fusion $^{40}Ar/^{39}Ar$ age of 33.51 ± 0.06 Ma, indicating that it was emplaced shortly after formation of the Hall Creek caldera. However, a second sample from only ~600 m to the west yielded a sanidine laser fusion $^{40}Ar/^{39}Ar$ age of 36.61 ± 0.08 Ma, substantially older than the caldera. These rocks are indistinguishable in the field and thin section, so it is difficult to know how much of the body mapped as unit Tr in figure 4 is pre- or post-caldera. If the caldera structural margin is indeed in the vicinity of the rhyolite dome, the older age may indicate a small outcrop of pre-caldera lava preserved along the otherwise-concealed caldera rim.

Post-Caldera Sedimentary Rocks, Tuffs, and Lava Flows

Caetano Tuff

The Caetano Tuff (unit Tct, fig. 4) directly overlies the tuff of Hall Creek everywhere both tuffs are exposed. Within the Hall Creek caldera the Caetano Tuff is about 100–200 m thick. The Caetano Tuff is a crystal-rich (40 volume percent) high-silica rhyolite with phenocrysts of smoky quartz, plagioclase, sanidine, minor biotite, and trace hornblende (John and others, 2008)—the high phenocryst content and abundant smoky quartz distinguish it from the underlying tuff of Hall Creek. The tuff was erupted from the Caetano caldera in the northern Toiyabe and southern Shoshone Ranges, about 30 km north of the Hall Creek caldera (fig. 2). The Caetano Tuff has an $^{40}Ar/^{39}Ar$ sanidine age of 34.00 ± 0.5 Ma (mean of 14 samples; Henry and John, 2013) that is indistinguishable within uncertainty from the age of the tuff of Hall Creek, indicating it was erupted less than 100 k.y. after formation of the Hall Creek caldera.

Lava Flows

In the eastern and northern parts of the Hall Creek caldera, the Caetano Tuff and tuff of Hall Creek are overlain by lava flows (unit Ta, fig. 4), and tuffaceous sedimentary rocks interbedded with small-volume lava flows and ash-flow tuffs (composite unit Tts, fig. 4). On the northern caldera margin, just outside the caldera, lavas consist of plagioclase-biotite dacite flows about 250 m thick and repeated by several northeast-striking faults. Biotite from a sample of these flows yielded an $^{40}Ar/^{39}Ar$ plateau age of 33.63 ± 0.06 Ma (sample H14-111), indicating eruption a few hundred k.y. after formation of the Hall Creek caldera. On the east side of the caldera, these flows consist of dark, reddish-weathering, fine-grained rocks with sparse plagioclase phenocrysts and trace pyroxene. Based on the Stewart and McKee (1977) mapping, these flows are up to 800 m thick along A–A' but pinch out only a few km to the north and south (fig. 4). This highly discontinuous outcrop pattern is probably due to the flows constructing a local edifice that was later surrounded and buried by younger sediments and tuffs.

Tuffaceous Sedimentary Rocks with Interbedded Tuffs and Lava Flows

On the east side of the Hall Creek caldera, Caetano Tuff and post-caldera lava flows are overlain by up to 500 m of variably reworked pale, poorly-welded, crystal-poor tuff, ledges of more densely welded pumice and crystal-rich tuff with abundant biotite and plagioclase and rare sanidine, reddish-weathering pebble conglomerate and sandstone with clasts of Paleozoic basement and andesite-dacite lava (probably unit Ta), and rare fine-grained crystal-poor lava flows (composite unit Tts, fig. 4). At one locality, a fine-grained lava flow (sample H11-40) and underlying conglomerate and sandstone are deposited in a well-preserved channel cut into poorly-welded tuff and tuffaceous sedimentary rocks (fig. 12). The discontinuous map pattern and variable thickness of this unit suggest deposition onto paleotopography with substantial relief created by both caldera formation and eruption of the older andesite lava flows. Rocks within the Tts unit are

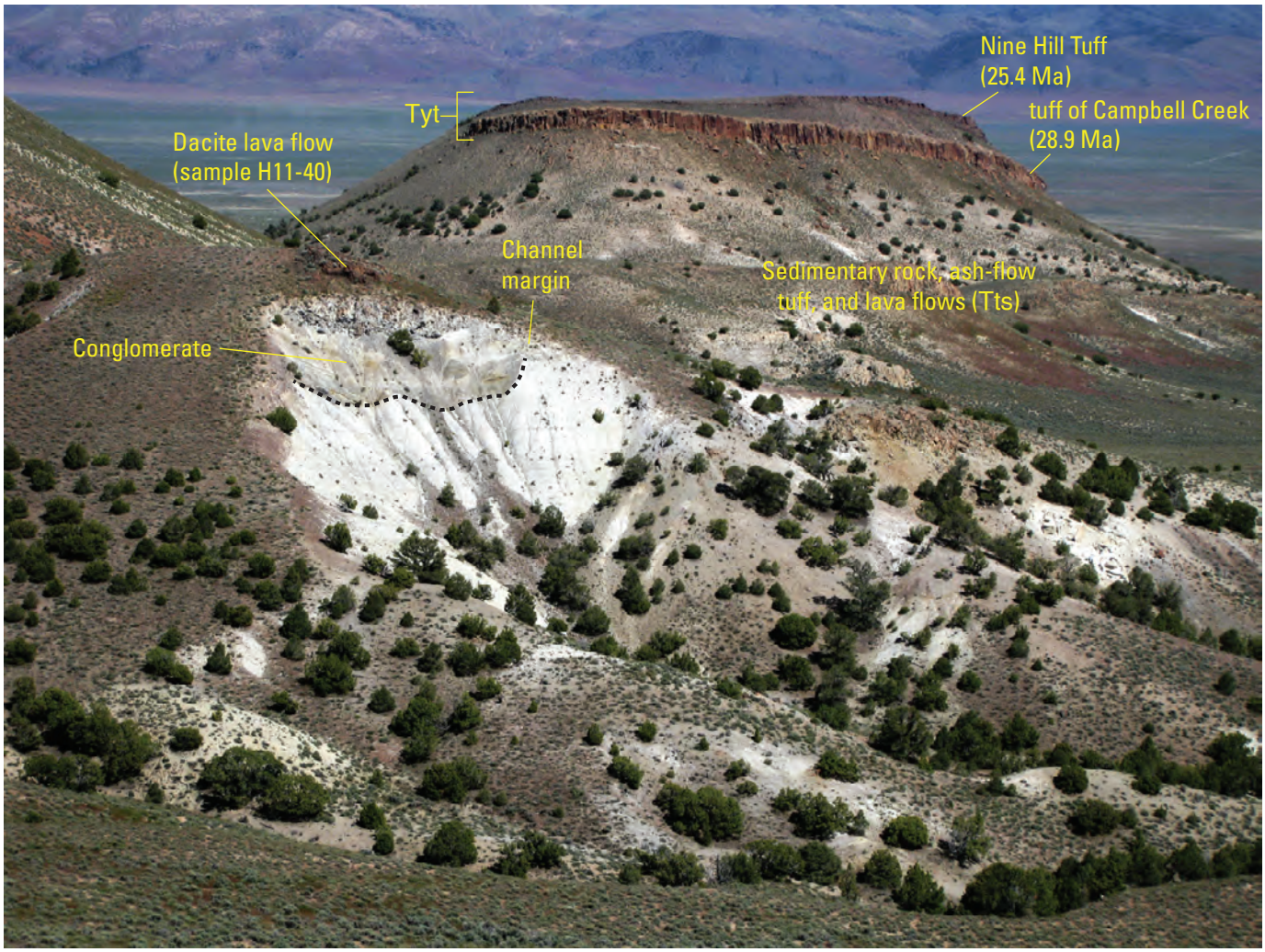

Figure 12. View east of post-caldera sedimentary rocks, lava flows, and tuffs (units Tts and Tyt, fig. 4) in the upper part of the caldera fill sequence on the west side of Grass Valley. Section dips 10–20° east away from viewer. Brecciated dacite lava flow on small knob in left center of photo is sample locality H11-40 (Ma, mega-annum).

undated but must be older than the 29 Ma tuff of Campbell Creek, which locally makes up the lower part of the Tyt map unit (see next section), constraining them to the latest Eocene or early Oligocene (34–29 Ma).

Distal Oligocene Ash-Flow Tuffs

The youngest ash-flow tuffs in the study area (unit Tyt, fig. 4) include several far-traveled Oligocene ignimbrites erupted elsewhere in the Basin and Range Province. On the east side of the Hall Creek caldera, this unit includes both the tuff of Campbell Creek and the Nine Hill Tuff (fig. 12). The tuff of Campbell Creek is an orange, nubbly-weathering, densely welded, sparsely porphyritic tuff with phenocrysts of plagioclase, sanidine, distinctive vermicular quartz, and minor biotite. It erupted ca. 28.9 Ma from a caldera in the Desatoya Mountains (fig. 1) ~75 km to the southwest of the study area and is one of the most widely distributed tuffs in the Great Basin (Henry and others, 2012). The Nine Hill Tuff is a distinctive orange to gray weathering, very densely welded, sparsely porphyritic tuff with phenocrysts of sanidine, lesser plagioclase and anorthoclase, and traces of quartz and biotite. It was erupted ca. 25.4 Ma and is also widely distributed, but its source caldera has not been found (Deino, 1989; Henry and John, 2013). These tuffs are variably deposited on older lava flows (unit Ta), tuffaceous sedimentary rocks (unit Tts), Caetano Tuff, and the tuff of Hall Creek, in a pattern indicating eruption onto paleotopography with substantial relief. In one preserved channel remnant on the north edge of the caldera, 25° east-dipping tuff of Campbell Creek thickens by nearly a factor of 10 across a single ridge top (fig. 13). In the northwestern corner of the map area, distal Oligocene tuffs are deposited directly on the tuff of Hall Creek, and include the 30.3 Ma tuff of Cove Spring (also present to the south of the caldera at Italian Creek, see Oligocene Rhyolite Domes section of this report) and the tuff of Campbell Creek, which is highly altered here and was originally mapped by Stewart and McKee (1977) as rhyolite lava.

Figure 13. View north of 28.9 Ma tuff of Campbell Creek deposited on post-caldera lava flows ~1 kilometer north of northern margin of Hall Creek caldera. Regional tilt is 25–30° east; note dramatic westward thickening of tuff over short distance across hillside, attributed to deposition on paleotopography developed on post-caldera lava flows.

Oligocene Rhyolite Domes

Two rhyolite domes each about 1 km across crop out in the east-central part of the map area (unit Tyr, fig. 4). They consist of strongly flow-banded, commonly glassy, sparsely porphyritic rhyolite lava with small phenocrysts of sanidine. A hand sample from the northern dome contained small (less than 1 cm) xenoliths of granitic rock. We initially mapped these domes as post-caldera rhyolite domes similar to the 33.5 Ma dome (map unit Tr) in the northeastern part of the map area. However, both proved to be late Oligocene—sample H11-156 from the northern dome yielded an $^{40}Ar/^{39}Ar$ sanidine age of 25.20 ± 0.04 Ma, and sample H11-158 from the southern dome yielded an $^{40}Ar/^{39}Ar$ sanidine age of 25.22 ± 0.04 Ma (table 2).

Boulder Conglomerate

Along the northern caldera margin at Rosebush Creek (figs. 3 and 4), lava flows (Ta) are overlain by a sedimentary deposit consisting of poorly exposed soft matrix with boulders up to 2 m across weathering out onto the ground surface (unit Ttg). Boulders include the tuff of Hall Creek, Caetano Tuff, andesite lava, and flow-banded rhyolite lava similar to unit Tr. This deposit strongly resembles deposits mapped as Miocene alluvial fans (unit QTg), but the lack of Oligocene tuff boulders—notably the tuff of Campbell Creek and Nine Hill Tuff—raises the possibility that it predates those tuffs, and is therefore assigned to a separate unit.

Tuff of Dry Creek West of Hall Creek Caldera

Smith (1989) mapped the area west of figure 4, north of Bernd Creek, as “tuff of China Spring” deposited on andesite flows and older sedimentary rocks. Smith correlated the tuff of China Spring with the Caetano Tuff, which would mean the underlying andesite flows predated the Hall Creek caldera, the tuff of Hall Creek was not present, and therefore the area was outside of the Hall Creek caldera. The best exposures of the stratigraphic section in this area are along lower Bernd Creek, which we re-examined in the course of this study. Figure 14 shows our reinterpretation of the Smith (1989) map in this area, based on new field observations, $^{40}Ar/^{39}Ar$ dates, and geochemical analyses. Field observations demonstrate that the Smith (1989) “tuff of China Spring” is actually the 28.9 Ma tuff of Campbell Creek, locally overlain by the 25.4 Ma Nine Hill Tuff (shown separately in figure 14 where directly observed in the field; elsewhere lumped in a single

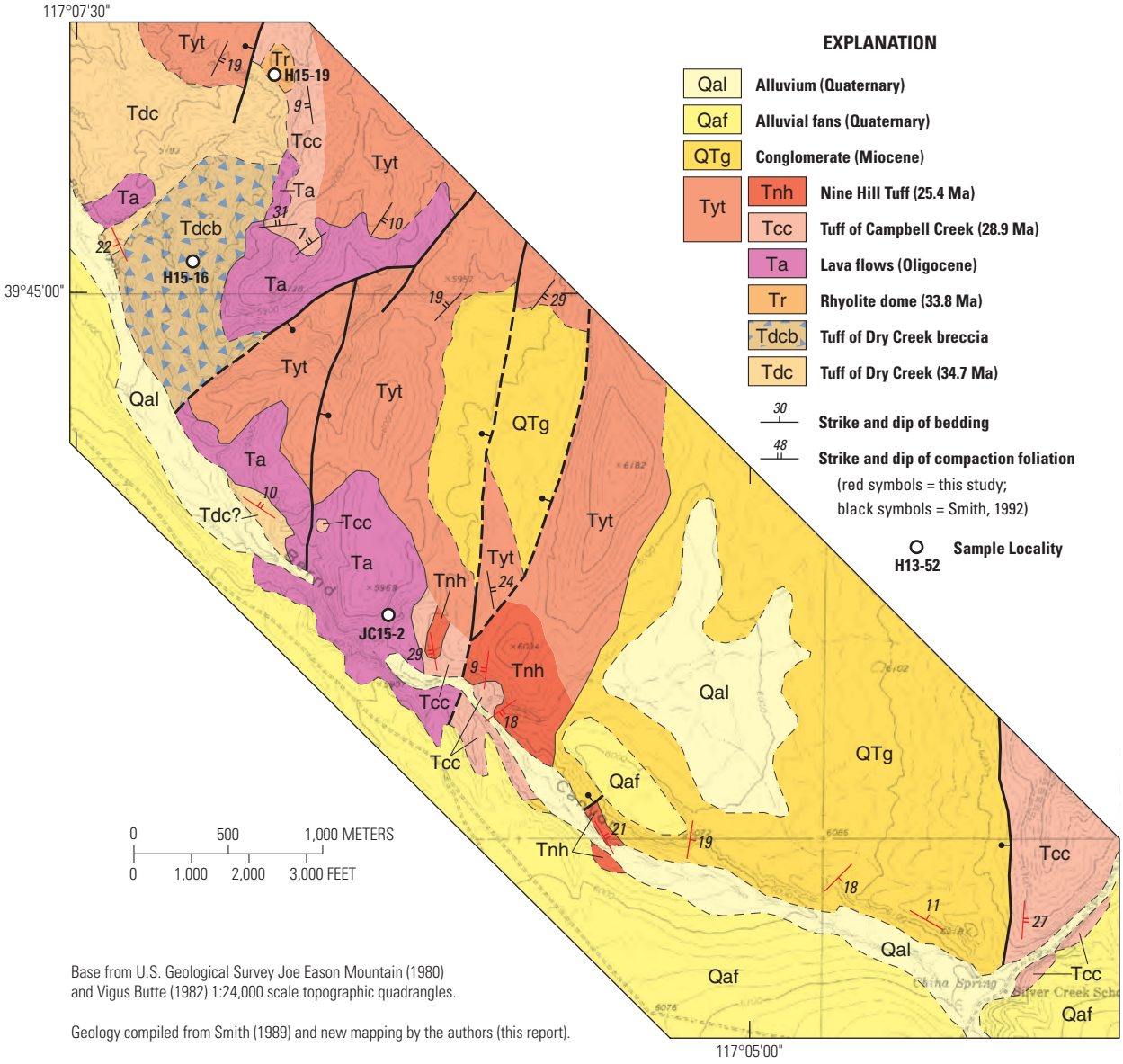

Figure 14. Bernd Creek area west of the Hall Creek caldera, modified from Smith (1989). Unit Tyt was mapped by Smith (1989) as the "tuff of China Spring" (34.0 Ma Caetano Tuff) overlying older lava flows and sedimentary rocks. It actually consists of the 28.9 Ma tuff of Campbell Creek (Tcc) and 25.4 Ma Nine Hill Tuff (Tnh), overlying lava flows correlative with post-caldera flows in the Hall Creek caldera (Ta; fig. 4), in turn overlying the 34.7 Ma tuff of Dry Creek (Tdc). Neither the Caetano Tuff nor the tuff of Hall Creek are present (Ma, mega-annum).

unit). Underlying andesite flows (unit Ta, fig. 14) are orange-weathering, platy, dark gray, crystal poor lava flows similar to the post-caldera andesites (unit Ta, fig. 4) that underlie the tuff of Campbell Creek within the mapped Hall Creek caldera (fig. 4). They are distinctly different from the porphyritic, hornblende-bearing pre-caldera andesites (unit Tad, fig. 4) that underlie the tuff of Hall Creek within its source caldera.

North of Bernd Creek on the west side of figure 14, Oligocene tuffs and lava flows overlie an ash-flow tuff that was clearly deposited inside a caldera. It includes outcrops of white, poorly-welded, well-bedded (probably reworked) deposits of ash and pumice, as well as about 1 km^2 of coarse megabreccia (Tdcb, fig. 14) composed of angular, brecciated blocks up to 3 m across in a matrix of poorly exposed lithic-rich, mostly densely-welded tuff (fig. 15). Breccia blocks consist primarily of chert, with lesser quartzite and carbonate probably sourced from lower Paleozoic bedrock, as well as less abundant boulders of hornblende-rich andesite similar to the pre-caldera lava flows (unit Tad, fig. 4) within the Hall Creek caldera. The tuff matrix of the breccia is indistinguishable in outcrop and hand sample from the tuff of Hall Creek and we initially interpreted it as such. However, it yielded an $^{40}Ar/^{39}Ar$ sanidine age of 34.79 ± 0.03 Ma with a

Figure 15. Strongly brecciated dark reddish chert blocks in matrix of pale lithic-rich tuff of Dry Creek, along Bernd Creek drainage. Sample locality H15-16 is between the two chert blocks in left-center of photograph. Hammer is 40 centimeters.

K/Ca of 38.9 ± 4.0 (sample H15-16, table 2), indistinguishable from the tuff of Dry Creek exposed at Bates Mountain 35 km to the southeast. Accordingly, we interpret the tuff outcrops along Bernd Creek to be within the source caldera for the tuff of Dry Creek. A possible outline of the caldera is shown in figure 2, although the full extent is unknown; most of it would be buried beneath younger volcanic rocks and alluvium. For the purpose of the present study, the stratigraphic section along Bernd Creek demonstrates that the tuff of Hall Creek is not present, and therefore the Hall Creek caldera does not extend west of figure 4.

Distribution of Outflow Tuff from Hall Creek and Other Calderas

Dry Canyon and Caetano Caldera

Between Corral Canyon and Dry Canyon to the north of the Hall Creek caldera (fig. 2), Caetano Tuff was deposited directly on older volcanic rocks and Paleozoic basement; tuff of Hall Creek is not present. At Dry Canyon 15 km north of the Hall Creek caldera (fig. 2), outflow Caetano Tuff with an $^{40}Ar/^{39}Ar$ age of 33.90 ± 0.07 Ma (sample H11-26) overlies a gray-weathering, pumice and lithic-rich, moderately crystal-rich tuff with phenocrysts of sanidine, plagioclase, quartz, and trace biotite. Based on its age (older than the Caetano Tuff) and phenocryst assemblage, this tuff is either the tuff of Hall Creek or the tuff of Dry Creek (fig. 16). A similar tuff (sample 06-DJ11) underlies Caetano Tuff just south of the Caetano caldera near Wood Spring (fig. 2), indicating that one or both of the tuffs of Hall Creek and Dry Creek flowed as far north as the southern margin of the Caetano caldera; neither has been found farther to the north (John and others, 2008; Colgan and others, 2011).

Italian Creek Paleovalley

About 13 km south of the Hall Creek caldera along Italian Creek on the west side of the Toiyabe Range (fig. 2), a 2–3 km wide swath of Tertiary volcanic rocks crops out for a northwest–southeast distance of about 8 km. They are deposited on lower Paleozoic rocks of the Roberts Mountains allochthon and were mapped by Stewart and McKee (1977) as Bates Mountain Tuff with subordinate andesite lava flows. We measured two sections in this outcrop belt about 2 km apart (fig. 17), to determine if outflow tuff of Hall Creek was present, and if so, establish its stratigraphic setting.

The lowest exposed tuff in the western section is densely welded and pumice-rich with sparse phenocrysts of sanidine, smoky quartz, plagioclase, and biotite. The base is obscured by brush along Italian Creek, but it is at least 100 m thick. A sample of this tuff (H12-169) yielded a sanidine laser fusion $^{40}Ar/^{39}Ar$ age of 31.46 ± 0.01 Ma. On the basis of its age and composition, this tuff correlates with the tuff of Hardscrabble Canyon (Henry and John, 2013), which is overlain by ~10 m of poorly exposed conglomerate consisting of small andesite clasts weathering out on a soft slope.

The tuff of Hardscrabble Canyon is overlain by an orange, nubbly weathering, pumice-rich tuff with abundant large sanidine and plagioclase (both to ~6 millimeters), with sparse quartz and biotite and ranges from moderately to densely welded and forms three distinct ledges that may represent multiple cooling units. This tuff is between 140 and 230 m thick (the top is obscured by the younger tuff of Cove Spring). A sample of this tuff (H12-170) yielded a sanidine laser fusion $^{40}Ar/^{39}Ar$ age of 31.25 ± 0.01 Ma (table 2). On the basis of its age and composition, this tuff correlates with the tuff of Rattlesnake Canyon (unit A of the Bates Mountain Tuff of Gromme and others, 1972) (Henry and John, 2013). The tuff of Rattlesnake Canyon is overlain by an undated tuff that is anywhere from 100 to 200 m thick (the base is concealed by the younger tuff of Cove Spring).

The uppermost tuff in the section is about 50 m thick and includes an orange-weathering, distinctly biotite-rich, poorly welded lower part overlain by a densely welded upper part with abundant sanidine and trace biotite and that forms a prominent red ledge; the entire tuff is probably a single compositionally zoned ignimbrite. A sample of this tuff from the upper ledge (H12-174) yielded a sanidine laser fusion $^{40}Ar/^{39}Ar$ age of 30.57 ± 0.01 Ma (table 2). On the basis of its age, stratigraphic position, and variable phenocryst assemblage, this tuff correlates with the tuff of Sutcliffe (unit B of the Bates Mountain tuff).

The youngest tuff in the section is not at the top, but rather lower on the slope (fig. 17), welded against the upper part of the tuff of Rattlesnake Canyon and the lower part of the unknown tuff. This tuff has distinct platy weathering and is very sparsely porphyritic with trace sanidine and may be up to 100 m thick if it dips the same as the rest of the section. A sample of this tuff (H12-177) yielded a sanidine laser fusion $^{40}Ar/^{39}Ar$ age of 30.37 ± 0.01 Ma (table 2), which tentatively correlates it with the tuff of Cove Spring (Henry and John, 2013).

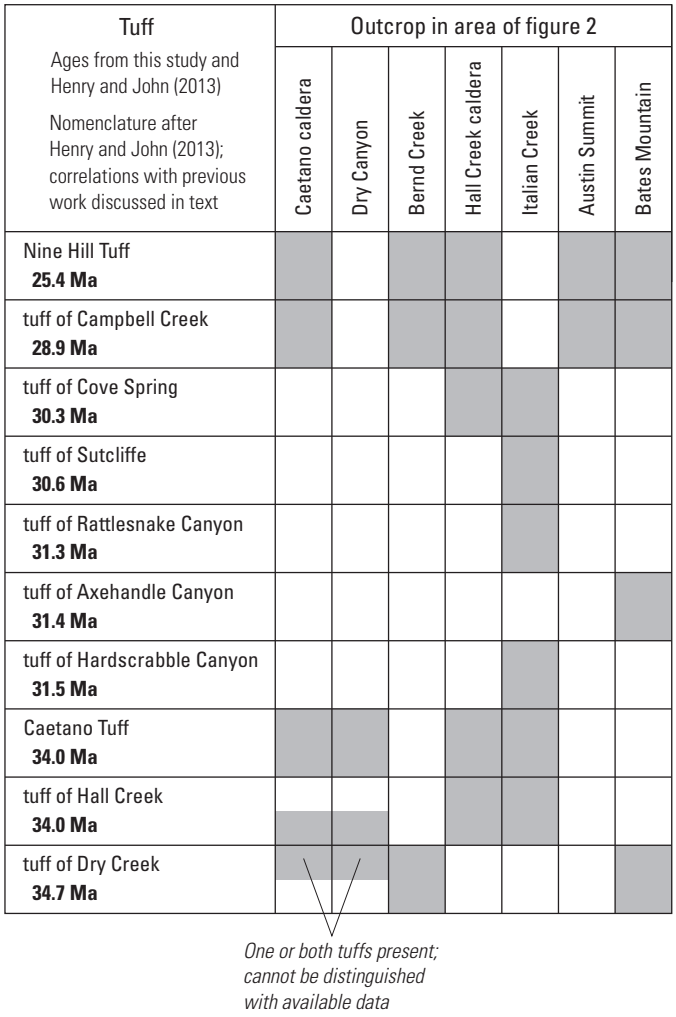

Figure 16. Ages, names, and distribution of ash-flow tuffs identified in the study area. Tuff names are those used by Henry and John (2013); alternative names and correlations are discussed in the text. Note that additional unidentified tuffs may be present at any of the localities shown here; this figure only shows those that were specifically identified and correlated as part of this study (Ma, mega-annum).

The lowest exposed tuff in the eastern section consists of ~100 m of moderately crystal-rich tuff with sanidine, plagioclase, vermicular quartz, and trace biotite and contains abundant collapsed pumice and small lithic fragments of Paleozoic sedimentary rocks and less common andesite lava This tuff is moderately to densely-welded with a basal vitrophyre 2 m thick where it rests directly on tightly folded lower Paleozoic argillite. A sample of this tuff (H12-182) yielded a sanidine laser fusion $^{40}Ar/^{39}Ar$ age of 33.92 ± 0.02 Ma (table 2). On the basis of its age, composition, and phenocrysts, this tuff correlates with the tuff of Hall Creek. It is overlain by about 20 m of poorly exposed conglomerate consisting of small (mostly less than 10 cm) andesite clasts with scattered large (up to 2 m) boulders of tuff of Hall Creek weathering onto the slope.

The tuff of Hall Creek is overlain by approximately 160 m of crystal-rich tuff with phenocrysts of plagioclase, sanidine, distinctly smoky quartz, and lesser biotite. This tuff is moderately pumice-rich, devitrified, and moderately to densely welded. A sample of this tuff (H12-185) yielded a sanidine laser fusion $^{40}Ar/^{39}Ar$ age of 33.93 ± 0.02 Ma (table 2). On the basis of its age, stratigraphic position, and presence of distinctive smoky quartz, this tuff correlates with the Caetano Tuff. It is overlain by a poorly exposed conglomerate interval 20 m thick with andesite clasts weathering onto a soft slope. Above the conglomerate is about 40 m of orange-weathering tuff with a poorly welded base overlain by a densely welded upper part that forms prominent, dark red ledges. The lower part is biotite-rich with a distinctive mix of dark and light pumice; the upper part contains abundant sanidine, plagioclase, and only trace quartz and biotite. This tuff correlates with the 30.6 Ma tuff of Sutcliffe, the same red ledge-forming tuff that caps the western section.

The outcrop pattern of ash-flow tuffs in the Italian Creek section indicates that they were deposited in a roughly 500-m deep paleovalley carved into the Paleozoic bedrock sometime prior to 34 Ma (fig. 17). The sequence of deposition is shown schematically in figure 18. The first tuffs to fill the paleovalley were the tuff of Hall Creek and Caetano Tuff at 34 Ma. They were subsequently partially eroded and the valley was refilled with the tuffs of Hardscrabble and Rattlesnake Canyons and the "unknown tuff." These tuffs and the older Caetano Tuff were then overlapped by the 30.6 Ma tuff of Sutcliffe, which in turn was partially eroded and the valley partly refilled by the tuff of Cove Spring (fig. 18). This cycle of continued partial erosion and redeposition of ash-flow tuffs is a common feature of middle Tertiary paleovalley sequences in the Great Basin (for example, Henry and others 2008, 2012; Cassel and others, 2009).

Austin Summit and Bates Mountain

At Austin Summit along U.S. Highway 50 a few km east of Austin (fig. 2), the 28.9 Ma tuff of Campbell Creek rests directly on Jurassic granite and is overlain by the 25.4 Ma Nine Hill Tuff (fig. 19). Both units are thin here, 8 m for the tuff of Campbell Creek and 5 m for the Nine Hill Tuff. At Bates Mountain at the south end of the Simpson Park Mountains (fig. 2), Stewart and McKee (1968) mapped a sequence of Eocene and Oligocene tuffs consisting of the tuff of Dry Creek, the tuff of Bottle Summit, and Bates Mountain Tuff resting directly on over 300 m of ca. 35 Ma andesite lava flows. Field examination, geochemistry, and $^{40}Ar/^{39}Ar$ dating confirm that the oldest tuff in this section is the 34.7 Ma tuff of Dry Creek (fig. 19), which probably erupted from a caldera just west of the Hall Creek caldera on the west side of the modern Toiyabe Range (figs. 2 and 14). Based on phenocryst assemblage, composition, age (31.44 ± 0.04 Ma; sample H11-36, table 2), and sanidine K/Ca, the tuff of Bottle Summit

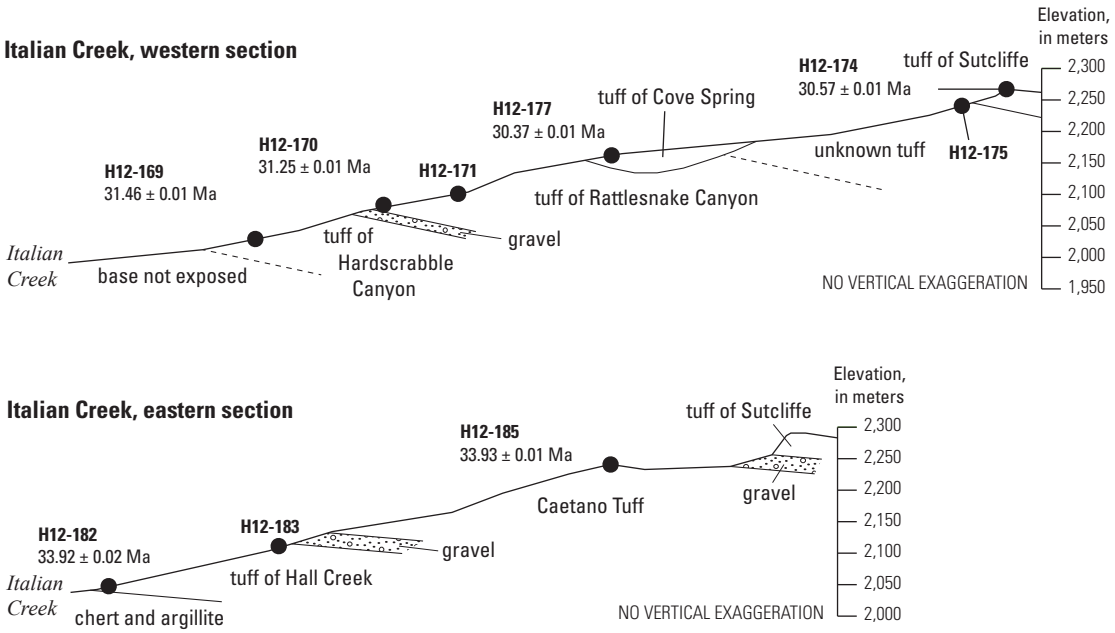

Figure 17. Outflow tuff in the Italian Creek drainage on the west flank of the Toiyabe Range south of Mount Callaghan, showing sample localities, ages, and unit boundaries. Sections are about 1 kilometer apart (Ma, mega-annum).

probably correlates with the widespread tuff of Axehandle Canyon (figs. 16 and 19) (Henry and John, 2013). The Bates Mountain Tuff at Bates Mountain consists of the 28.9 Ma tuff of Campbell Creek and the 25.4 Ma Nine Hill Tuff (fig. 19) (units C and D, respectively, of the Bates Mountain Tuff; Gromme and others, 1972; John and others, 2008). Both units are much thicker here than at Austin Summit, about 50 m for the tuff of Campbell Creek and 20 m for the Nine Hill Tuff. Neither the tuff of Hall Creek nor the Caetano Tuff are present in this section, nor have they been found farther south. Geologic relations at Austin Summit and Bates Mountain therefore indicate that the tuff of Hall Creek probably did not flow farther south than the Italian Creek paleovalley. However, the possibility cannot be totally ruled out that the tuff was deposited and completely eroded away in the brief interval prior to deposition of ca. 31 Ma tuffs.

Cenozoic Normal Faulting

Tertiary rocks within and around the Hall Creek caldera are moderately to gently east-tilted and cut by predominantly north-striking, west-dipping normal faults (fig. 4). Several minor faults cut the eastern part of the caldera, offsetting the overlying Caetano Tuff less than 1 km in total (fig. 4). Based on offset and repetition of the caldera floor along A–A′, there is about 2,700 m of slip on the west-dipping Iowa Canyon fault, which cuts through the middle of the caldera along Iowa Canyon (fig. 4). The Iowa Canyon fault strikes 020° along the west side of Mount Callaghan, cuts the southern caldera margin, and gradually curves to a strike of 315° before merging with (or truncating against) the northern caldera margin fault. Several minor faults cut the hanging wall of the Iowa Canyon fault west of Mount Callaghan; presumably they strike north into the caldera but cannot be reliably mapped through the expanse of breccia-rich tuff there. A concealed, west-dipping fault bounds the west edge of the exposed Hall Creek caldera; there is about 3–4 km offset on this fault based on its juxtaposition of post-caldera ash-flow tuffs (unit Tyt) with pre-caldera rocks (units PzTrm and Tad). While the southern caldera margin fault was cut and offset by normal faults, the originally down-to-the-south northern caldera margin fault was reactivated along Rosebush Creek (fig. 3) with the opposite sense of slip, juxtaposing post-caldera rocks outside the caldera against a topographically more prominent ridge of altered intracaldera tuff to the south. Displacement during reactivation, which could have occurred during later extension that tilted the caldera to the east, was apparently greatest to the east and died out to the west of Hall Creek (fig. 4).

Stewart and McKee (1968; 1977) mapped a low-angle thrust contact between Ordovician-Silurian carbonates and underlying Cambrian shale and limestone in the vicinity of Bernd Canyon (fig. 6*C*). Smith (1992) reinterpreted this contact as a low-angle normal fault—the “Bernd Canyon detachment”—and mapped the 3–4 km^2 carbonate body on the south side of Bernd Canyon as a klippe detached from the underlying basement (fig. 6*B*). As noted previously, we reinterpret the southern part of this contact as a down-to-the-north normal fault, part of the structural margin of the Hall Creek caldera (fig. 6*A*). The northern segment just uphill from Bernd Creek does appear to be a low-angle, younger-on-older structural contact. On the north side of Bernd Canyon, Smith (1992) mapped a subhorizontal fault contact between

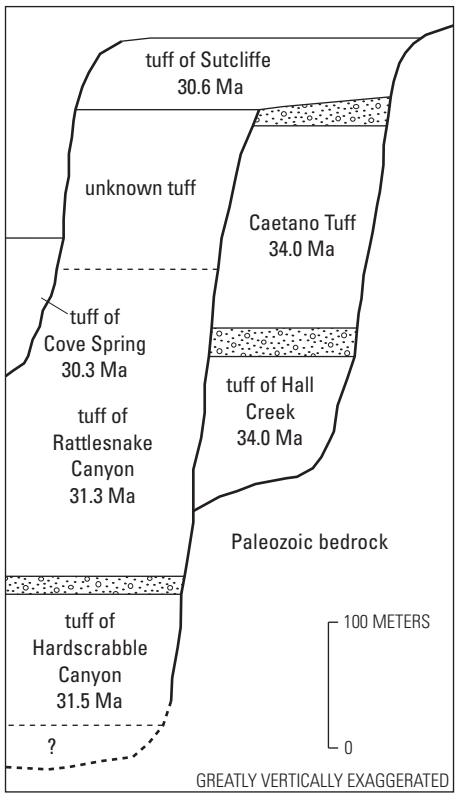

Figure 18. Outflow tuff in the Italian Creek drainage (based on sections in figure 17), illustrating sequential erosion and redeposition of paleovalley-filling tuff during late Eocene and early Oligocene volcanism (Ma, mega-annum).

Ordovician and Cambrian rocks that offsets the base of the tuff of Hall Creek and strikes north for about 6 km, cutting intracaldera tuff of Hall Creek but disappearing locally in the vicinity of Boone Creek (fig. 6*B*). We examined this area in detail and were unable to find any evidence for low-angle faulting within the tuff of Hall Creek, nor any evidence that the base of it was offset as shown in figure 6*B*. However, the amount of offset at the base of the tuff on the Smith (1989) map is so small—only 100 m at most—and the breccia-rich intracaldera tuff so lacking in stratigraphic markers, that is impossible to prove or disprove minor offset of either by any faults, low or high angle. The simplest explanation of the field relations is intracaldera tuff of Hall Creek deposited on Paleozoic basement and older andesite flows with no low-angle fault (as shown in figures 4 and 6*A*).

On the north side of Bernd Canyon, Ordovician rocks overlie Cambrian rocks along a forested slope with sparse outcrop; both units strike north and dip east in a manner that requires a structural contact (figs. 4 and 6). While searching for the Bernd Canyon detachment in this area, we found the Hall Creek tuff dike (unit Thci) described in the previous section and shown in figures 4 and 6*A*. The dike has subvertical foliation and can be traced in float and sparse outcrop for at least 500 m along strike, coincident with the map trace of the Bernd Canyon detachment. A similar basement-on-basement fault filled with a tuff dike is found on the northeastern margin of the Caetano caldera (fig. 2) (Moore and Henry, 2010; Colgan and others, 2011). The Caetano dike was a feeder for the early part of the Caetano Tuff eruption and intrudes a within-basement normal fault that accommodated part of the caldera collapse. The Hall Creek tuff dike in Bernd Canyon probably also intrudes a high angle, west-striking fault related to caldera collapse. This fault is coincident with a structure mapped as a low-angle fault by Stewart and McKee (1968) (fig. 6*C*) and Smith (1992) (fig. 6*B*), and it is possible their low-angle fault may actually may be a high-angle, down to-the north normal fault related to collapse of the Hall Creek caldera (for example, fig. 6*A*). However, the paucity of outcrop and lack of significant drainages to provide three-point constraints on the dip of the contact makes both high- and low-angle fault interpretations possible for the contact between the Ordovician and Cambrian rocks.

Geochemistry

Major and trace element geochemical data were obtained from the tuff of Hall Creek and related volcanic rocks, along with representative samples of other Tertiary igneous rocks in the study area. Forty-six samples were analyzed for major and trace elements. Twenty-five samples were analyzed by the U.S. Geological Survey contract laboratory (SGS Minerals, Toronto, Canada), 19 samples were analyzed by Washington State Geoanalytical (Pullman, Wash.), and two samples were analyzed at both laboratories. At SGS Laboratories, major oxide abundances were analyzed by wavelength-dispersive X-Ray fluorescence (XRF) spectrometry, and 55 trace elements were analyzed by inductively-coupled plasma mass spectrometry (ICP-MS) and inductively-coupled plasma atomic emission spectrometry (ICP-AES) (Taggart, 2002); these data are

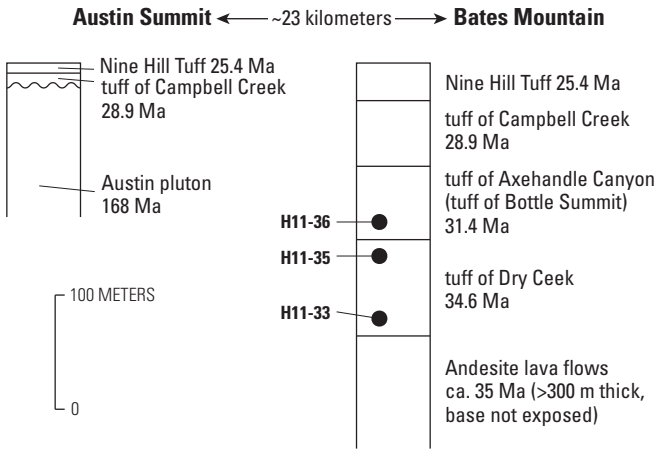

Figure 19. Outflow tuffs at Austin Summit in the Toiyabe Range and Bates Mountain in the southern Simpson Park Mountains (m, meters; km, kilometers; Ma, mega-annum; >, more than; ~, approximately; ca., around).

archived in the U.S. Geological Survey National Geochemical Database (NGDB). At Washington State Geoanalytical, 27 major oxides and trace elements were analyzed by XRF, and 27 trace elements were analyzed by ICP-MS (Johnson and others, 1999). Analytical data are available from the USGS ScienceBase Catalog (Colgan and Henry, 2017).

Samples include both vitrophyres and devitrified rock, and ash-flow tuff samples include both whole rocks and individual pumice clasts (table 1). Major oxide abundances in figures 20 and 21 are normalized to 100% volatile free. Some samples, mostly of hydrated vitrophyres, have undergone significant alkali mobility, and analyses with K_2O >6% and rhyolites with Na_2O <2.8% are omitted from figure 20 and plotted separately in figures 21 and 23.

The tuff of Hall Creek is a low- to high-silica rhyolite, zoned from about 77 to 71percent SiO_2 (fig. 20). This compositional range is similar to the better-studied Caetano Tuff to the north (Watts and others, 2016), but sample density is insufficient to determine if the tuff of Hall Creek is stratigraphically zoned from more to less felsic upsection like the Caetano Tuff (John and others, 2008), or if more- and less-evolved parts of the magma chamber were tapped simultaneously (for example, Lipman and others, 2015). Major elements follow expected variation patterns with increasing SiO_2 content, similar to the trends observed in the Caetano Tuff (fig. 21). Trace elements compatible in major and accessory mineral phases (for example, Ba [sanidine], Zr [zircon], La [allanite]) generally decrease with increasing SiO_2 content, while relatively incompatible elements (for example, Rb) tend to increase (fig. 21). Although both the tuff of Hall Creek and the Caetano Tuff span about the same range in SiO_2 content, a plot of Zr compared with Nb (fig. 22) indicates that the Hall Creek caldera is lacking the more highly evolved (high Nb/low Zr, for example, sample H11-26) fraction present in the Caetano Tuff. Only a small amount of the estimated ~1,100 km^3 Caetano Tuff is this highly evolved, however (Watts and others, 2016), and sampling at Hall Creek is not complete enough to detect a similarly small amount of highly evolved tuff.

Chondrite-normalized rare earth element (REE) data from the tuff of Hall Creek show enrichment in light REE relative to a flatter profile for the heavier elements (fig. 23*A*). All samples have a negative (Eu) anomaly; those with deeper Eu anomalies have somewhat flatter overall REE profiles (fig. 23*A*). With increasing SiO_2 content, the depth of the Eu anomaly (Eu/Eu*) increases (fig. 21*H*), while the slope of the overall REE pattern decreases as indicated by La/Yb (fig. 21*G*). Watts and others (2016) interpreted similar overall trace element and REE patterns from the Caetano caldera as evidence that fractional crystallization generated most of the observed compositional variation in the Caetano Tuff. Decreasing REE slope with increasing SiO_2 is consistent with fractionation of allanite, which is present in the Caetano Tuff but has not been found at Hall Creek. Much more limited data from Hall Creek are consistent with a similar process, but a detailed geochemical and petrologic study based on a larger sample set would need to be done to evaluate this hypothesis.

Analyses of outflow Caetano Tuff from the study area overlap with those from intracaldera Caetano Tuff and range from about 74 to 77% SiO_2 (figs. 21 and 22). This compositional range spans both the "upper" (less evolved) and "lower" (more silicic) compositional members of the zoned intracaldera Caetano Tuff, indicating that outflow tuff in the study area represents both

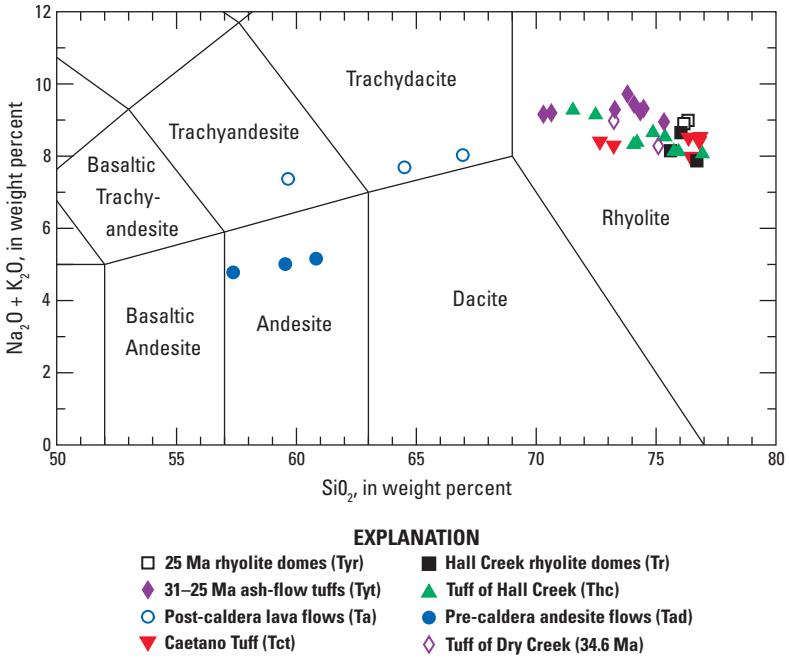

Figure 20. Total alkali–silica plot of all geochemical samples analyzed in this study. Field boundaries from Le Maitre (1989). Analyses normalized to 100 percent volatile free. Altered samples not plotted (Ma, mega-annum).

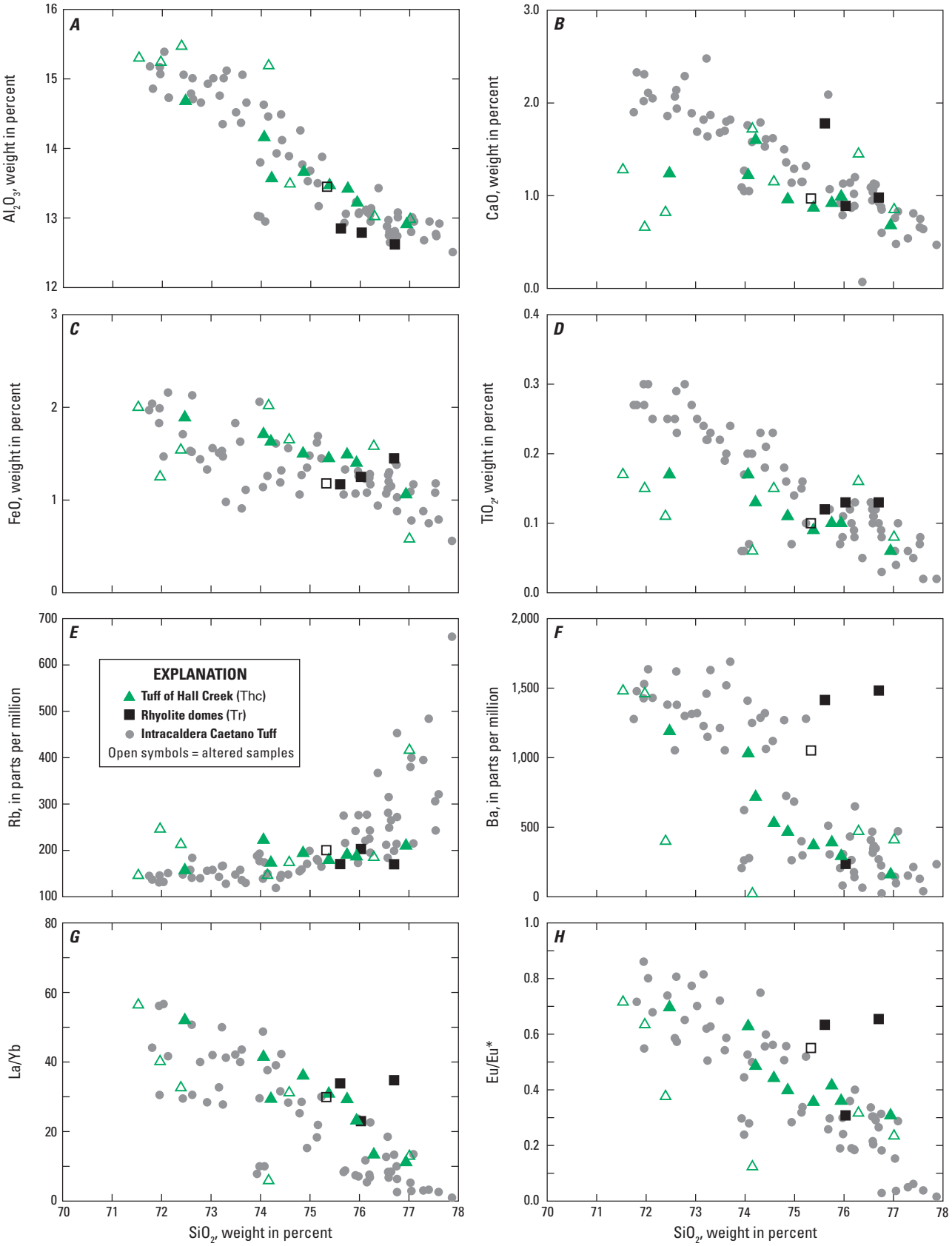

Figure 21. Whole rock analyses of the tuff of Hall Creek and related rhyolite domes, compared to data from intracaldera Caetano Tuff. Analyses normalized to 100 percent volatile free. FeO* is total Fe as FeO. Altered samples (Na_2O less than 2.8 percent) shown as open symbols. Caetano Tuff data from Watts and others (2016).

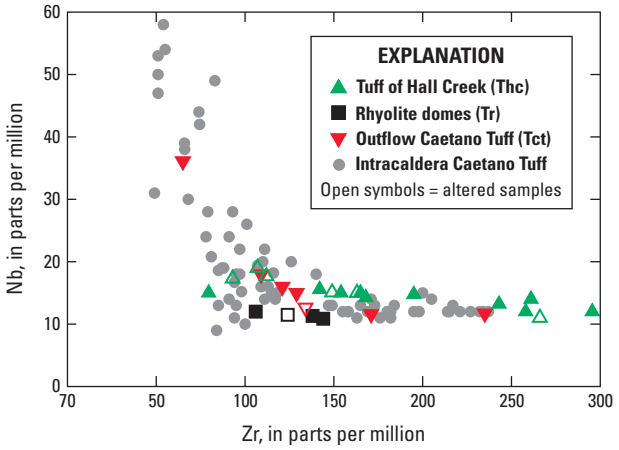

Figure 22. Zr compared with Nb for analyses of the tuff of Hall Creek, related rhyolite domes, and outflow Caetano Tuff analyzed in this study, compared to analyses of intracaldera Caetano Tuff from Watts and others (2016). Altered samples (Na_2O less than 2.8 percent) shown as open symbols.

early and late phases of the Caetano eruption. One Caetano Tuff sample (H11-26) has a very deep Eu anomaly (fig. 23*C*) and high Nb/Zr ratio (fig. 22), similar to the highly evolved fraction of the intracaldera Caetano Tuff that Watts and others (2016) interpreted as the earliest erupted product of the Caetano caldera.

Pre- and post-caldera lavas are geochemically distinct from each other. Pre-caldera lavas (unit Tad) are medium-K andesites, in the lower range of total alkalis from other middle Tertiary intermediate rocks in the Great Basin (fig. 20) (Best and others, 2009; Henry and John, 2013). Post-caldera lavas (unit Ta) are high-K andesite to dacites, in the higher range of total alkalis of the intermediate rock compositions compiled by Best and others (2009). The pre-caldera andesites have exceptionally high Sr contents, 1,630 to 3,070 parts per million (ppm), higher than any reported in the compilation of Best and others (2009). The high Sr contents and abundant hornblende suggest a water-rich magma. Pre- and post-caldera lavas in and near the Caetano caldera are also medium- and high-K, respectively, but all are andesites with Sr contents less than 800 ppm (Watts and others, 2016).

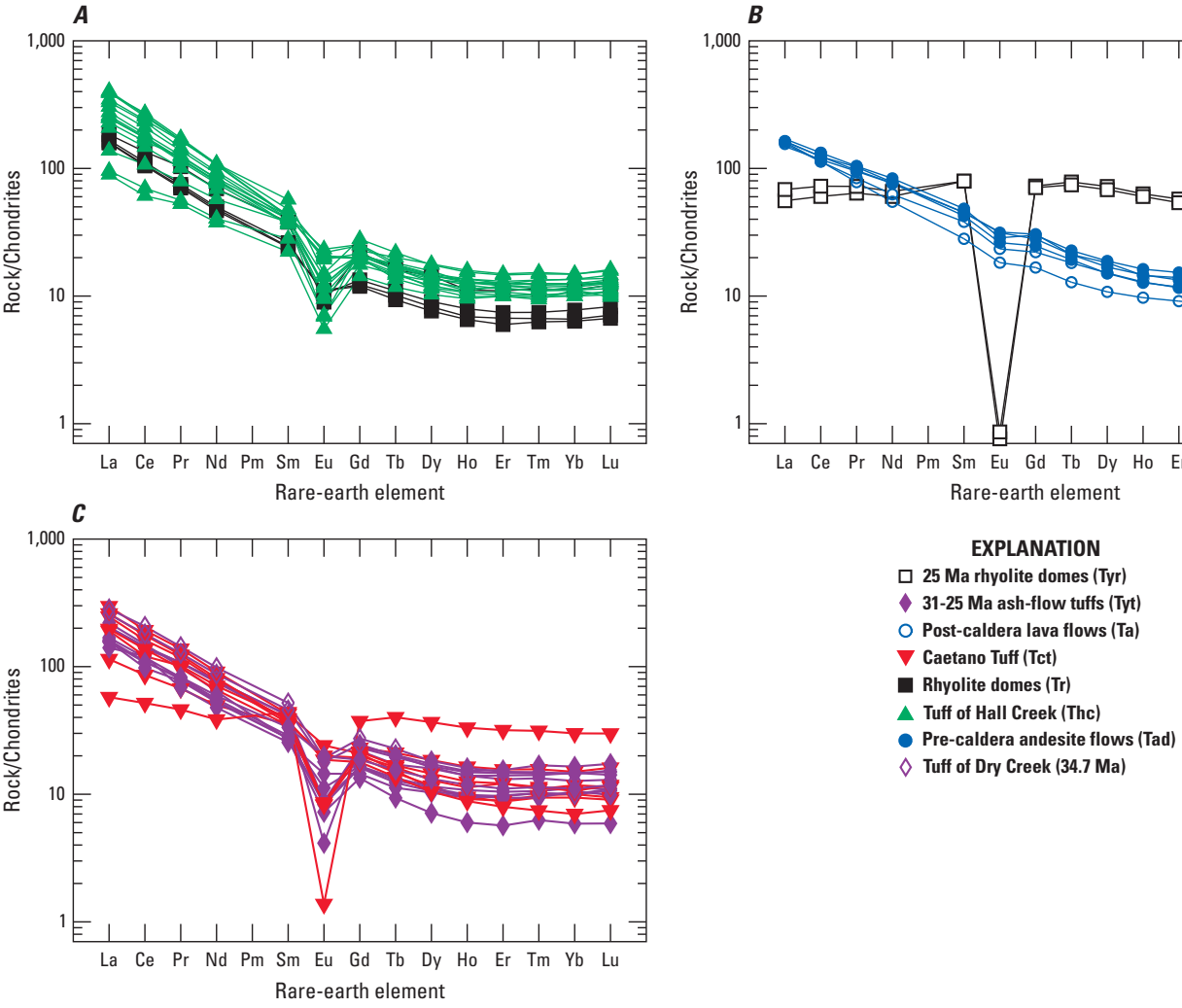

Figure 23. Chondrite-normalized (Sun and McDonough, 1989) rare-earth element diagrams for all samples analyzed in this study (Ma, mega-annum).

Major and trace element patterns in post Hall Creek distal outflow tuffs in the study area (Tyt) are typical for Great Basin ignimbrites (for example, Henry and John, 2013); these data were useful for correlating samples to known tuffs but do not bear on the history of the Hall Creek caldera as they erupted far away and much later. Although indistinguishable in the field from the 34 Ma ring-fracture rhyolite domes (unit Tr), the 25 Ma rhyolite domes (unit Tyr) are geochemical outliers in all respects, with extremely high Zn, Ga, Rb, Y, Nb, Ta, and heavy REE, low Sr and light REE, and extreme negative Eu anomalies (fig. 23*B*). The southern dome may have been emplaced along the caldera ring fracture but are otherwise completely unrelated to the Hall Creek caldera or the other Eocene magmas.

Discussion

Formation of the Hall Creek Caldera

The Hall Creek caldera displays all the classic features of large rhyolite collapse calderas: thick intracaldera tuff juxtaposed across steep fault contacts with pre-caldera rocks; abundant megabreccia composed of pre-caldera rocks surrounded by and locally interfingered with tuff; and pre- and post-caldera volcanic rocks including lava domes and caldera-fill sedimentary rocks. Other, more rarely seen features that are informative about the process of caldera collapse include the large expanse of exposed caldera floor, the tuff dike preserved near the caldera margin, and apparent "overfilling" of the caldera as indicated by major burial of the caldera wall by tuff. Figure 24 illustrates the process of caldera formation at Hall Creek in the context of regional paleogeography, based on a north-south section through the caldera and surrounding area reconstructed from field and geologic map relations.

Prior to the onset of Eocene volcanism, the early Tertiary erosional surface in the area of the future Hall Creek caldera exposed progressively shallower Paleozoic rocks from south to north, from Cambrian limestone and shale to the Roberts Mountains allochthon and its Pennsylvanian-Permian cover rocks (fig. 24*A*). As discussed in the next section, the Mount Callaghan area in the Eocene was probably the topographically high core of an antiformal structure (fig. 2) formed in the Mesozoic (fig. 24*A*). Andesite lava flows were erupted onto the Eocene erosional surface ca. 35–34 Ma (fig. 24*B*). Although they probably built local edifices on the landscape, they were primarily deposited in a topographic low along the north flank of the Mount Callaghan uplift. This low area was probably in part the western extension of the andesite-filled erosional low area in the Simpson Park Mountains to the east (fig. 2), and may also have been a pre-caldera fault-bounded basin. Together with coeval, more voluminous flows in the nearby Simpson Park Mountains (fig. 2), these andesite flows represent one of the more voluminous episodes of pre-caldera intermediate volcanism in the Great Basin. In the area of figure 4, they thicken to the north across what would become the Hall Creek caldera, and appear to terminate abruptly against the normal fault bounding the north side of the caldera (fig. 24*B*). Down-to-the-south slip on this fault obviously postdates the andesite flows, meaning that either the fault formed earlier—affecting subsequent distribution of the andesite flows—and was reactivated as part of the caldera collapse structure, or that the caldera margin fault coincidentally formed along the margin of the Eocene topographic low in which the andesite flows ponded. The presence of andesite blocks in megabreccia (unit Thbc) on the north margin of the caldera suggests some andesite may have been deposited on the Roberts Mountains allochthon just north of the caldera, but probably not a significant amount. It is unlikely that a substantial volume of andesite there would have been completely eroded away in the less than 1 m.y. interval between the andesite eruptions and deposition of the tuff of Hall Creek.

The tuff of Hall Creek erupted ca. 34 Ma, forming a caldera that collapsed to an average depth of about 2.5 km and perhaps as deep as 3 km along its southern margin where the caldera floor is not exposed (fig. 24*C* and *D*). Although no Eocene plutonic rocks are exposed in the study area, the tuff of Hall Creek was most likely sourced from a large silicic magma chamber that began forming at least several hundred k.y. prior to the main eruption, as was the case for the nearby Caetano caldera (John and others, 2008; Watts and others, 2016), and is typical for large silicic calderas (for example, Lipman and Bachmann, 2015). The eruption was fed by tuff venting along the ring-fracture faults that accommodated caldera collapse (fig. 24*C*), a remnant of which is preserved as a porphyritic tuff dike intruding a bedrock fault in the southwestern corner or floor of the caldera. The caldera floor is exposed for 6–7 km along strike in both the footwall and hanging wall of the Iowa Canyon fault (fig. 4). The contact between intracaldera tuff and caldera floor andesite is more or less planar over that distance and the caldera floor block is intact, consistent with piston-like caldera subsidence during eruption (for example, Lipman, 1997), with the exception of a small area along the southern caldera margin.

Coarse mega- and mesobreccia of Paleozoic wall-rock blocks were shed into the caldera during collapse. While the presence of megabreccia is nearly ubiquitous in large calderas, the concentration of breccia low in the caldera fill sequence at Hall Creek–locally on the caldera floor itself—is unusual compared to other calderas. Typically megabreccia accumulates higher in the fill sequence after more substantial collapse has taken place. Lipman and others (2015) described megabreccia deposited on or close to the caldera floor in the Bonanza caldera in Colorado, which they attributed to pre-caldera topography causing early-erupted tuff to disperse away from the caldera rather than ponding inside it, allowing subsequent catastrophic collapse to shed voluminous breccias directly onto the caldera floor. At Hall Creek, virtually all of the erupted tuff ponded inside the caldera or close it, and caldera-floor megabreccia is concentrated in the southwestern part of the caldera

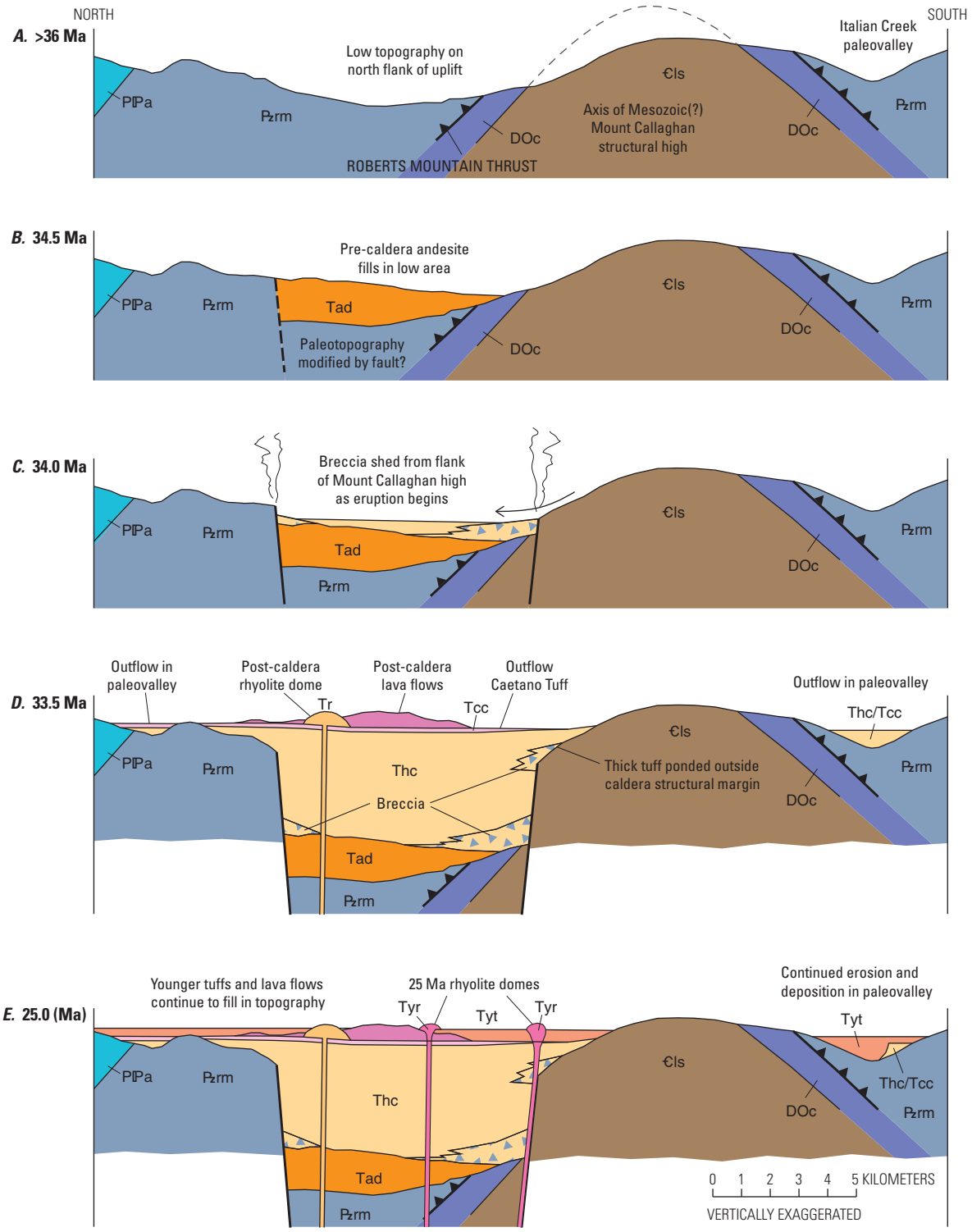

Figure 24. Schematic north-south sequential cross sections illustrating the formation of the Hall Creek caldera (Ma, mega-annum).

just north of Mount Callaghan (fig. 4). The geographic and stratigraphic position of these breccia deposits is likely related to formation of the caldera in the pre-caldera topographic low north of the Mount Callaghan structural and topographic high (fig. 24*C*). This low was at least in part an andesite-filled, west-trending paleovalley connected to a similar andesite-filled paleovalley in the Simpson Park Mountains. When the eruption began, breccia could have been shed directly from the already high, steep flanks to the north and south, even before significant collapse had taken place. Envisioning a scenario in which substantial collapse could take place without concurrent drawdown of the underlying magma chamber by venting of tuff is otherwise difficult.

Tuff of Hall Creek ponded as much as 1 km thick just outside the southern structural margin of the caldera, and ponded several hundred meters thick just outside the northern structural margin (fig. 24*D*). Geologic mapping (this study; Stewart and McKee, 1968) rules out additional collapse faults both north and south of the main caldera margin, suggesting that local topography at the time of eruption caused the tuff to pond in the immediate vicinity of the caldera. This topography is probably a combination of pre-caldera erosional topography and a topographic caldera rim that extended several kilometers outward from the structural margin of the caldera. Topographic caldera rims form as blocks of the caldera wall slump into the caldera during and immediately after ash-flow eruption and caldera subsidence (Lipman, 1984, 1997; Best and others, 2013). The presence of abundant megabreccia in the Hall Creek caldera demonstrates that the caldera margin grew outward by this process, but distinguishing a topographic caldera rim from pre-caldera topography is difficult. Their topographic expressions are similar (apparent erosion upsection away from the caldera), and at Hall Creek the relevant field relations are covered by younger rocks or modified by normal faults.

North of the caldera margin, tuff of Hall Creek is deposited on bedrock and older volcanic rocks as far north as the Caetano caldera (fig. 2). Between Cowboy Rest Creek (north edge of fig. 4) and the mapped caldera margin, tuff of Hall Creek is overlain by thick post-caldera lava flows (Ta), in turn overlain by coarse sediments of unknown age (unit Ttg). These units may represent deposits adjacent to a topographic caldera rim extending 1–2 km north of the caldera structural margin. North of Cowboy Rest Creek, the tuff of Hall Creek and the Caetano Tuff are overlain directly by the 28.9 Ma tuff of Campbell Creek, consistent with sequential outflow tuffs filling paleotopography. The eastern caldera margin is concealed, but we interpret the structural margin to be close to the post-caldera rhyolite dome (unit Tr), with post-caldera rocks (units Tyt and Tts) ponded between there and a caldera topographic rim ~2 km to the east, buried beneath Grass Valley (fig. 4). The thick tuff of Hall Creek ponded outside the southern caldera structural margin is probably partly within the caldera topographic rim, but the relevant field relations there are covered by alluvium (fig. 4) and it is unclear how far south the topographic rim would be. Thickness of ponded tuff may have been enhanced by pre-caldera high topography south of the caldera (fig. 24*A*). A topographic rim 1–2 km outside the caldera structural margin is consistent with better-exposed field relations at the nearby Caetano caldera, which also has abundant coarse megabreccia along its margins that defines a roughly 1 km wide, topographic rim (John and others, 2008; Colgan and others, 2011; Moore and Henry, 2011).

Immediately following caldera collapse, outflow tuff from the Caetano caldera flowed south onto the tuff of Hall Creek, both inside and outside its caldera basin (fig. 24*D*). Two rhyolite domes and substantial flows of andesite and dacite erupted in and around the caldera within 400 ka of the main tuff eruption. One rhyolite intruded the eastern caldera margin at 33.5 Ma (fig. 4), and the other about 5 km west of the Hall Creek caldera into the older Dry Creek caldera at about 33.8 Ma (fig. 14). The intermediate lavas generated irregular topography inside the caldera and spread outside (or were erupted separately) along the northern margin (fig. 24*E*). The post-caldera rhyolite domes indicate that at least some residual magma existed in the chamber following the eruption, but no resurgent plutons large enough to dome the caldera floor and fill were emplaced at Hall Creek, as is common in other calderas (for example, John and others, 2008; Best and others, 2013; Lipman and others, 2015). The andesite and dacite lavas are much less evolved than the tuff of Hall Creek, while also more alkalic and less crystal-rich than the hornblende-rich pre-caldera lava flows. Relatively crystal-poor intermediate lava flows also erupted at the Caetano caldera within 500 ka of the main tuff eruption, where they are interpreted to be sourced from the same mid-crustal zone of melting that produced the Caetano Tuff, but not directly from the Caetano magma chamber itself (Watts and others, 2016). The post-caldera lavas at Hall Creek may have a similar origin.

For the next 10 m.y., tuffaceous sediments and distal ash-flow tuffs accumulated in the caldera and surrounding lowlands, filling in topography accentuated by the earlier caldera collapse and lava eruptions. At 25 Ma, a small volume of highly evolved rhyolite magma locally intruded the caldera ring-fracture faults, forming several lava domes (fig. 24*E*). Post-34 Ma volcanism had migrated progressively farther west and south of the Hall Creek–Caetano area with time; by 25 Ma, magmatism was most active in the Stillwater–Clan Alpine region ~100 km to the southwest (fig. 1) (Henry and John, 2013). The reason why 25 Ma magmatism affected areas to the east and north that had been quiescent for almost 10 m.y. at that point is unclear, but it appears to have been a fairly widespread phenomenon—the Fish Creek Mountains caldera in the northwestern corner of figure 2 formed ca. 24.9 Ma (Henry and John, 2013; Cousens and others, 2014), nearly 10 m.y. after volcanism in the area had ceased following eruption of the Caetano and Hall Creek calderas.

Distribution of Outflow Tuff and Middle Tertiary Paleogeography

Late Eocene to Oligocene volcanic rocks in the study area are deposited on pre-Tertiary strata ranging from Lower Cambrian to Triassic. Stratigraphic relations and the presence of Cambrian rocks in megabreccia demonstrate that rocks at least as old as Cambrian limestone and shale (unit €ls) were exposed at Mount Callaghan when the Hall Creek caldera formed ca. 34 Ma, with progressively younger rocks exposed to the north and south (fig. 2). Across Carico Lake Valley to the west, Oligocene tuffs in the Ravenswood area were also deposited directly on Cambrian rocks, with younger Paleozoic rocks beneath this unconformity to the north and south (fig. 2). Together, these patterns indicate that the Mount Callaghan area is at the core of an east-west trending anticlinal uplift that involves Triassic rocks and formed prior to the onset of Eocene volcanism. This structure probably formed during the Cretaceous Sevier orogeny, although exhumation of Cambrian rocks is unusual this far west of the main Sevier thrust front (for example, Long, 2012), and the east-west trend is unusual compared to the more north-south Mesozoic folds in northern Nevada (for example, Long, 2015). Whenever it formed, the core of this structure formed an east-west elongate topographic high in the Eocene, as evidenced by the paucity of Eocene and Oligocene volcanic rocks preserved directly on it (figs. 2 and 24), compared to areas to the north and south. Either no tuffs were deposited there, or they were thin enough (for example, fig. 19) to be easily eroded away.

Andesite lava flows more than 300 m thick in the Simpson Park Mountains are overlain by younger tuffs on Bates Mountain, including the 28.9 Ma tuff of Campbell Creek. At Austin Summit along U.S. Highway 50 only 20 km to the west, a thin layer (8 m) of the tuff of Campbell Creek is deposited directly on the Jurassic Austin pluton and overlain by a similarly thin layer of Nine Hill Tuff (fig. 19), clearly indicating that the andesite lava flows were deposited in a topographic low relative to the surrounded bedrock. Had they instead built large edifices on a low-relief bedrock landscape, the younger tuffs would have flowed around these volcanoes in the lowlands, rather than being deposited more thickly on top of them. The fact that the tuff of Campbell Creek overlies both the andesite flows and bedrock indicates that the top of the andesite sequence was roughly level with the surrounding bedrock erosional surface by 30 Ma. Contacts between the andesite flows and Paleozoic basement are everywhere depositional (fig. 2), suggesting this topography was primarily erosional. The Simpson Park topographic low extended around the north side of the Mount Callaghan structural high to the site of the future Hall Creek caldera, where thick andesite flows ponded immediately prior to the caldera eruption (fig. 24*B*). The 34.7 Ma tuff of Dry Creek was able to flow east from its source caldera at least as far as Bates Mountain (fig. 2), probably around the north side of the Mount Callaghan structural high.

As described in the previous section, most erupted tuff of Hall Creek ponded within or immediately adjacent to its source caldera, but some of the outflow did disperse more widely in the area of figure 2. Any Eocene topographic barrier on the north side of the Hall Creek caldera was much lower than on the south side, and outflow tuff of Hall Creek was able to flow as far north as the site of the future Caetano caldera; the Caetano Tuff in turn flowed south and ponded in the Hall Creek caldera (fig. 24*D*). Despite the presence of high topography immediately south of the Hall Creek caldera, both outflow tuff of Hall Creek and Caetano Tuff flowed into the Italian Creek paleovalley on the south side of Mount Callaghan (figs. 2 and 18, 24*D*). It is unclear whether small amounts of both tuffs flowed directly south over the top of the Mount Callaghan uplift, or if the Eocene Italian Creek drainage extended far enough east that tuffs could flow east around the Mount Callaghan uplift and then west into the Italian Creek paleovalley.

Overall, the distribution of Eocene lava flows and tuffs north and east of Austin is consistent with significant Eocene topography that strongly affected the distribution of volcanic rocks, but there is no evidence for a major north-south trending middle Tertiary ridge that served as a barrier to the east-west dispersal of ash-flow tuffs. Rather, the area was characterized by east-west trending paleovalleys and intervening ridges that facilitated east-west dispersal of ash-flow tuffs, while generally limiting their north-south extent (figs. 2 and 24). These erosional patterns, together with structural relations in Paleozoic rocks, argue against a Tonopah-Austin paleodivide being the pronounced edge of a major orogenic plateau controlled by crustal-scale reverse faults and enhanced by erosion and isostatic uplift (Best et al., 2013). Such a structure would be much more extensive along strike, and any north-trending, west-dipping thrust faults would be associated with north-south trending folds and faults, not localized east-west trending domes like the one in figure 2. If a middle Tertiary Austin-Tonopah paleodivide was present, it is more likely to have been related to more localized, near surface processes.

Whether the Eocene-Oligocene paleodivide was close to the study area or farther east, all previous interpretations place it east of the study area (fig. 1). Numerous tuffs sourced from western Nevada were nonetheless able to flow into and through the study area ca. 32–25 Ma, including the tuff of Campbell Creek from the Desatoya Mountains (fig. 1) and the Nine Hill Tuff, from an unknown source in the vicinity of the Stillwater–Clan Alpine caldera complex (Deino, 1989; Henry and John, 2013). This either indicates that the drainage divide was farther west than previously thought, or that the topographic gradient was low enough for tuffs with sufficient kinetic energy to flow long distances up a gentle slope. The latter is consistent with results from Cassel and others (2009, 2014), who interpreted stable isotope data to indicate the middle Cenozoic Sierra Nevada had a steep westward gradient that decreased eastward into a much flatter area in what is now the Great Basin.

Timing and Kinematics of Cenozoic Extension

Field relations in the study area indicate that Cenozoic extension took place mostly on west-dipping, high-angle normal faults, was of moderate to low magnitude, and postdates Oligocene tuffs as young as ca. 25 Ma. As discussed previously, there is no evidence for a low-angle Bernd Canyon detachment cutting the tuff of Hall Creek (Smith, 1992), although a low-angle fault contact does separate Cambrian and Ordovician units on the south side of Bernd Canyon (fig. 4 and 6). This fault could be an earlier (post Paleozoic, pre-Eocene) normal fault, but its limited outcrop area makes it unlikely to have accommodated significant Cenozoic extension. Other Cenozoic detachment faults in the Great Basin are typically mapped for tens of km to over 100 km along strike and juxtapose substantially different stratigraphic levels (for example, Miller and others, 1999; Howard, 2003), while the Bernd Canyon fault only crops out for a few km along strike and does not juxtapose greatly different levels of the Paleozoic stratigraphy. Smith (1992, fig. 9) interpreted the Toiyabe Range north of Austin as a locus of large-magnitude Cenozoic extension, with as much as 100–200 percent strain in the area of figure 4. Restored post-tuff of Hall Creek (younger than 34 Ma) extension along cross section *A–A′* (fig. 4) is about 3 km or 15% strain, mostly accommodated by the Iowa Canyon fault. Although more detailed mapping could refine this estimate, nothing in the mapped geology supports large-magnitude post-Eocene extension (100–200 percent strain) in the study area.

Although compaction foliation in the Eocene and Oligocene tuffs is variable, there is no evidence for progressively less tilting in younger units that would indicate protracted extension from 34 to more recently than 25 Ma (Smith, 1992). Foliation in the intracaldera tuff of Hall Creek can vary because of welding against breccia blocks and caldera walls, and foliation in younger tuffs is highly variable because of welding against local topography (for example, fig. 13). Post-caldera lava flows built edifices and flowed into topographic lows, leading to a highly irregular distribution. Overall the package of late Eocene and Oligocene volcanic rocks in the study area dips consistently east (cross section, fig. 4), consistent with block tilting after deposition of the youngest tuffs ca. 25 Ma. Colgan and others (2008) interpreted synextensional basin fill within the Caetano caldera (40 km north of the Hall Creek caldera; fig. 2) to record middle Miocene (around 16–10 Ma) extension on west dipping faults. Stockli (1999) interpreted 15 Ma apatite fission track ages to record rapid middle Miocene extensional unroofing of the Toiyabe Range at the latitude of Austin (30 km south of the Hall Creek caldera; fig. 2) on a west-dipping fault system. In the absence of more direct constraints, the simplest interpretation is that post-25 Ma slip on west-dipping faults in the study area also took place in the middle Miocene (16–10 Ma) concurrently with areas to the north and south, perhaps with more recent late Miocene and Pliocene slip. Extensional faulting in the Hall Creek area thus appears to be part of the middle Miocene episode of Basin and Range extension that affected much of the northern Great Basin (for example, Colgan and Henry, 2009), rather than intimately related to Eocene magmatism.

Conclusions

Prior to the onset of late Eocene volcanism, the northern Toiyabe Range of central Nevada was characterized by a structurally controlled, east-west trending high ridge in the area of present-day Mount Callaghan. Andesite lava flows ponded hundreds of meters thick in topographically lower areas to the north, and to the east in the modern Simpson Park Mountains. A probable caldera for the tuff of Dry Creek formed ca. 34.7 mega-annum (Ma), and the main Hall Creek caldera formed ca. 34.0 Ma during eruption of the tuff of Hall Creek. Collapse of the Hall Creek caldera was piston-like with an intact floor block, and the caldera filled with thick intracaldera tuff and interbedded breccia lenses shed from the caldera walls. Much of this breccia was deposited close to or directly on the caldera floor itself. Tuff ponded thickly in the immediate vicinity of the caldera and dispersed a short distance, mostly to the north. Both silicic and intermediate post-caldera lavas were locally erupted within 400 k.y. of the main eruption, and for the next 10 m.y. sedimentary rocks and distal outflow tuff ponded in the caldera basin and filled other topographic low areas nearby. Patterns of deposition in these tuffs indicate that the region was characterized by east-west trending paleovalleys and ridges in the late Eocene and Oligocene, which facilitated the dispersal of ash-flow tuffs erupted farther to the west. Extensional faulting of the Hall Creek caldera area postdates 25 Ma and is of modest magnitude (15-percent strain); there is no evidence for major slip on Eocene detachment faults in the study area.

References Cited

Armstrong, R.L., Ekren, E.B., McKee, E.H., and Noble, D.C., 1969, Space-time relations of Cenozoic volcanism in the Great Basin of the western United States: American Journal of Science, v. 267, p. 478–490, doi:10.2475/ajs.267.4.478.

Best, M.G., and Christiansen, E.H., 1991, Limited extension during peak Tertiary volcanism, Great Basin of Nevada and Utah: Journal of Geophysical Research, v. 96, p. 13509–13528.

Best, M.G., Barr, D.L., Christiansen, E.H., Gromme, C.S., Deino, A.L., and Tingey, D.G., 2009, The Great Basin altiplano during the middle Cenozoic ignimbrite flareup: Insights from volcanic rocks: International Geology Review, v. 51, no. 6, p. 1–45.

Best, M.G., Christiansen, E.H., and Gromme, S., 2013, Introduction: The 36-18 Ma southern Great Basin, USA, ignimbrite province and flareup: Swarms of subduction-related supervolcanoes: Geosphere, v. 9, p. 260–274, doi:10.1130/GES00870.1.

Cassel, E.J., Breecker, D.O., Henry, C.D., Larson, T.E., and Stockli, D.F., 2014, Profile of a paleo-orogen: High topography across the present-day Basin and Range from 40 to 23 Ma: Geology, v. 42, p. 1007–1010, doi:10.1130/G35924.1.

Cassel, E.J., Calvert, A.T., and Graham, S.A., 2009, Age, geochemical composition, and distribution of Oligocene ignimbrites in the northern Sierra Nevada, California—Implications for landscape morphology, elevation, and drainage divide geography of the Nevadaplano: International Geology Review, v. 51, p. 723–742, doi:10.1080/00206810902880370.

Colgan, J.P., and Henry, C.D., 2009, Rapid middle Miocene collapse of the Mesozoic orogenic plateau in north-central Nevada: International Geology Review, v. 51, p. 920–961.

Colgan, J.P., and Henry, C.D., 2017, Geochemical and geochronologic data from the Hall Creek caldera, Toiyabe Range, Nevada: U.S. Geological Survey [ScienceBase] data release, available online at https://doi.org/10.5066/F7JD4TX8.

Colgan, J.P., Henry, C.D., and John, D.A., 2011, Geologic map of the Caetano caldera, Lander and Eureka Counties, Nevada: Nevada Bureau of Mines and Geology Map 174, scale 1:75,000.

Colgan, J.P., John, D.A., and Henry, C.D., 2008, Large-magnitude Miocene extension of the Eocene Caetano caldera, Shoshone and Toiyabe Ranges, Nevada: Geosphere, doi:10.1130/GES00115.1.

Coney, P.J., 1978, Mesozoic–Cenozoic Cordilleran plate tectonics, *in* Smith, R.B., and Eaton, G.P., eds., Cenozoic tectonics and regional geophysics of the western Cordillera: Geological Society of America Memoir 152, p. 33–50.

Cousens, B., Stevens, C., Varve, S., Henry, C.D., and John, D.A., 2014, Volcanism in the Fish Creek Mountains, Battle Mountain area, central Nevada–a microcosm of central Great Basin igneous activity during the Cenozoic: Geological Society of America Abstracts with Programs, v. 46, no. 6, p. 551.

DeCelles, P.G., 2004, Late Jurassic to Eocene evolution of the Cordilleran thrust belt and foreland basin system, western U.S.A.: American Journal of Science, v. 304, p. 105–168, doi: 10.2475/ajs.304.2.105.

Deino, A.L., 1989, Single crystal $^{40}Ar/^{39}Ar$ dating as an aid in correlation of ash flows—Examples from the Chimney Springs/New Pass Tuffs and the Nine Hill/Bates Mountain Tuffs of California and Nevada: New Mexico Bureau of Mines and Mineral Resources, Continental magmatism abstracts, v. 131, p. 70.

Dickinson, W.R., 2006, Geotectonic evolution of the northern Great Basin: Geosphere, v. 2, no. 7, p. 353–368; doi: 10.1130/GES00054.1.

du Bray, E.A., and Pallister, J.S., 1991, An ash flow caldera in cross section—Ongoing field and geochemical studies of the Mid-Tertiary Turkey Creek Caldera, Chiricahua Mountains, SE Arizona: Journal of Geophysical Research, v. 96, p. 13435–13457.

Gans, P.B., Mahood, G.A., and Schermer, E., 1989, Synextensional magmatism in the Basin and Range Province—A case study from the eastern Great Basin: Geological Society of America Special Paper 233, 53 p., doi: 10.1130/SPE233-p1.

Gromme, C.S., McKee, E.H., and Blake, M.C., Jr., 1972, Paleomagnetic correlations and potassium-argon dating of middle Cenozoic ash-flow sheets in the eastern Great Basin, Nevada and Utah: Geological Society of America Bulletin, v. 83, p. 1619–1638, doi:10.1130/0016-7606(1972)83[1619:PCAPDO]2.0.CO;2.

Heizler, M.T., 2011, Introducing the ARGUS VI mass spectrometer to geo and thermochronology: American Geophysical Union, Fall Meeting 2011, abstract V51A–2508.

Heizler, M.T., McIntosh, W.C., Ross, Jake, and Hamilton, Doug, 2014, 10e13 Ohm Faraday multi-collection: Striving for accuracy to match ultrahigh precision $^{40}Ar/^{39}Ar$ measurements: Sacramento, Calif., Goldschmidt 2014 Abstracts, p. 957.

Henry, C.D., 2008, Ash-flow tuffs and paleovalleys in northeastern Nevada: Implications for Eocene paleogeography and extension in the Sevier hinterland, northern Great Basin: Geosphere, v. 4, p. 1–35, doi: 10.1130/GES00122.1.

Henry, C.D., Hinz, N.H., Faulds, J.E., Colgan, J.P., John, D.A., Brooks, E.R., Cassel, E.J., Garside, L.J., Davis, D.A., and Castor, S.B., 2012, Eocene-Early Miocene paleotopography of the Sierra Nevada–Great Basin–Nevadaplano based on widespread ash-flow tuffs and paleovalleys: Geosphere, v. 8, no. 1, p. 1–27, doi:10.1130/GES00727.1.

Henry, C.D., and John, D.A., 2013, Magmatism of the ignimbrite flareup in the western Nevada volcanic field, Great Basin, USA: Geosphere, v. 9, p. 951–1008.

Howard, K.A., 2003, Crustal structure in the Elko-Carlin region, Nevada, during Eocene gold mineralization: Ruby-East Humboldt metamorphic core complex as a guide to the deep crust: Economic Geology, v. 98, p. 249–268.

Hudson, M.R., John, D.A., Conrad, J.E., and McKee, E.H., 2000, Style and age of late Oligocene-Early Miocene deformation in the southern Stillwater Range, west central Nevada: Paleomagnetism, geochronology, and field relations: Journal of Geophysical Research, v. 105, p. 929–954.

John, D.A., 1995, Tilted mid-Tertiary ash-flow calderas and subjacent granitic plutons, southern Stillwater Range, Nevada: Cross-sections of an Oligocene igneous center: Geological Society of America Bulletin, v. 107, p. 180–200.

John, D.A., Henry, C.D., and Colgan, J.P., 2008, Magmatic and tectonic evolution of the Caetano caldera, north-central Nevada—A tilted mid-Tertiary eruptive center and source of the Caetano Tuff: Geosphere, v. 4, p. 75–106.

Johnson, D.M., Hooper, P.R., and Conrey, R.M., 1999, XRF analysis of rocks and minerals for major and trace elements on a single low-dilution Li-tetraborate fused bead: Advances in X-Ray Analysis, v. 41, p. 843–867.

Kuiper, K.F., Deino, A., Hilgen, F.J., Krijgsman, W., Renne, P.R., and Wijbrans, J.R., 2008, Synchronizing rock clocks of Earth history: Science, v. 320, p. 500–504.

Le Maitre, R.W., 1989, A classification of igneous rocks and glossary of terms: Boston, Blackwell Scientific, 193 p.

Lipman, P.W., 1984, The roots of ash-flow calderas in western North America: Windows into the tops of granitic batholiths: Journal of Geophysical Research, v. 89, p. 8801–8841.

Lipman, P.W., 1997, Subsidence of ash-flow calderas: relation to caldera size and magma-chamber geometry: Bulletin of Volcanology, v. 59, p. 198–218.

Lipman, P.W., and Bachmann, O., 2015, Connecting ignimbrite to batholith in the Southern Rocky Mountains: Integrated perspectives from geological, geophysical, and geochronological data: Geosphere, v. 11, p. 705–743, doi:10.1130/GES01091.1.

Lipman, P.W., Zimmerer, M.J., and McIntosh, W.C., 2015, An ignimbrite caldera from the bottom up—Exhumed floor and fill of the resurgent Bonanza caldera, Southern Rocky Mountain volcanic field: Geosphere, v. 11, p. 1902–1947, doi:10.1130/GES01184.1.

Long, S.P., 2012, Magnitude and spatial patterns of erosional exhumation in the Sevier hinterland, eastern Nevada and western Utah, USA: Insights from a Paleogene paleogeologic map: Geosphere, v. 8, p. 881–901, doi:10.1130/GES00783.1.

Long, S.P., 2015, An upper-crustal fold province in the hinterland of the Sevier orogenic belt, eastern Nevada, U.S.A.—A Cordilleran Valley and Ridge in the Basin and Range: Geosphere, v. 11, doi:10.1130/GES01102.1.

Masek, J.G., Isacks, B.L., Gubbels, T.L., and Fielding, E.J., 1994, Erosion and tectonics at the margins of continental plateaus: Journal of Geophysical Research, v. 99, p. 13941–13956.

Mason, B.G., Pyle, D.M., and Oppenheimer, C., 2004, The size and frequency of the largest volcanic eruptions on earth: Bulletin of Volcanology, v. 66, p. 735–748, doi:10.1007/s00445-004-0355-9.

Mars, J.C., 2013, Hydrothermal alteration maps of the central and southern Basin and Range Province of the United States from Advanced Spaceborne Thermal Emission and Reflection Radiometer (ASTER) data: U.S. Geological Survey Open-File Report 2013–1139, 5 p. 13 plates, scale 1:300,000, accessed July 18, 2011, at http://dx.doi.org/10.3133/ofr20131139.

McIntosh, W.C., Heizler, M., Peters, L., and Esser, R., 2003, $^{40}Ar/^{39}Ar$ geochronology at the New Mexico Bureau of Geology and Mineral Resources: New Mexico Bureau of Geology and Mineral Resources Open File Report OF-AR-1, 10 p.

McKee, E.H., and Silberman, M.L., 1970, Geochronology of Tertiary igneous rocks in central Nevada: Geological Society of America Bulletin, v. 81, no. 8, p. 2317–2328.

Miller, E.L., Dumitru, T.A., Brown, R.W., and Gans, P.B., 1999, Rapid Miocene slip on the Snake Range–Deep Creek Range fault system, east-central Nevada: Geological Society of America Bulletin, v. 111, p. 886–905.

Miller, E.L., Gans, P.B., and Garing, J., 1983, The Snake Range decollement: An exhumed mid-Tertiary brittle-ductile transition: Tectonics, v. 2, p. 239–263.

Miller, E.L., and Miller, M.M., 1992, Late Paleozoic paleogeographic evolution and tectonic evolution of the western U.S. Cordillera, *in* Burchfiel, B.C., Lipman, P.W., and Zoback, M.L., eds., The Cordilleran Orogen: Conterminous U.S.: Boulder, Colo., Geological Society of America, The Geology of North America, v. G-3.

Min, K., Mundil, R., Renne, P.R., and Ludwig, K.R., 2000, A test for systematic errors in $^{40}Ar/^{39}Ar$ geochronology through comparison with U/Pb analysis of a 1.1 Ga rhyolite: Geochimica et Cosmochimica Acta, v. 64, p. 73–98.

Moore, S.C., and Henry, C.D., 2010, Preliminary geologic map of the northeastern margin of the Caetano caldera, Lander County, Nevada: Nevada Bureau of Mines and Geology Open-File Report OF10-10, scale 1:6,000.

Murchey, B.L., 1990, Age and depositional setting of siliceous sediments in the upper Paleozoic Havallah sequence near Battle Mountain Nevada: Implications for the paleogeography and structural evolution of the western margin of North America: Geological Society of America Special Paper 255, p.137–155.

Roberts, R.J., Hotz, P.E., Gilluly, J., and Ferguson, H.G., 1958, Paleozoic rocks of north-central Nevada: American Association of Petroleum Geologists Bulletin, v. 42, p. 2813–2857.

Samson, S.D., and Alexander, E.C., Jr., 1987, Calibration of the interlaboratory $^{40}Ar/^{39}Ar$ dating standard, MMhb-1: Chemical Geology Isotope Geoscience, v. 66, p. 27–34.

Silberling, N.J., and Roberts, R.J., 1962, Pre-Tertiary stratigraphy and structure of northwestern Nevada: Geological Society of America Special Paper 72, 58 p.

Silberman, M.L., and McKee, E.H., 1971, Potassium-argon ages of plutons in north-central Nevada: Isochron/West, v. 71, no. 1, p. 15–32.

Smith, D.L., 1989, Structural geology and tectonic development of the Toiyabe Range, Lander and Nye Counties, Nevada: Stanford, Calif., Stanford University, Ph.D. thesis, 169 p.

Smith, D.L., 1992, History and kinematics of Cenozoic extension in the northern Toiyabe Range, Lander County, Nevada: Geological Society of America Bulletin, v. 104, p. 789–801.

Speed, R., Elison, M.W., and Heck, F.R., 1988, Phanerozoic tectonic evolution of the Great Basin, *in* Ernst, W.G., ed., Metamorphism and crustal evolution of the western United States—Rubey Volume VII: Englewood Cliffs, N.J., Prentice-Hall, p. 572–605.

Steiger, R.H., and Jäger, E., 1977, Subcommission on geochronology: Convention on the use of decay constants in geo- and cosmochronology: Earth and Planetary Science Letters, v. 36, p. 359–362.

Stewart, J.H., and McKee, E.H., 1968, Geologic map of the Mount Callaghan quadrangle, Lander County, Nevada: U.S. Geological Survey Geologic Quadrangle Map GQ–730, scale 1:24,000.

Stewart, J.H., and McKee, E.H., 1969, Geologic map of the Hall Creek and western part of the Walti Hot Springs quadrangles, Lander County, Nevada: U.S. Geological Survey Open-File Report 69–269, scale 1:62,500.

Stewart, J.H., and McKee, E.H., 1977, Geology and mineral resources of Lander County, Nevada: Nevada Bureau of Mines and Geology Bulletin 88, 106 p., 1 plate, 1:250,000 scale.

Stockli, D.F., 1999, Regional timing and spatial distribution of Miocene extension in the northern Basin and Range Province: Stanford, Calif., Stanford University, Ph.D. thesis, 239 p.

Sun, S.-S., and McDonough, W.F., 1989, Chemical and isotopic systematics of oceanic basalts: Implications for mantle composition and processes, *in* Saunders, A.D., and Norry, M.J., eds., Magmatism in the ocean basins: Geological Society of London Special Publication 42, p. 313–345, doi:10.1144/GSL.SP.1989.042.01.19.

Taggart, J.E., Jr., 2002, Analytical methods for chemical analysis of geologic and other materials: U.S. Geological Survey Open-File Report 02–0223, available online at http://pubs.usgs.gov/of/2002/ofr-02-0223/OFR-02-0223.pdf.

U.S. Geological Survey, 1999, 30-meter digital elevation model, available online at https://nationalmap.gov/elevation.html.

Watts, K.E., John, D.A., Colgan, J.P., Henry, C.D., Bindeman, I.N., and Schmitt, A.K., 2016, Probing the volcanic-plutonic connection and the genesis of crystal-rich rhyolite in a deeply dissected supervolcano in the Nevada Great Basin: Source of the late Eocene Caetano Tuff: Journal of Petrology, v. 57(8), p. 1599–1644, doi: 10.1093/petrology/egw051.

Appendix 1. $^{40}Ar/^{39}Ar$ Methods and Sample Data

Minerals were separated from crushed, sieved samples by standard magnetic and density techniques. Sanidine and plagioclase were leached with dilute HF to remove adhering matrix. All samples were hand-picked under a binocular microscope. Samples and neutron flux monitor Fish Canyon Tuff sanidine were irradiated in Al disks for 7 hours at the Nuclear Science Center in College Station, Tex., or at the USGS reactor in Denver, Colo. Individual sanidine crystals were fused with a CO_2 laser at 5W; laser fusion data available from the USGS ScienceBase Catalog (Colgan and Henry, 2017). Biotite, plagioclase, and hornblende were step heated with a diode laser at progressively higher powers; step-heating data are available from the USGS ScienceBase Catalog (Colgan and Henry, 2017). Analyses of extracted gases of samples collected during or before 2011 (H11- and H08-) were performed on a Mass Analyzer Products model 215-50 single-collector mass spectrometer operated in static mode, according to methods summarized in McIntosh and others (2003). Samples collected more recently (H12- and JC13-) were analyzed on an ARGUS VI multi-collector mass spectrometer. All ages are calculated for an age of 28.201 Ma (Kuiper and others, 2008; Min and others, 2000) on Fish Canyon Tuff sanidine. Ages determined on the ARGUS VI mass spectrometer are significantly more precise and accurate than ages determined on the MAP 215-50 (Heizler, 2011; Heizler and others, 2014). However, methodology is evolving, and final calculations of uncertainties may differ slightly from those reported here. Weighted mean $^{40}Ar/^{39}Ar$ ages of sanidine calculated by the method of Samson and Alexander (1987). Decay constants after Min et al. (2000); total = 5.463×10^{-10} yr^1. Isotopic abundances after Steiger and Jäger (1977); $^{40}K/K = 1.167 \times 10^{-4}$.

Explanation of $^{40}Ar/^{39}Ar$ Single Crystal Laser Fusion Analytical Data Plots (figures 1–1 to 1–19)

EXPLANATION OF $^{40}Ar/^{39}Ar$ SINGLE CRYSTAL LASER FUSION ANALYTICAL DATA PLOTS
(Figures 1-1 to 1-19)

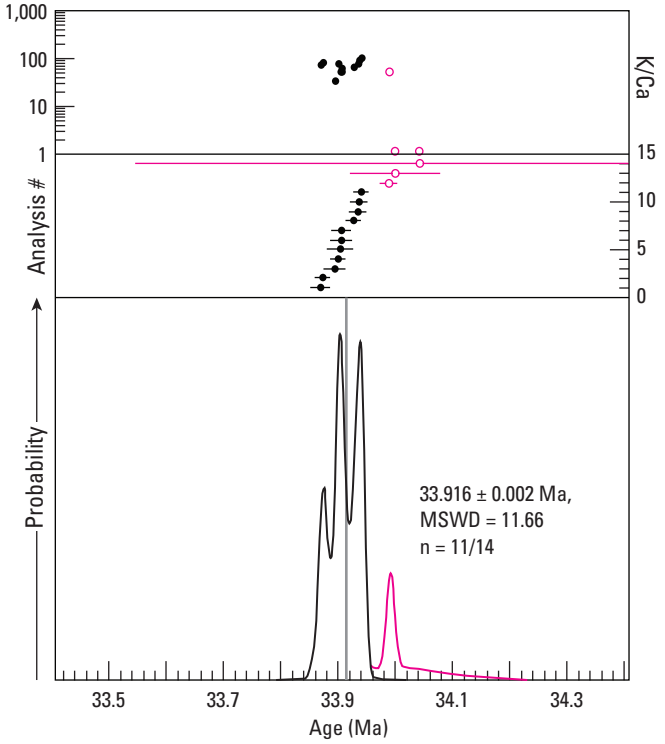

Upper plot is the potassium / calcium (K/Ca) ratio. Scale is logarithmic, open pink circles are analyses omitted from the final age calculation.

Middle plot shows uncertainty (1-sigma) on individual analyes, arranged from youngest to oldest. Open pink circles are analysis omitted from the final age calculation. Error bars smaller than symbols where not shown.

Bottom plot shows Probability Density Function (PDF) for all analyses (pink curve) and those used to calculate the final sample age (black curve).

Final age indicated by dark gray line with light gray uncertainty bounds (2-sigma); uncertainty is smaller than dark gray line if not shown.

Text box shows final age and uncertainty (2-sigma) in Ma, Mean Square of Weighted Deviates (MSWD), and number of grains analyzed compared to the total number analyzed.

X-axis for all plots is age in Ma

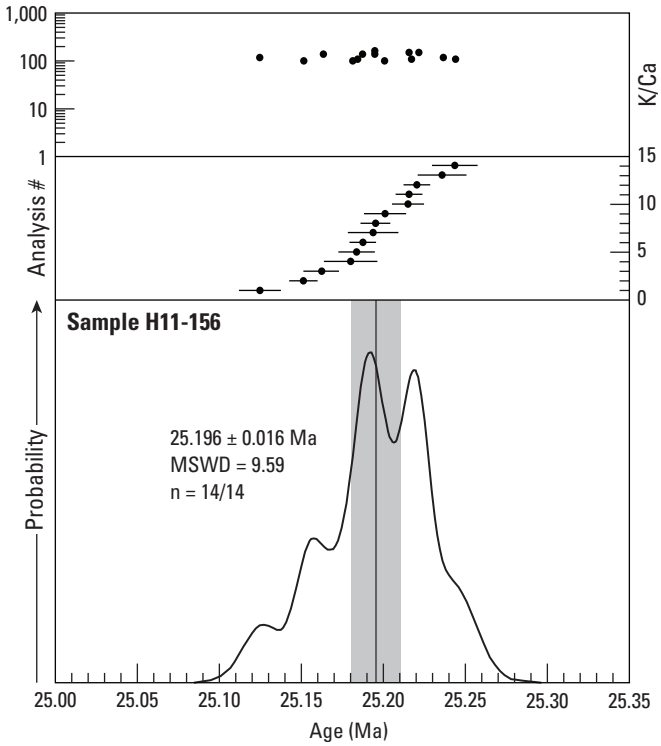

Figure 1–1. $^{40}Ar/^{39}Ar$ data for sample H11-156.

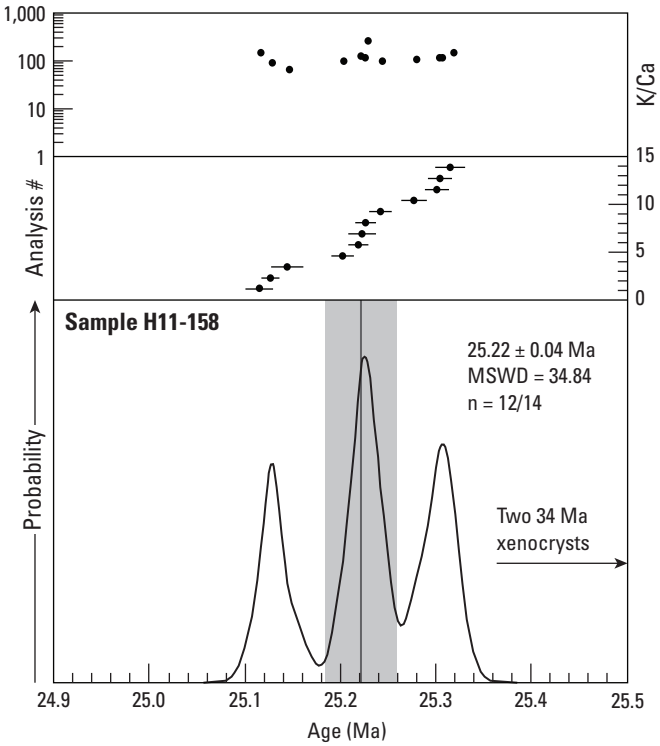

Figure 1–2. $^{40}Ar/^{39}Ar$ data for sample H11-158.

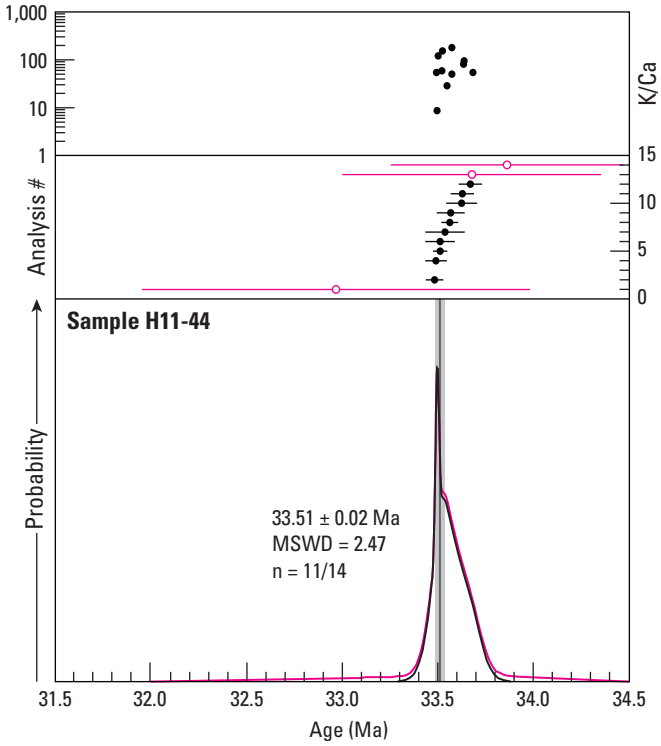

Figure 1–3. $^{40}Ar/^{39}Ar$ data for sample H11-44.

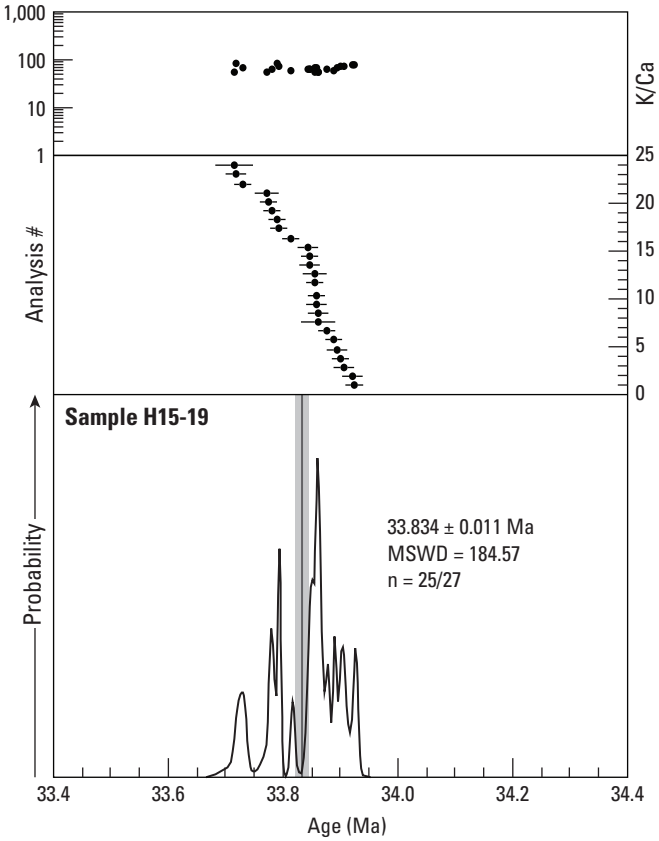

Figure 1–4. $^{40}Ar/^{39}Ar$ data for sample H15-19.

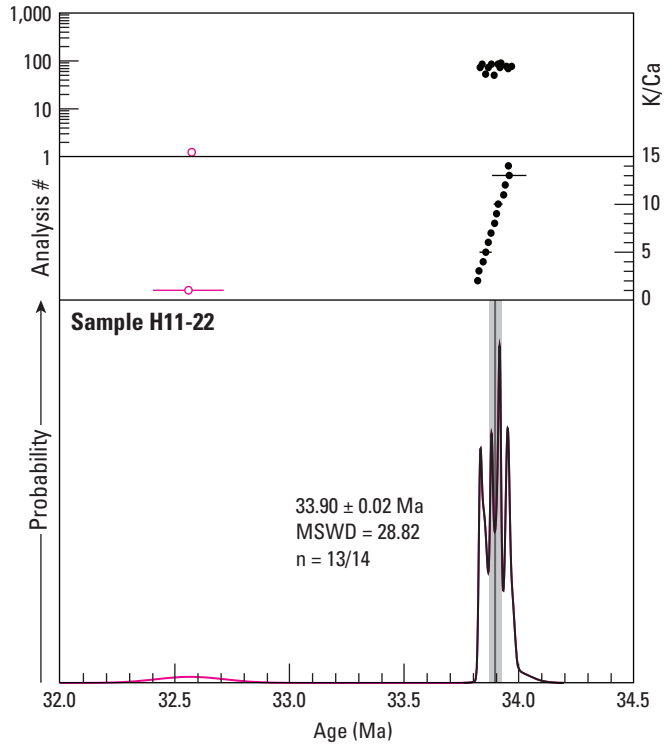

Figure 1–5. $^{40}Ar/^{39}Ar$ data for sample H11-22.

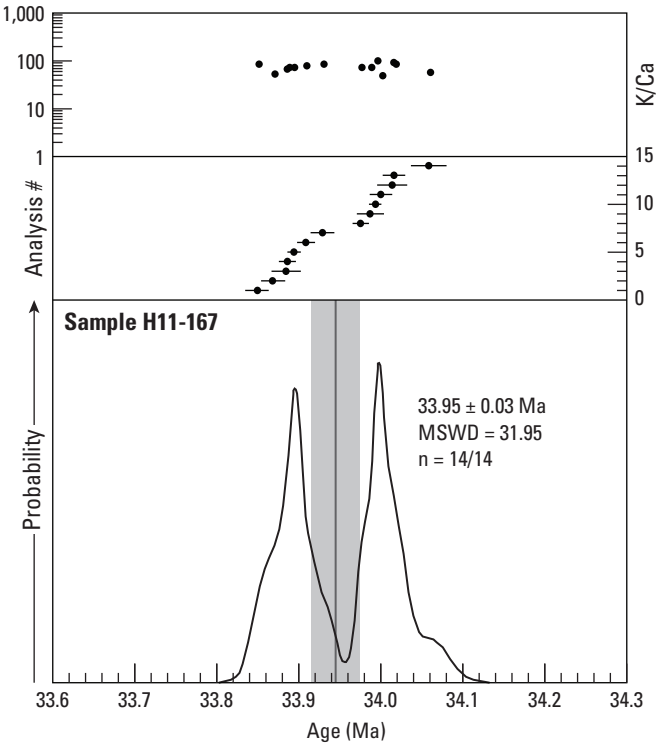

Figure 1–6. $^{40}Ar/^{39}Ar$ data for sample H11-167.

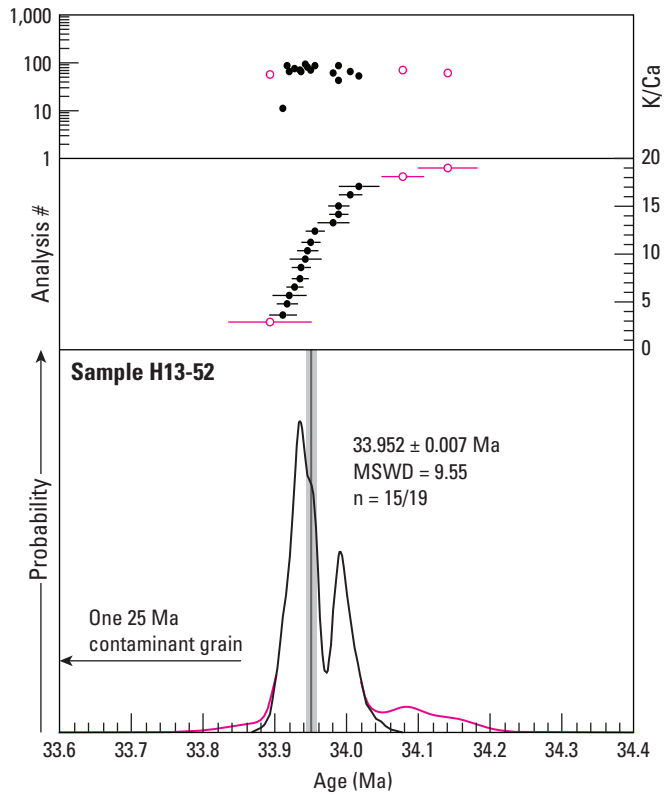

Figure 1–7. $^{40}Ar/^{39}Ar$ data for sample H13-52.

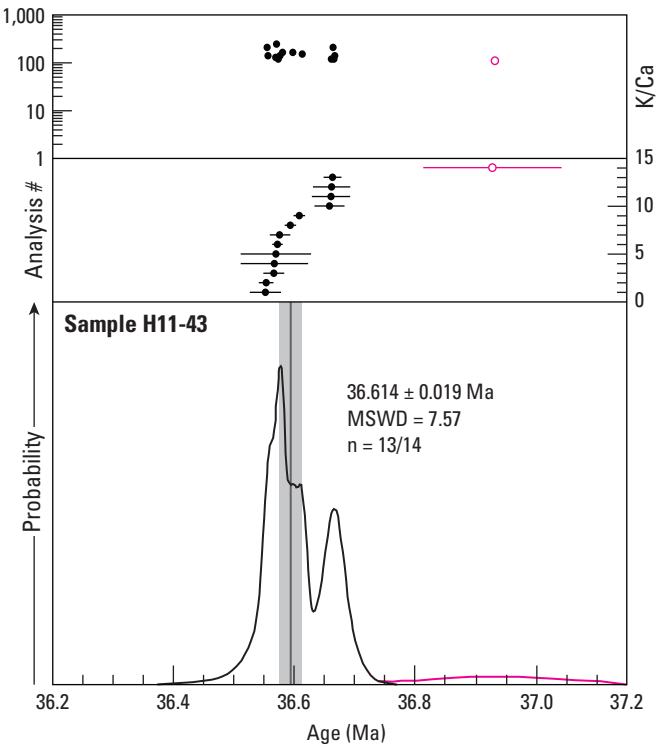

Figure 1–8. $^{40}Ar/^{39}Ar$ data for sample H11-43.

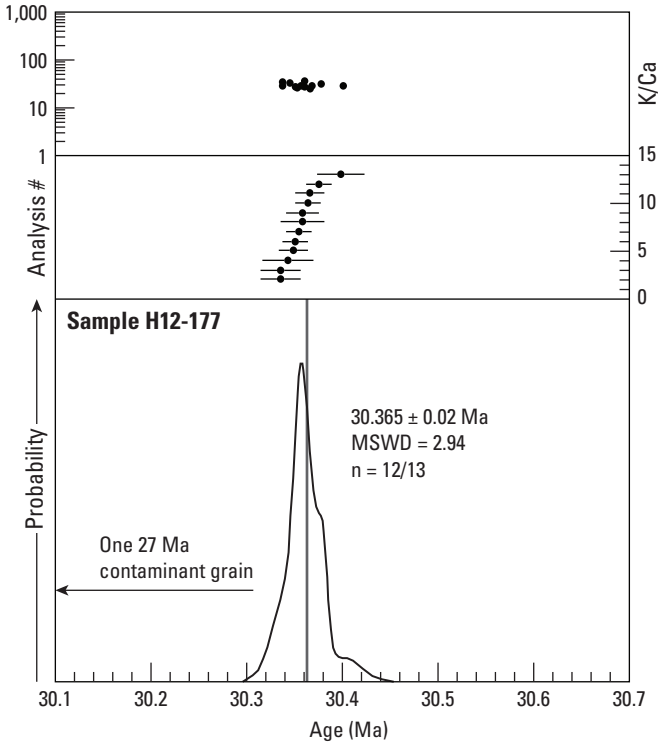

Figure 1–9. $^{40}Ar/^{39}Ar$ data for sample H12-177.

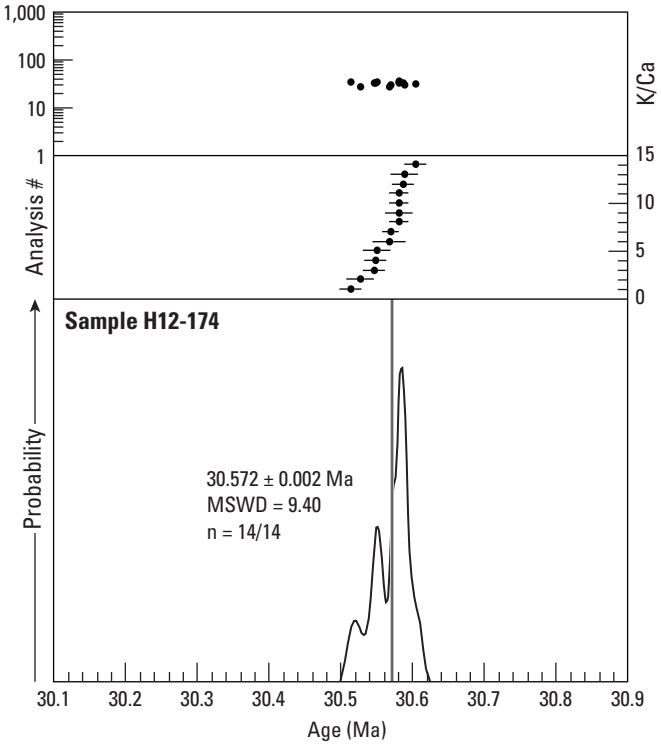

Figure 1–10. $^{40}Ar/^{39}Ar$ data for sample H12-174.

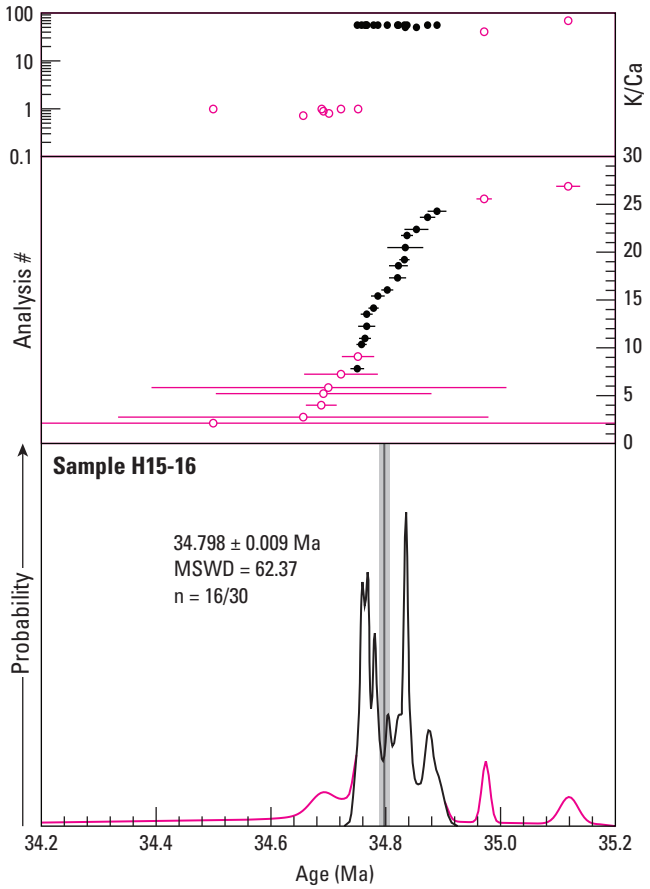

Figure 1–11. $^{40}Ar/^{39}Ar$ data for sample H15-16.

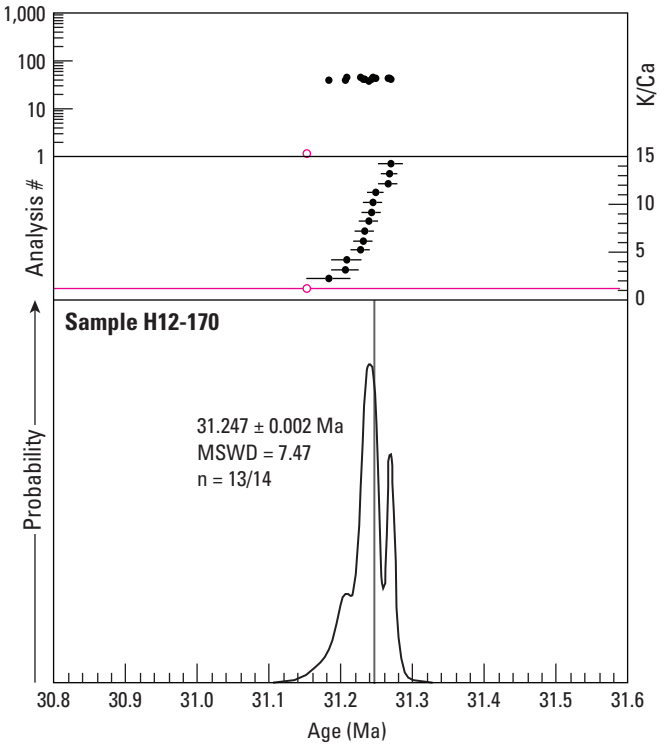

Figure 1–12. $^{40}Ar/^{39}Ar$ data for sample H12-170.

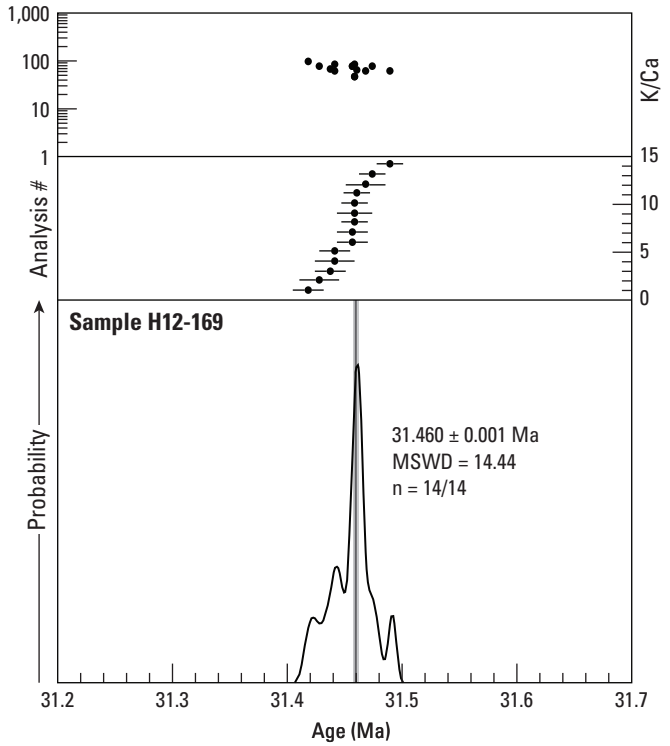

Figure 1–13. $^{40}Ar/^{39}Ar$ data for sample H12-169.

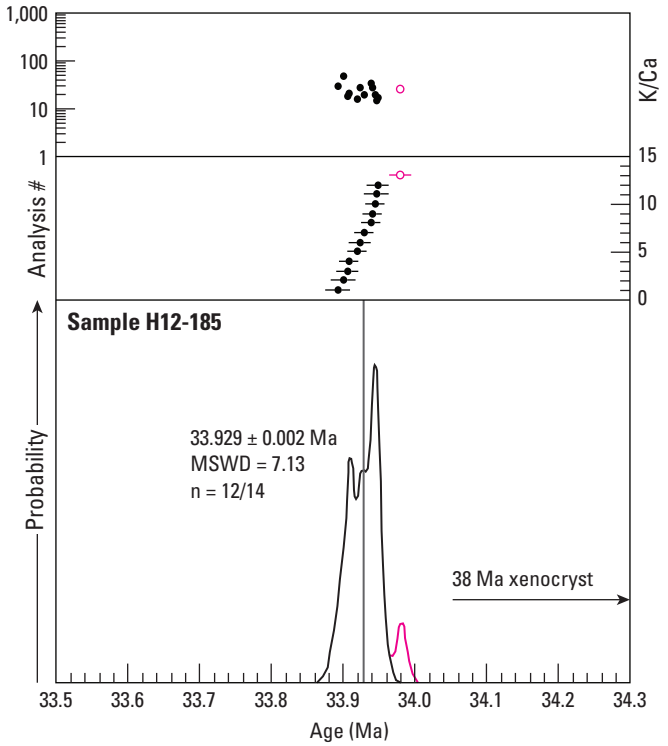

Figure 1–14. $^{40}Ar/^{39}Ar$ data for sample H12-185.

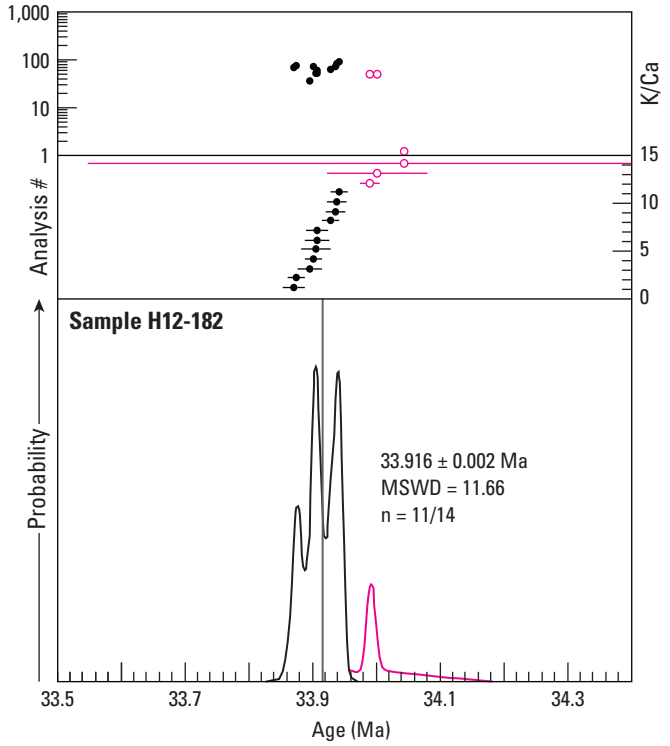

Figure 1–15. $^{40}Ar/^{39}Ar$ data for sample H12-182.

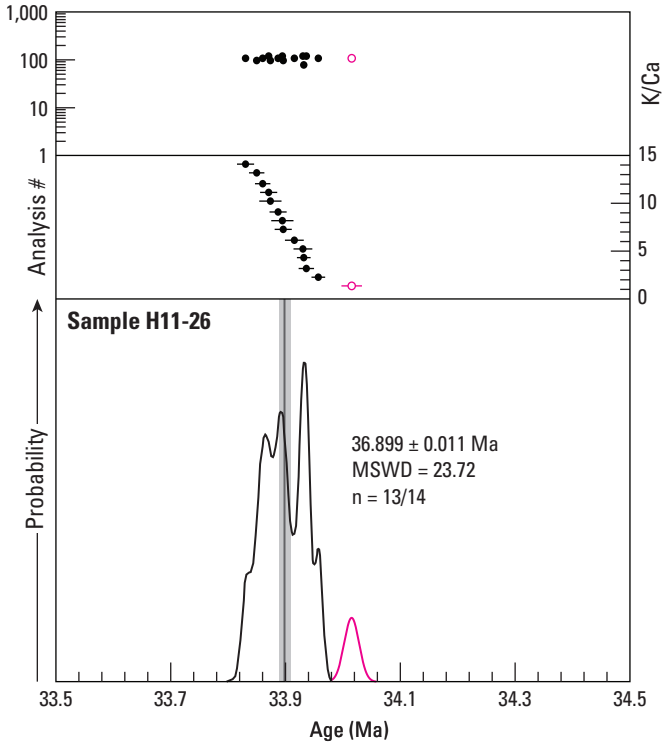

Figure 1–16. $^{40}Ar/^{39}Ar$ data for sample H11-26.

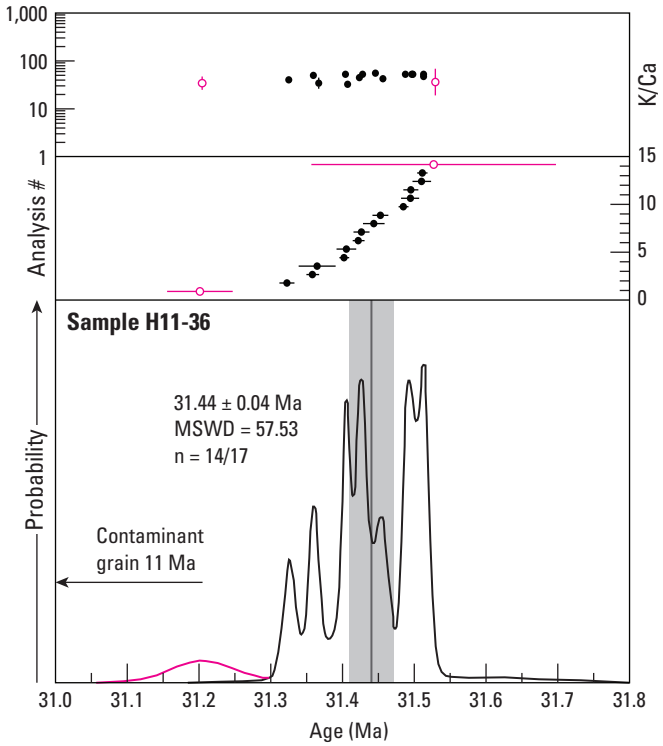

Figure 1–17. $^{40}Ar/^{39}Ar$ data for sample H11-36.

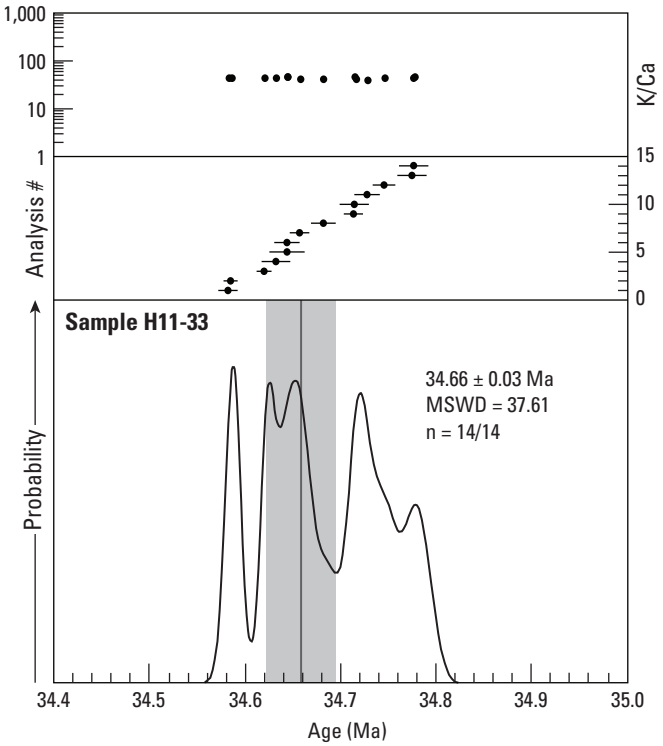

Figure 1–18. $^{40}Ar/^{39}Ar$ data for sample H11-33.

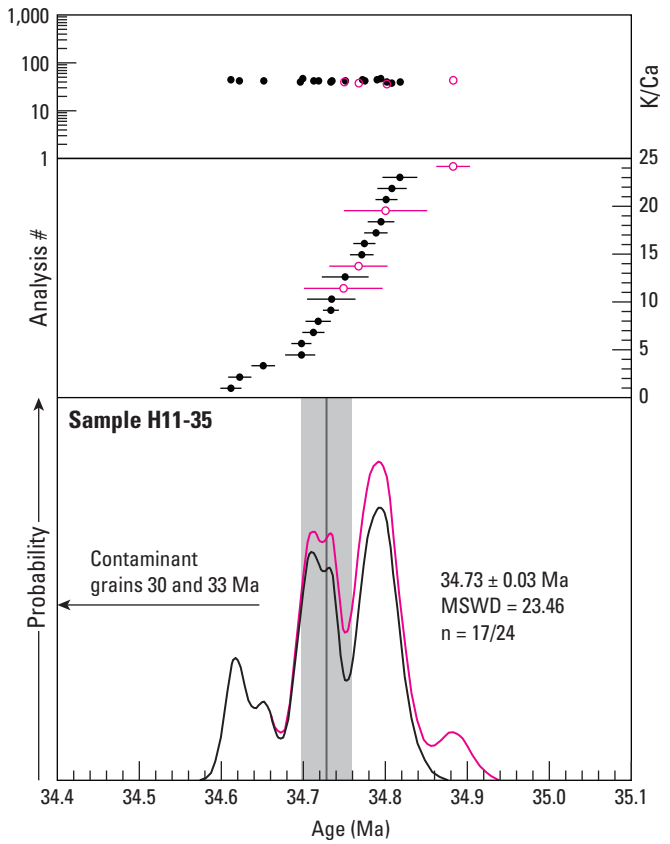

Figure 1–19. $^{40}Ar/^{39}Ar$ data for sample H11-35.

Explanation of $^{40}Ar/^{39}Ar$ Step Heating Analytical Data Plots (figures 1–20 to 1–22)

Upper left plot is the potassium / calcium (K/Ca) ratio.
Scale is logarithmic, box height indicates 1-sigma uncertainty.
Boxes/bars correspond to lettered steps in lower plot.

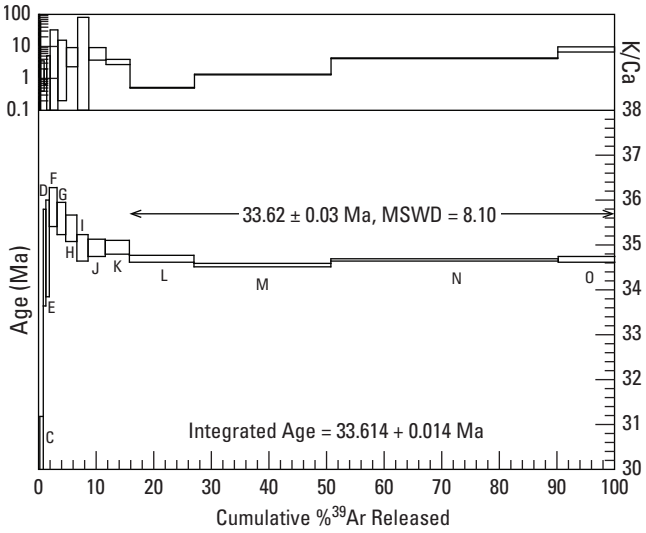

Lower left plot shows individual heating steps, indicated by letters.
Box height indicates 1-sigma age uncertainty, box width indicates percentage of ^{39}Ar released for that step. Y-axis is age in Ma.
Horizontal arrow and text indicates plateau age for indicated steps, with 2-sigma uncertainty and Mean Square of Weighted Deviates (MSWD).
Integrated age is the combined age for all steps, with 2-sigma uncertainty.

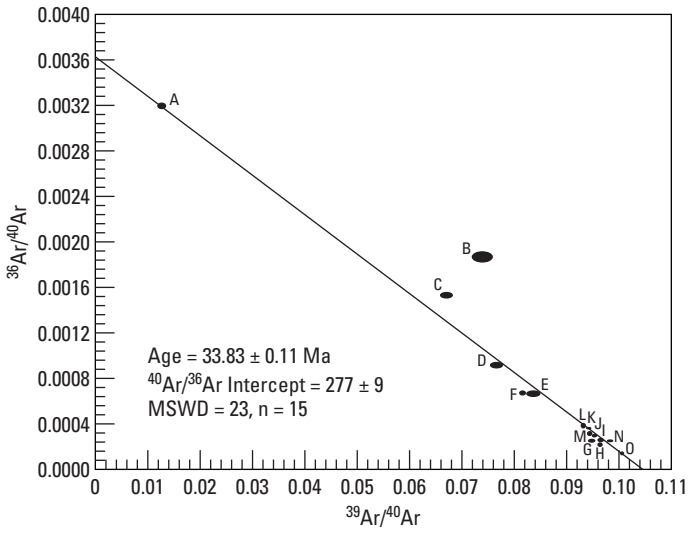

Right plot shows the isochron age. Black ellipses are 1-sigma uncertainty on individual analyses, letters correspond to lettered steps in left plot.
Black line is the best statistical fit to the individual analyses, and text box indicates the age (2-sigma uncertainty), initial $^{40}Ar/^{36}Ar$ ratio, MSWD, and number of included steps for the best fit line.

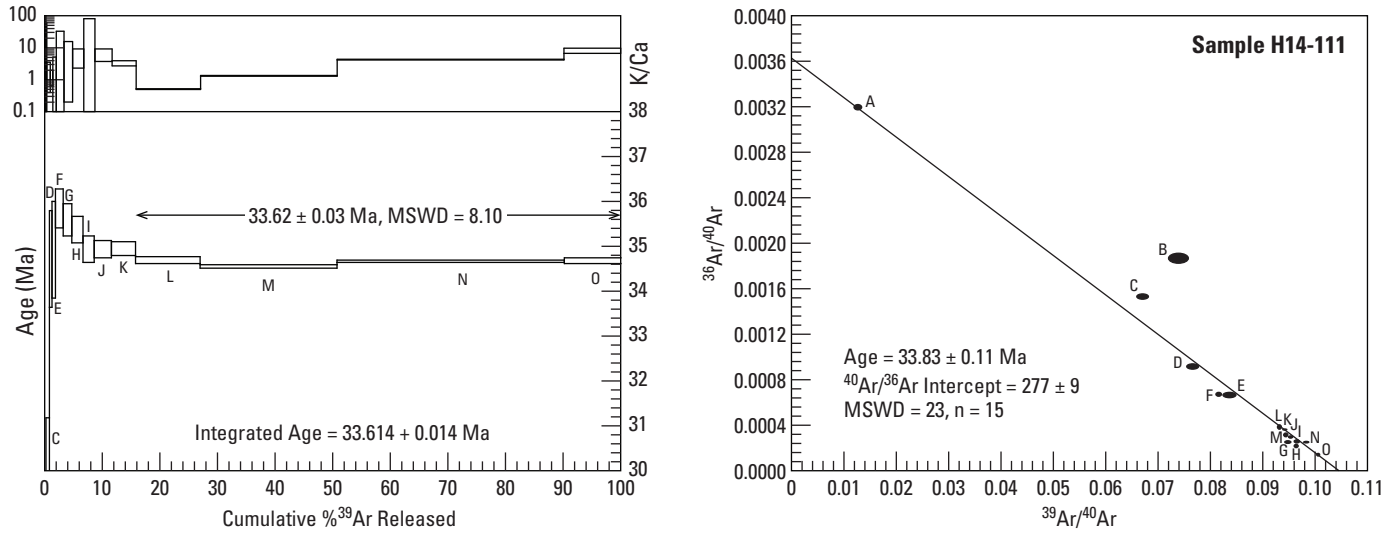

Figure 1–20. $^{40}Ar/^{39}Ar$ data for sample H14-111.

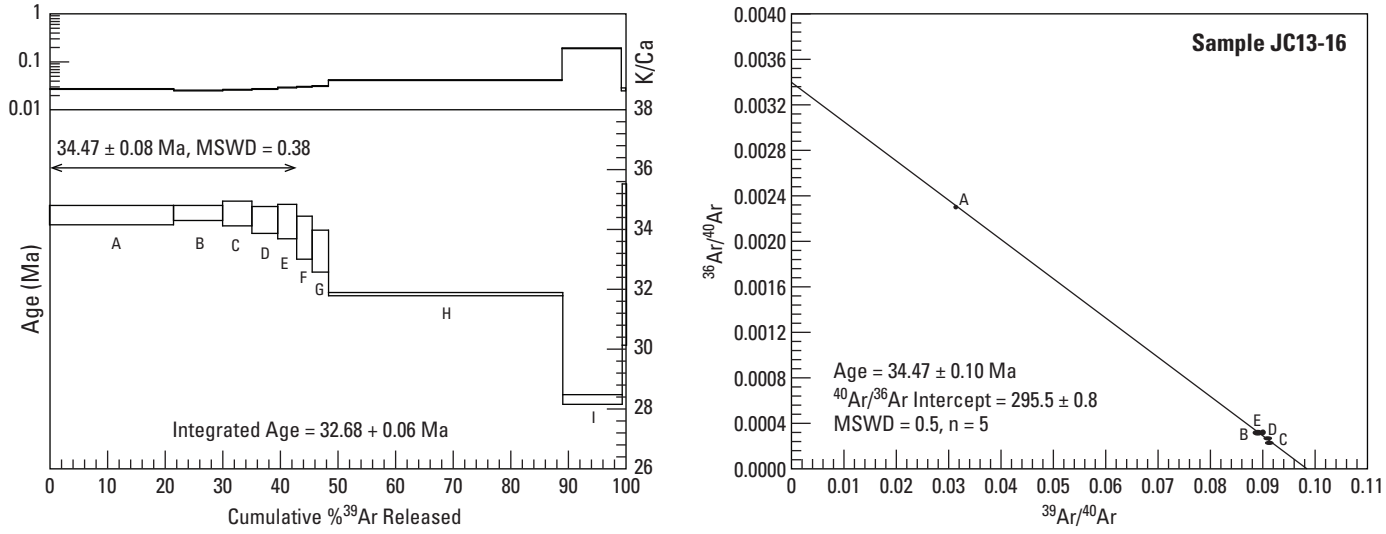

Figure 1–21. $^{40}Ar/^{39}Ar$ data for sample JC13-16.

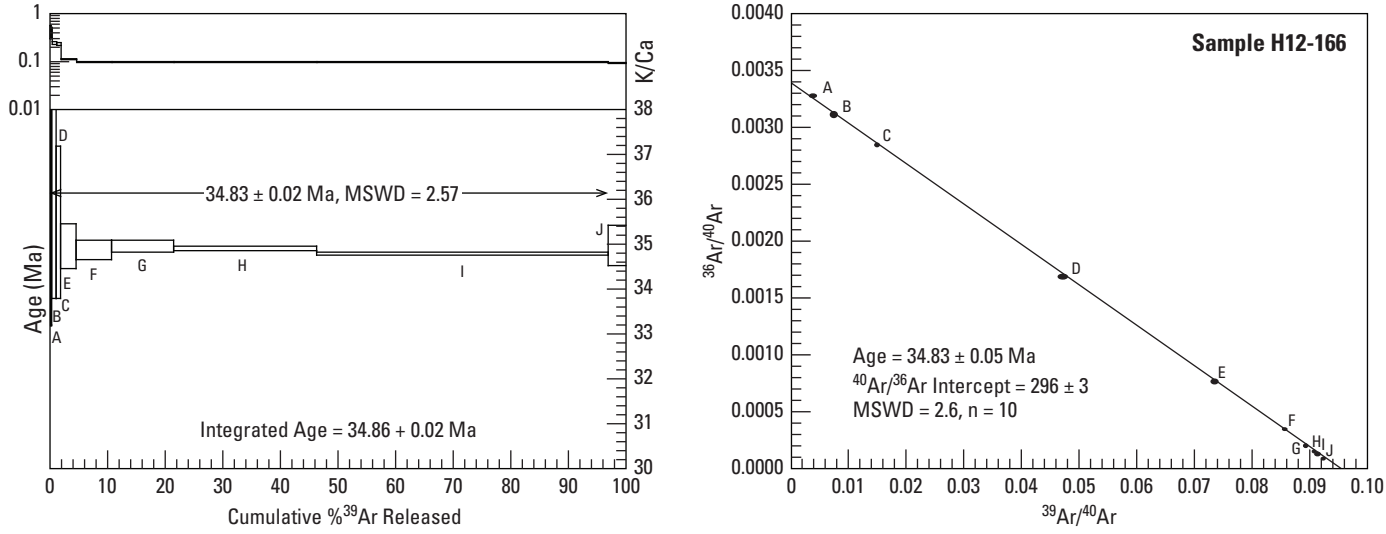

Figure 1–22. $^{40}Ar/^{39}Ar$ data for sample H12-166.

Publishing support provided by:
Denver Publishing Service Center, Denver, Colorado

For more information concerning this publication, contact:

Program Coordinator, National Cooperative Geologic Mapping Program
12201 Sunrise Valley Drive, Mail Stop 908
Reston, VA 20192
(703) 648-6053

Or visit the Geosciences and Environmental Change Science Center Web site at:
http://ncgmp.usgs.gov/

This publication is available online at:
http://dx.doi.org/10.3133/pp1832

ISSN 2330-7102 (online)
https://doi.org/10.3133/pp1832